Lap Au-Yeung, Team Manager
World Wide Convergence
66 Chancellors Circle
Winnipeg, Manitoba, R3T 2N2

December 04, 2019

Paul Labossiere, Ph.D., P.Eng
University of Manitoba
E2-372F EITC
Winnipeg, Manitoba, R3T 5V6

Re: Letter of Transmittal

Dear Dr. Labossiere,

On behalf of the team at World Wide Convergence (WWC), I submit herewith our final report entitled "Optimization of Non-Circular Void Concrete Extruder" as part of the fulfillment required for the course MECH 4860.

This report provides the details and related findings regarding the final optimized design of Ultra-Span's non-circular void concrete extruder. This document explains the project's process of examining the current design, identifying possible design concepts, evaluating the concepts, and suggesting a final design. WWC has proposed a simple design that does not require any additional components beyond what Ultra-Span already uses. The final design indicates that Ultra-Span may improve the pressure, viscosity, and velocity streamline performance of their concrete extruder by making minor modifications to their current auger configuration and material shield geometries. The project is completed on time with outcomes that satisfy all specified expectations of the client.

If you have any question or concerns on these matters, please contact Lap Au-Yeung at
or

Regards,

Lap Au-Yeung

University of Manitoba

Final Design Report

Optimization of Non-Circular Void Concrete Extruder

Client: Ultra-Span

Course Advisor: Dr. Meghan Guyot

Date of Submission: December 04, 2019

Created by: World Wide Convergence (WWC)

(MECH 4860 Group 2)

Mateus Braga ______________________________

David Penner ______________________________

Qiuhao Zheng ______________________________

Lap Au-Yeung ______________________________

Executive Summary

Ultra-Span, an industry leader in circular void concrete extruders is currently developing a non-circular void (NCV) concrete extruder. The current NCV design produces uneven concrete slabs and its extrusion speed is slow. Due to uneven compaction, the extruded concrete slabs are experiencing concrete starvation at the two top edges of the slab and the NCV extruder is also extruding at half the speed of its circular void counterpart (30 [*in/min*] versus 60 [*in/min*]).

The team at World Wide Convergence (WWC) undertook the project to optimize Ultra-Span's NCV concrete extruder. WWC's objectives for this project were to research other concrete extruders, develop concepts that improve the quality of the concrete slabs produced, increase the extrusion speed, evaluate the concepts using Computational Fluid Dynamics (CDF), and suggest an optimized final design. WWC served as CFD specialists to model the concrete flow within the extruder. The required deliverables included CFD analysis, detailed design optimization, 3D models of the optimized final design, a poster of the final design, and a final design report. Prototyping, physical testing, manufacturing, a bill of materials, and a cost summary were excluded from the scope.

Following an engineering design methodology 15 concepts were developed. After evaluating the performance of the concepts in compatibility for manufacture, minimal number of parts, pressure performance, viscosity performance, flow uniformity, and maintenance/cleaning ease, 11 concepts were eliminated in a screening process. The four concepts chosen for additional evaluation were to alternate the direction of rotation between the five augers, increase the length and close off the gaps between material shields, attach vanes on top of the mandrels, and add vanes to the sidewalls of the extruder cassette. Once the four concepts were evaluated using CFD a weighted decision matrix was used to select the advancing concepts. The advancing concepts were to alternate the direction of rotation between the five augers and increase the material shield length. These two designs were then combined in a final design optimization phase.

The final design developed by WWC integrates perfectly into Ultra-Span's existing NCV extruder with no additional components or new procedures. The simple yet effective final design extends Ultra-Span's original material shields from 6 [*in*] on the top and 15.75 [*in*] on

the bottom to 15.75 [*in*] at the top and at the bottom. The final design also re-configures Ultra-Span's current auger rotation directions to be Clockwise – Counter clockwise – Clockwise – Clockwise – Counter clockwise. The optimized design decreases the average outlet pressure by 39.31% from the current design and reduces shearing at the outlet (increases viscosity) by 53.91%. Less shearing along with uniform pressure at the outlet shows that WWC's design makes the flow uniform across the extruder, increasing the extrusion speed and satisfying the required slab geometry. In conclusion, the project is completed on time with outcomes that satisfy all specified expectations of the client.

Table of Contents

List of Figures

List of Tables

Abbreviations

WWC	World Wide Convergence
PDR	Project Definition Report
CDR	Concept Design Report
NCV	Non-Circular Void
CFD	Computational Fluid Dynamics
CSM	Concept Screening Matrix
CWM	Criteria Weighting Matrix
WDM	Weighted Decision Matrix
CAD	Computer Aided Design
CCW	Counter Clockwise
CW	Clockwise

1. Introduction

Ultra-Span, one of the leaders in the pre-cast concrete industry and inventors of the concrete extrusion technology, are experts in designing and manufacturing concrete extruders. Using augers and vibrational plates, concrete extruders simultaneously shear and compact wet concrete into slabs. Various shapes of concrete slabs can be made by extruding the concrete out of an opening set to a prescribed geometry. Ultra-Span's machines are capable of producing regular pre-cast concrete as well as hollow core slabs. Figure 1 shows one of Ultra-Span's concrete extruders and Figure 2 shows typical hollow core concrete slabs.

Figure 1. Ultra-Span's concrete extruder [1]

Figure 2. Pre-cast, circular void concrete slabs [1]

Engineers have determined that there are benefits to creating non-circular void hollow core slabs. However, as non-circular void concrete extruders are relatively new to the industry, the technology is still under development and there are some issues with the quality, consistency, and speed of the concrete extrusion.

1.1. Problem Description

Currently, Ultra-Span's non-circular void (NCV) concrete extruder produces uneven concrete slabs, and its extrusion speed is slow. Inconsistent flow through the compaction chamber is leading to uneven compression between the top and bottom half of the augers, as well as from the middle to the outside augers. Due to the uneven compression, the extruded concrete slabs, as seen in Figure 3, are experiencing concrete starvation at the two top edges of the slab, making it not suitable for its structural use. The NCV extruder is also extruding at roughly half the speed of its circular void counterpart (30 [*in/min*] versus 60 [*in/min*]). The lower speed extrusion means lower productivity and is less efficient for Ultra-Span's clients.

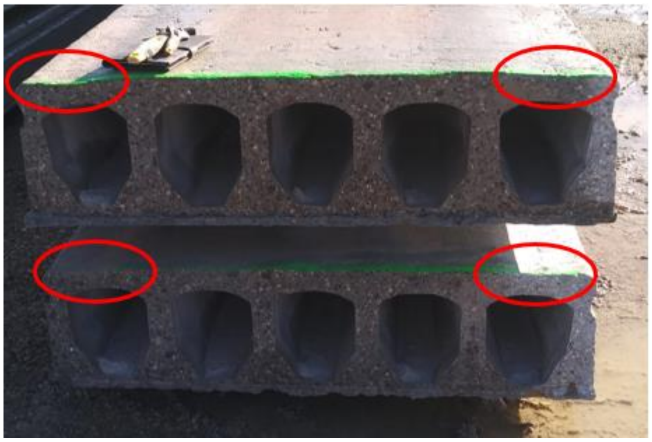

Figure 3. Pre-cast concrete slabs with non-circular voids. The zones of concrete starvation circled in red [1]

The team at World Wide Convergence (WWC) undertook the project to optimize Ultra-Span's NCV concrete extruder. WWC's primary objectives for this project were to research other concrete extruders, optimize the existing design, and analyze the concrete fluid flow coming from Ultra-Span's NCV extruder. The goal of the project is to suggest optimizations to the current extruder, to improve the quality of the concrete slabs produced, and to increase the extrusion speed all while maintaining the outlet geometry of the concrete slab prescribed by structural engineers.

1.2. Ultra-Span's Extrusion Process

To provide context for the report that follows, Ultra-Span's hollow core extrusion process [2] is explained below:

1. Fresh concrete is poured into a vertical hopper. Figure 4 shows the hopper.

Figure 4. Top view of the hopper from Ultra-Span's concrete extruder [1]

2. Highly powered augers rotate to draw the concrete downward and force the concrete downstream.
3. Downstream from the augers, the concrete passes around the vibrating mandrels, gradually taking the outlet shape and forming the voids. The mandrels are located in the compaction chamber where there is a vibrating plate that presses on the top of the concrete. The purpose is to consolidate the concrete and remove any air pockets that are trapped inside the concrete.
4. The flow exits the compaction chamber holding its overall trapezoidal shape and the shape of the voids by flowing around follower tubes until it is hardened enough to maintain its shape. Figure 5 shows a computer-generated model of the augers, mandrels, and follower tubes.

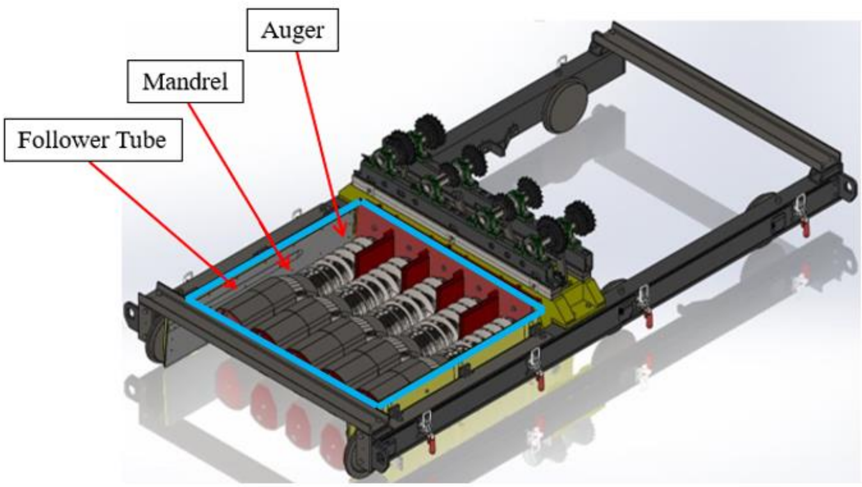

Figure 5. Extruder mechanism sectional cut. Compaction chamber highlighted in light blue, follower tube, mandrel, and auger labeled [1]

5. The concrete exits the extruder in its final shape, hard enough to withstand the weight of a person immediately at the outlet. Figure 6 shows the extruder outlet.

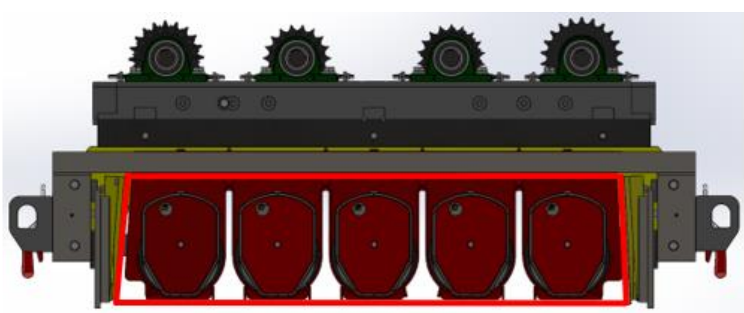

Figure 6. Extruder outlet highlighted in red [1]

The shape of the voids can be made either circular or non-circular by modifying the follower tubes. The circular void extruders operate by allowing the mandrels and the follower tubes to rotate at the same speed as the auger. However, the NCV extruders do not allow for the mandrels or the follower tubes to be rotated. Therefore, the concrete flow is facilitated by the rotation of the augers along with vibration of the mandrel.

1.3. Project Definition

WWC's role in this project was to serve as Computational Fluid Dynamics (CFD) specialists. Ultra-Span has minimal access to CFD software and their personnel with CFD experience is limited. However, they are well equipped with manufacturing specialists and are proficient with the current operation of their manufacturing shop. It is for this reason WWC is responsible for presenting CFD results to Ultra-Span's technical team given WWC's access to CFD software and expertise in CDF simulations. The goal is to equip Ultra-Span with the knowledge necessary to better understand their NCV extruder so they may implement modifications to the NCV extruder themselves. The technical analysis and optimization suggestions by WWC may provide valuable information that encourages design changes within Ultra-Span.

The scope of work that WWC undertook at the onset of this project included performing CFD analysis, giving detailed design optimization, creating 3D models of the optimized final design, and producing technical drawings of the optimized design. WWC and Ultra-Span agreed that the project would not include any prototyping, physical testing or manufacturing related work such as a bill of materials and a cost summary.

1.4. Ultra-Span's Needs and Required Specifications

All needs identified by WWC are included in Table I. Upon consultation with Ultra-Span, WWC has ranked the needs on a scale of low, medium or high depending on their severity and urgency.

TABLE I. LIST OF NEEDS TO OPTIMIZE ULTRA-SPAN'S NCV EXTRUDER

Needs #	Needs Statement	Importance
1	The extruder design needs to use Ultra-Span's existing platform	High
2	The extruded concrete needs to have a flat top surface	High
3	The extruded concrete needs to have uniform properties throughout the slab	High
4	The extruded concrete needs to be in the shape of the specified technical drawings	High
5	The concrete needs to hold its shape immediately after the outlet of the extruder	High
6	The concrete needs to be a fluid (not solid) until right after the outlet of the extruder	High
7	The manufacturing of the extruder cassette needs to be possible within Ultra-Span's existing infrastructure	High
8	The design needs to be safe	High
9	The concrete needs to be extruded at 60 [*in/min*]	High
10	The extruder needs to operate normally for any of Ultra-Span's recommended aggregate/cement mixes	High
11	The extruder needs to work in various locations around the world	Medium
12	The extruder needs to maintain performance during operation	Medium
13	The extruder cassette needs to have few moving parts	Medium
14	The design needs to last a long time	Medium
15	The design needs to be low cost	Low
16	The extruder cassette needs to be easily accessible for maintenance	Low
17	The extruder cassette needs to allow for easy replacement of worn parts	Low

WWC's optimization process does not change the fundamentals of the original design, thus the low and medium needs, which were met by the current design will still be met after optimization and are not considered further. Of the 17 needs identified ten were considered high importance. After further consultation with Ultra-Span the important needs were refined. The most important needs to be addressed by WWC's optimizations are as follows:

- The extruder design needs to use Ultra-Span's existing platform
- The concrete needs to be extruded at a minimum rate of over 60 [*in/min*]
- The extruder needs to operate normally for any of Ultra-Span's recommended aggregate/cement mixes
- Any suggested design changes need to be possible within Ultra-Span's existing infrastructure
- The location of all the voids as well as the overall dimension of the extruded concrete slabs must remain unchanged

1.5. Constraints and Limitations

In order to meet the client's needs, several constraints and limitations were imposed on the project. The most important constraint is that the final concrete slab quality and geometry cannot be compromised. Following a civil engineering analysis, Ultra-Span has indicated that any optimizations to the NCV extruder must maintain the structure, safety and usability of the precast concrete produced. The implications and additional constraints ensuing from this are further explained in the following list:

- The final cross section of the follower tubes cannot be modified
- The location of the follower tubes at the outlet cannot be modified
- The voids must be in the pre-existing location
- The outlet cassette geometry must stay the same
- The final slab geometry must be conserved
- The width of the extruder cannot be wider than the 47 7/8 [*in*] bed rails of the extruder

In brief, the location of all the voids as well as the overall dimension of the extruded concrete slabs must remain unchanged. Therefore, the modified design must comply with the technical drawings dimensioned in Figure 7.

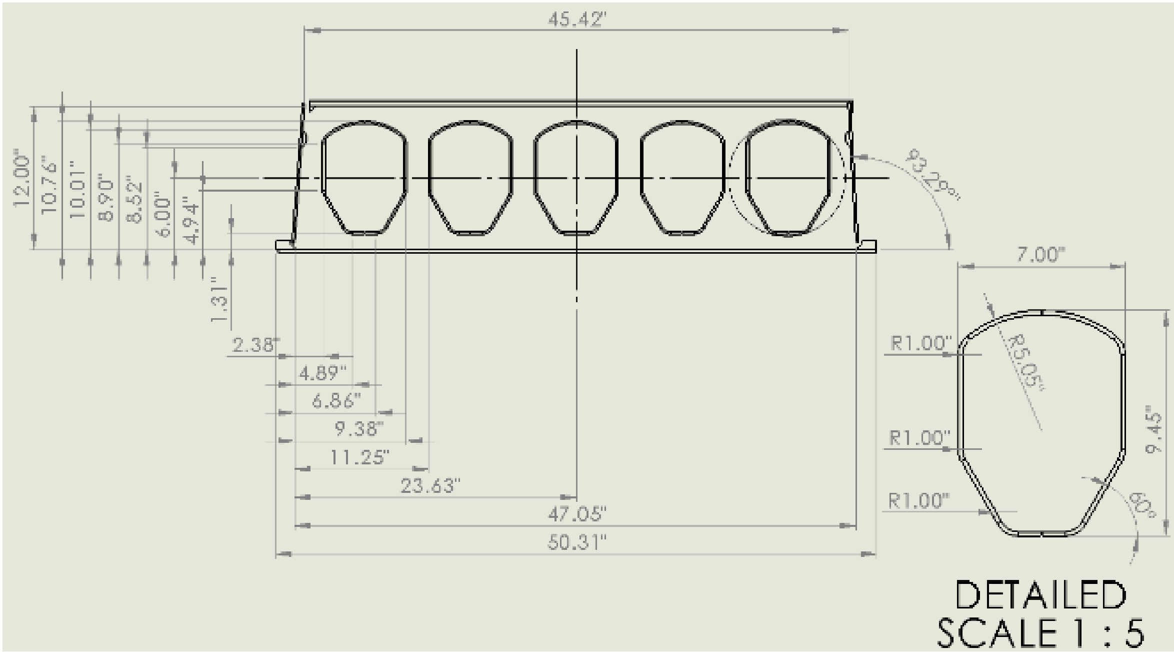

Figure 7. Desired geometry of the concrete slabs produced by the NCV extruder

1.6. Scope Modification

After the submission both of the Project Definition Report (PDR) and Concept Design Report (CDR) and meeting with the client, a modification to the project scope was made. Previously the required deliverables included producing technical drawings of the optimized design. However, due the complex, technical, and specialized nature of CFD, technical drawings for the final design are no longer required and are beyond the scope of this project. The client has deemed rigorous CFD analysis as the primary focus and will create their own technical drawings within their well-established manufacturing department. Therefore, the new deliverables include CFD analysis, detailed design optimization, 3D models of the optimized final design, a poster of the final design, and a final design report. Prototyping, physical testing, manufacturing, a bill of materials, and a cost summary remain excluded from the scope.

The scope change affects the project such that upon competition of WWC's work, the client will not directly have a ready-to-implement design. The CFD results and corresponding designs provided by WWC will need to be verified with experiments, made into technical drawings, and be subject to an engineering economic analysis before they are implemented.

1.7. Report Structure

This report explains the project's process from examining the current design, identifying advancing concepts, evaluating the outstanding concepts, and suggesting a final design. Further recommendations are given followed by a conclusion of the final design and closure of the project.

Ultimately, this document is presented as a CFD investigation, numerically analyzing the concrete flow in Ultra-Spans' NCV concrete extruder. The information will equip Ultra-Span with the knowledge to optimize their existing NCV concrete extruders by presenting a solution that satisfies their specific needs and resolves the current quality issues with their NCV concrete extruder.

2. Current Specifications

To facilitate design optimization, the current specifications are detailed to help understand the flawed design and identify where changes could be made. Based on the information provided by Ultra-Span, the overall layout of the final concrete slab produced cannot change as previously shown in Figure 7. Figure 8 is a technical drawing of the current outlet cassette on the NCV extruder. The location of each component in Figure 8 is constrained from changing because in doing so would cause structural changes to the concrete slab.

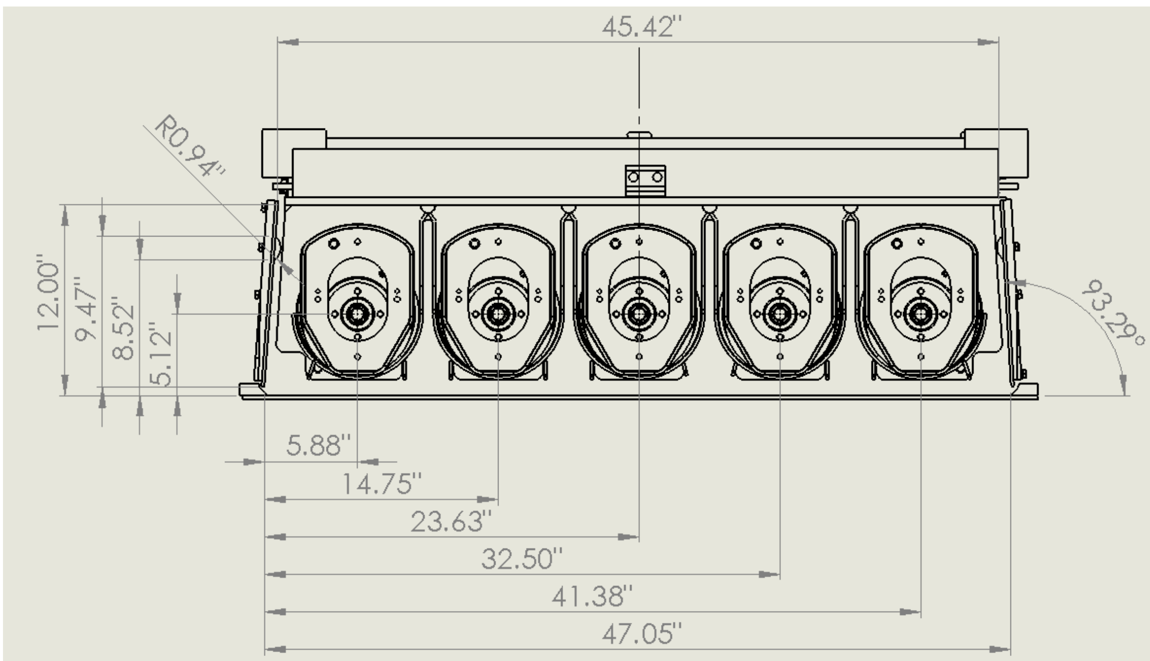

Figure 8. Current outlet cassette of the NCV extruder

What is permitted to be optimized is the speed and direction of the augers, the mandrel shape and length, the material shields, and the addition of minor components such as vanes or pushing plates to re-direct the flow. Figure 9 provides an overview of the speed and rotation of each individual auger in the mechanism. Currently the three augers on the left rotate counter clockwise (CCW) and the two augers on the right rotate clockwise (CW). Additionally, the two outer most augers spin faster than the two inner augers.

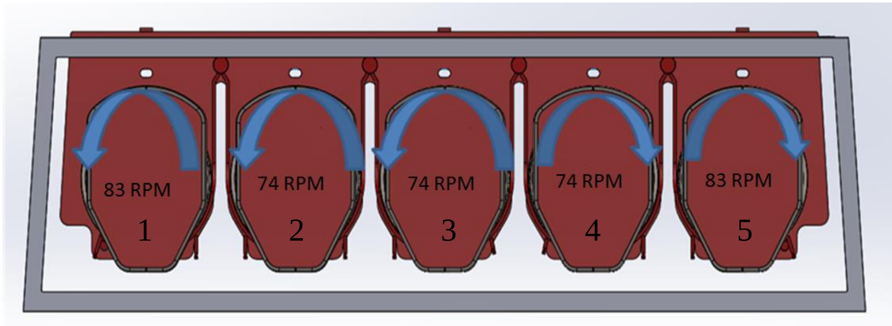

Figure 9. Overview of current auger rotation [2].

Table II presents the information from Figure 9 in tabular form.

TABLE II. CURRENT AUGER SPEED AND ROTATION [1]

Auger	**1**	**2**	**3**	**4**	**5**
Speed [*rpm*]	83	74	74	74	83
Rotation	CCW	CCW	CCW	CW	CW

Figure 10 shows the current mandrels. The purpose of the mandrels are to facilitate the transition in size from the auger to the follower tubes.

Figure 10. Current mandrels

Figure 11 shows the current material shields. Rough dimensions are shown to provide a general understanding of the current length of the material shield. The material shield provides separation between individual augers for about half the length of the augers, approximately 6

[*in*]. The current material shield supports the bottom of the augers for about 15.75 [*in*] on the outside augers and 12 [*in*] for the inside augers. There are also small gaps in between each material shield, one of these gaps is circled in red in Figure 11.

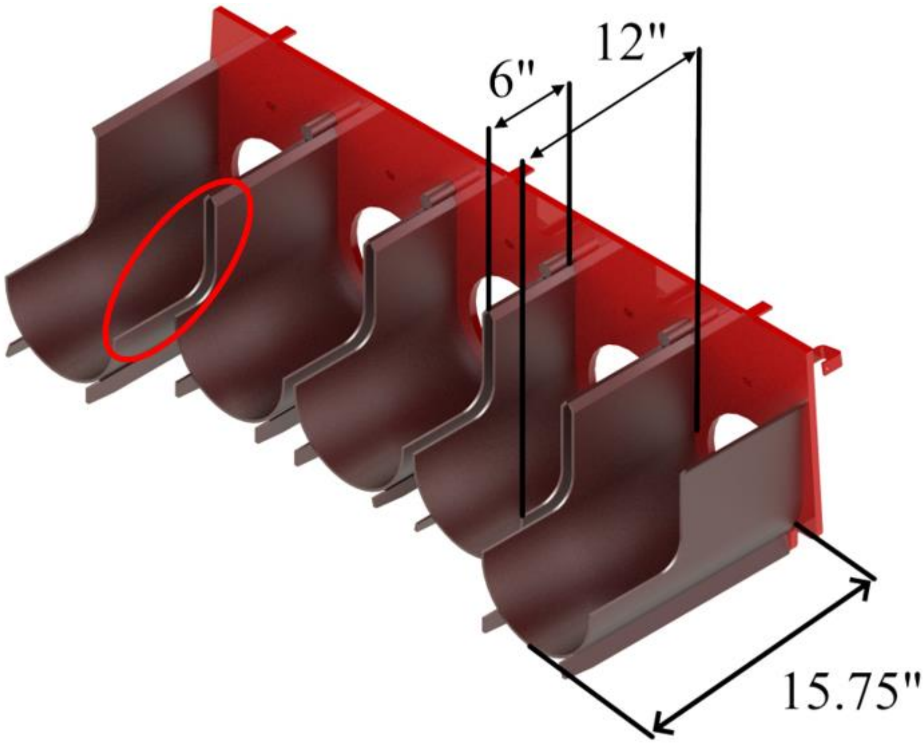

Figure 11. Current material shields with rough dimensions, gaps between material shield circled in red

Figure 12 shows one of the sidewalls of the extruder cassette. The horizontal rib is an existing feature necessary for the required slab geometry and cannot be modified.

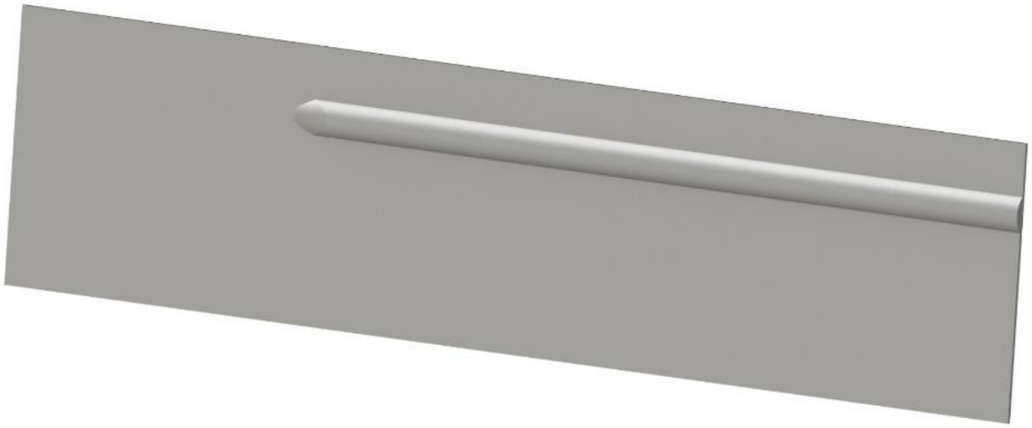

Figure 12. Current extruder cassette sidewalls

Systematically each of these components were evaluated and were subject to an engineering analysis and design process.

3. Design Methodology

To improve upon Ultra-Span's current non-circular void extruder and meet the clients needs, WWC's design methodology was as follows:

1. Understand Ultra-Span's field of operation and needs
2. Research concrete extrusion and existing extruder design
    2.1. Consult with the client and gather data about the current NCV extruder
3. Identify features of the current NCV extruder that are to be optimized
    - Augers
    - Mandrels
    - Follower tubes
    - Overall cassette geometry
4. Develop design concepts that improve upon the identified features
5. Screen the concepts against the selection criteria
    - Compatibility for manufacture
    - Minimal number of parts
    - Pressure performance
    - Viscosity performance
    - Flow uniformity
    - Maintenance /cleaning ease
6. Evaluate the concepts using Siemens STAR-CCM+ CFD software
7. Select concepts that have the greatest optimization potential
8. Combine the two concepts that had the greatest impact for further optimization
9. Analyze the combination
10. Interpret the results and make engineering conclusions
11. Develop a final design

A summary of the concepts that advanced from the screening phase and a discussion of their performance is provided in Section 4.

4. Summary of Advancing Concepts

In the CDR 15 concepts were developed. Based on the performance of the concepts in compatibility for manufacture, minimal number of parts, pressure performance, viscosity performance, flow uniformity, and maintenance/cleaning ease, 11 concepts were eliminated and four advanced to further analysis in the FDR. This section provides a summary of the concepts that have advanced from the screening phase in the CDR. Table III summarizes the advancing concepts. The concept letters on the left hand side of the table correspond to the letter assigned during the organization of the 15 concepts developed in the CDR and are therefore not in alphabetical order.

TABLE III. POST CONCEPT SCREENING RESULTS

Concept	Concept Description
B	Alternate the direction of rotation between the five augers
D	Close off gaps between material shields and increase material shield length
H	Attach vanes on top of mandrel to manipulate the flow direction
O	Add vanes to the side walls to redirect flow downstream

To begin the concept evaluation, each of the continuing concepts is modeled using SolidWorks computer aided design (CAD) software. Along with a brief explanation of each concept, the performance for each concept in compatibility for manufacture, minimal number of parts, and maintenance/cleaning ease is discussed. Discussion for pressure performance, viscosity performance, and flow uniformity is postponed until Section 6 where detailed CFD analysis is used to justify the concrete flow characteristics. Renders for each of the continuing concepts are shown in Figure 13 to Figure 17.

Concept B is the simplest design and maintains the most similarities to the current design. This concept only alters the direction of the auger rotation and maintains the same rotation speed for each auger. Table IV shows the adjusted auger rotations. Concept B attempts to increase the shear force applied to the concrete flow, helping to liquefy the concrete for a smoother and faster flow downstream. This modification utilizes existing parts where no new parts are needed, resulting in greater compatibility for manufacture. Furthermore, there are no new features that require additional maintenance needs. In brief, Concept B performs equally well as the current design in the areas of compatibility for manufacture, minimal number of parts, and maintenance / cleaning ease.

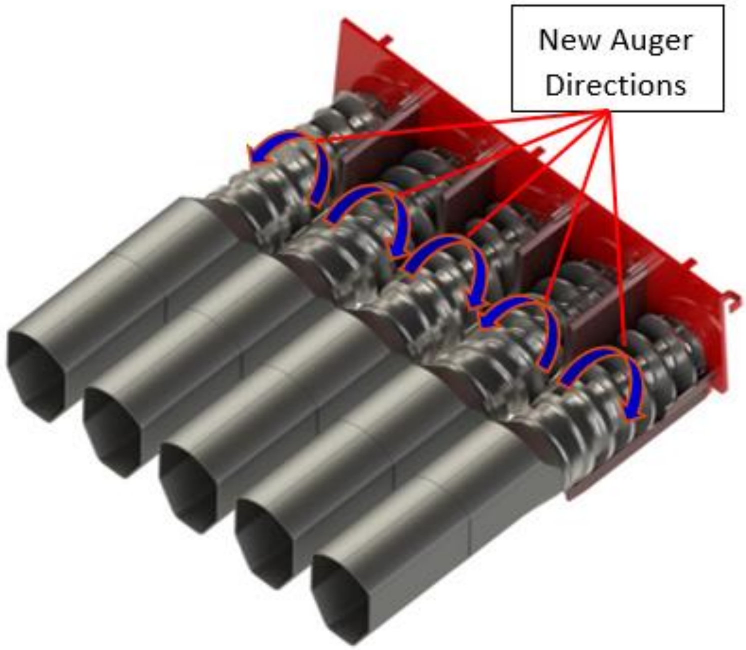

Figure 13. Concept B: Alternate Auger Rotations (isometric view)

TABLE IV. CONCEPT B: AUGER SPEED AND ROTATION

Auger	**1**	**2**	**3**	**4**	**5**
Speed [*rpm*]	83	74	74	74	83
Rotation	CCW	CW	CW	CCW	CW

Concept D features modification to material shields to seal off gaps and to elongate the shields surrounding the augers since hardened concrete build-up was found in gaps between the material shields and walls. The material shields are increased to a length of 15.75 [*in*], now they fully divide individual augers for the entire length of the auger, keeping the concrete sperate until reaching the mandrels. Concept D is attempting to keep concrete funneled and driven by the augers, potentially reducing the flow blockage. This modification does not generate extra parts but rather reduces the amount of labour needed for manufacture since the material shields are no longer required to be machined down to a finite curvature.

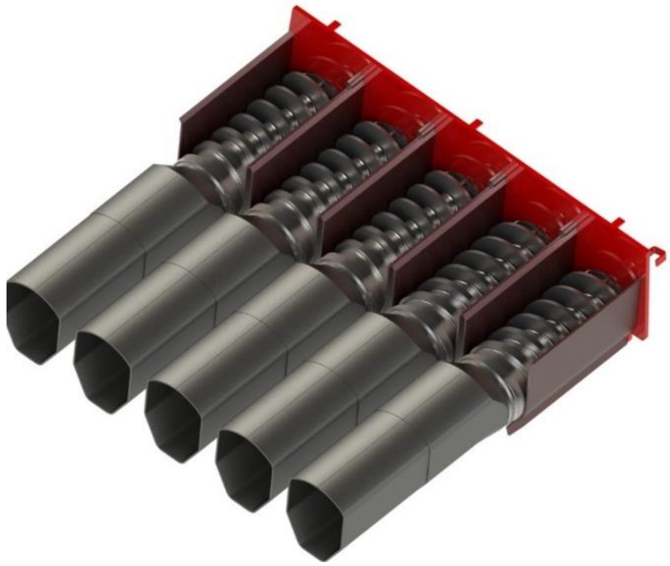

Figure 14. Concept D: Sealed and Elongated Material Shields (isometric view)

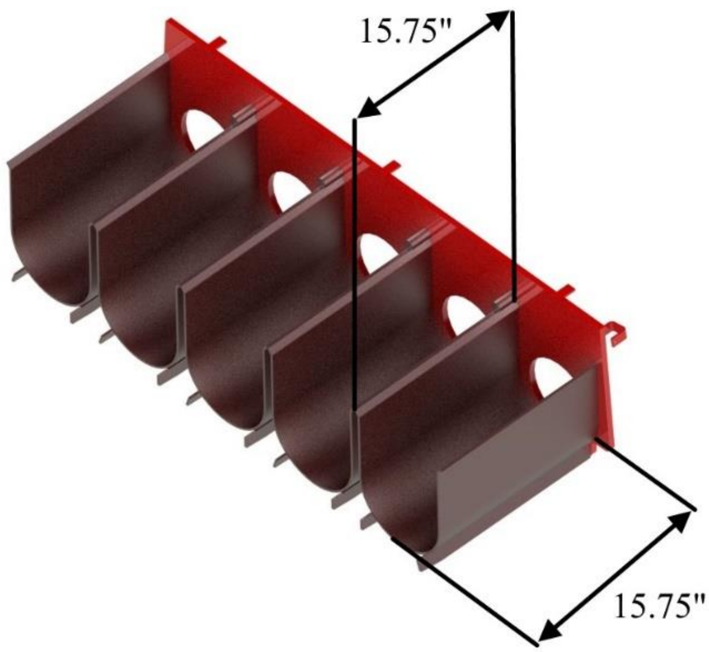

Figure 15. Concept D: Sealed and Elongated Material Shields with dimensions (isometric view)

Concept H features vanes that redirect material toward the regions of concrete starvation in an attempt to produce a uniform concrete slab. Uneven concrete distribution was found at the top of the extruded slab, thus vanes are added on the top of the mandrel. This concept increases the number of parts by two per mandrel, which sums up to a total of ten extra parts. The parts are generally obtained from metal plates, where they can be manufactured in-house. In terms of maintenance and cleaning ease, the extra components are considered as objects in the flow path where potential build-up cleaning or regular part replacement may be needed during maintenance period.

Figure 16. Concept H: Mandrel Vanes (isometric view)

Concept O adds sheet metal vanes to the sidewalls to redirect downward flow on the sidewalls into axial flow toward the outlet. The sidewalls can help to convert the vertical velocity into axial velocity so that the concrete flow is directed towards the starvation points. Similar to the previous Concept H, Concept O also requires six new metal parts to be machined in-house to modify two side walls. As in Concept H, the parts also interfere with the concrete flow, resulting in more regular concrete build-up leading to required maintenance and concrete removal.

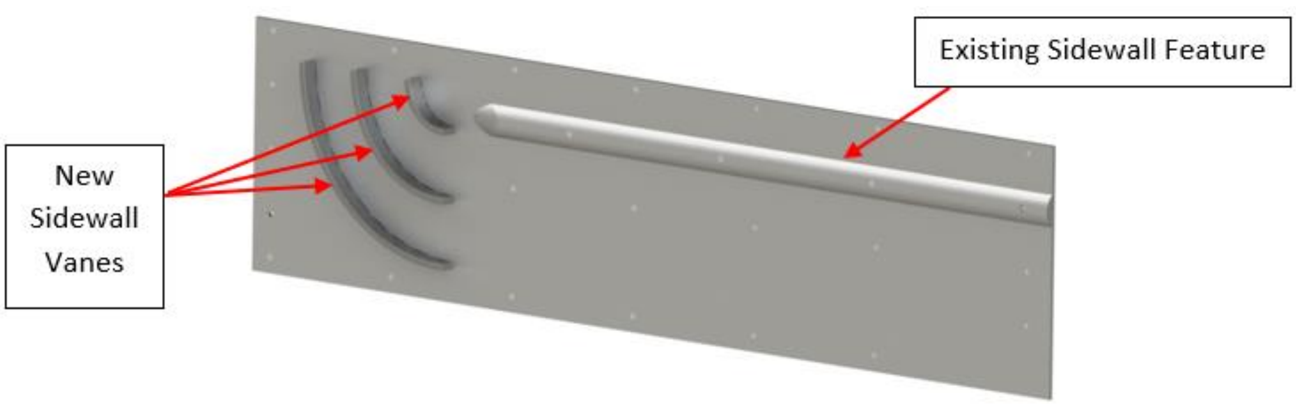

Figure 17. Concept O: Sidewall Vanes (isometric view)

5. CFD Analysis

There are many details and requirements necessary to properly perform CFD analysis. Due to the CFD focus of this project, part of the details of the design are found in the thorough and rigorous CFD setup, methodology, and solving process necessary to fully define the numerical simulation. These details are explained in this section by discussing the procedure and the setup WWC has taken to perform the CFD analysis. Additionally, the methodology in the presentation of the CFD results as well as the interpretation of the results are explained and justified.

5.1. CFD Procedure

All CFD simulations are performed using Siemens STAR-CCM+, with the CFD workflow being split up into the sections of geometry, meshing, setup, solving, and post-processing.

5.1.1. Geometry

The baseline geometry came from production CAD drawings of the NCV extruder, as provided by Ultra-Span. From this CAD, the fluid path of the concrete is modelled starting 130 [*cm*] upwards into the hopper until the plane where the concrete exits the extruder. For each concept simulation to be tested, modifications are made to this baseline geometry. The domain of the fluid flow and the internals of the fluid flow domain are shown in Figure 18. Additionally, the fluid flow domain relative to the overall NCV extruder is shown in Figure 19.

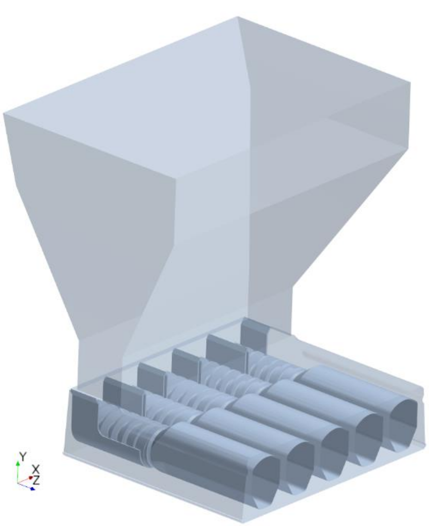

Figure 18. Fluid flow domain (light grey) and internals (darker grey)

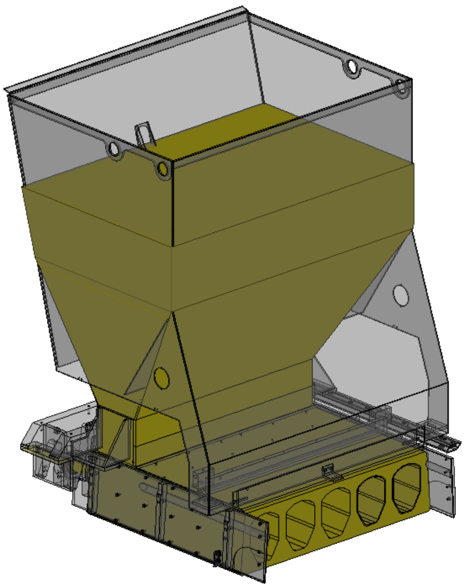

Figure 19. Fluid flow domain (yellow) relative to the NCV extruder

Minor modifications are made to the flow-path in order to facilitate simulation. These modifications include the removal of small air-gaps in the extruder walls and follower tubes, the removal of the 1/16 [*in*] gap between the augers and the material shield, as well as the removal of weld fillets.

In addition, the fluid flow domain is split up into two categories of volumes, the rotating volumes containing the augers, and the non-rotating volume containing the rest of the flow path. These volumes are created by forming a cylinder around each auger and subtracting it from the overall flow path. The cylinder is then combined with the auger to become the rotating volume. The cutout volume for the auger is shown in Figure 20.

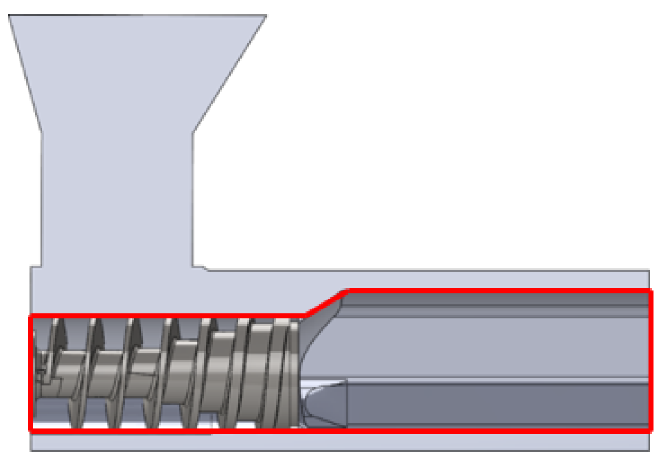

Figure 20. Auger cutout volume highlighted in red

5.1.2. Meshing

Using STAR-CCM+'s automated meshing process, for the purpose of preliminary concept evaluation, the fluid flow domain is meshed into polyhedral cells of arbitrary shape with a global resolution target of 10 [*mm*] as determined by a mesh convergence study in Appendix A. Polyhedral meshes created by STAR-CCM+ have an average of 14 faces per cell and are not aligned with any coordinate system. This method of meshing is used because of the high quality meshes produced, specifically the smooth gradient of cell sizes throughout the domain, as well as the efficient capturing of surface geometry. The various meshes are shown in Figure 21 to Figure 23.

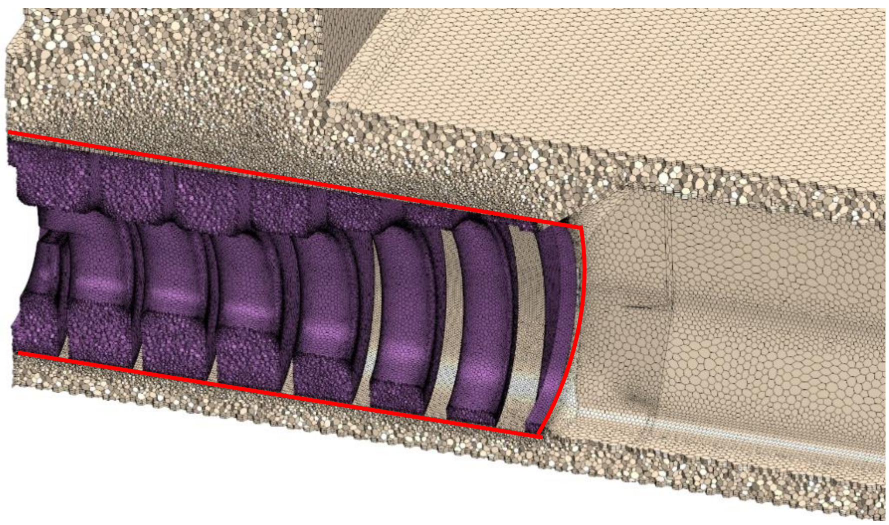

Figure 21. Mesh cross-section with interface between rotating auger and stationary background volumes outlined in red

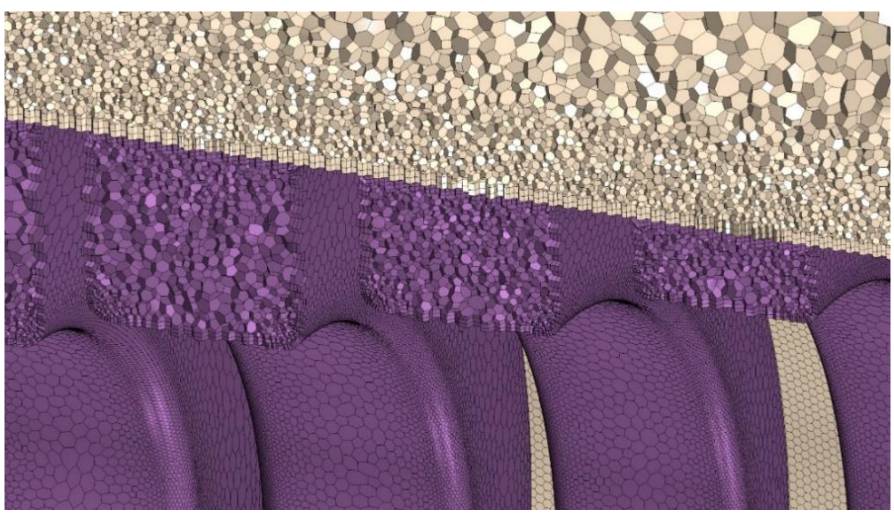

Figure 22. Closeup of auger mesh interface between rotating auger and stationary background volumes

Figure 23. Auger surface mesh closeup

In addition to the global resolution target of 10 [*mm*], a 2 [*mm*] refinement is placed on the cylindrical interface between the rotating auger and stationary background volumes in order to reduce numerical error at this interface.

To provide a set of high-resolution results for comparison between the initial and final designs, a final set of CFD analysis is performed with a 2 [*mm*] mesh comprising of 41.4 million cells. In performing this analysis, a notable difference in results is found compared to the 10 [*mm*] results used for the design process. While this difference is unexpected given the mesh independence study performed, the difference was minor in comparison to the differences between design concepts used to guide the design phase. As such, this mesh dependence is not found to impact the design process detailed in this report and the trends observed in the results are not influenced by the mesh sizes used.

5.1.3. Setup

For the physics setup, due to the extremely low Reynolds number of the flow, a laminar flow model is selected. A steady state approach is taken with the auger rotation being modelled by a rotating reference frame. Body forces due to gravity were applied, as the concrete density of 2000 [kg/m^3] has a significant impact on the flow. The viscosity is modelled using the non-Newtonian Herschel-Bulkley viscosity model as provided within STAR-CCM+. The Herschel-Bulkley viscosity model is selected due to the non-Newtonian nature of fresh concrete. The Herschel-Bulkley viscosity model is shown in Eq. 1. [3].

$$\mu(\dot{\gamma}) = \begin{cases} \mu_0 & , if \ \ \dot{\gamma} < \dfrac{\tau_0}{\mu_0} \\ \dfrac{\tau_0 + k\left(\dot{\gamma} - \dfrac{\tau_0}{\mu_0}\right)^n}{\dot{\gamma}} & , if \ \ \dot{\gamma} \geq \dfrac{\tau_0}{\mu_0} \end{cases} \qquad \text{Eq. 1}$$

Where:

k is the consistency factor

n is the power law exponent

τ_0 is the yield stress threshold

μ_0 is the yielding viscosity

γ is the shear rate

Ultra-Span has provided values to use with this model. The values are:

k = 132 [$Pa{\cdot}s$]

n = 1.7

τ_0 = 385 [Pa]

μ_0 = 2000 [$Pa{\cdot}s$]

For the boundary conditions used with the domain, the fluid flow is driven by a 60 [*in/min*] outflow velocity specified at the extruder outlet as well as a 60 [*in/min*] tangential bed velocity to simulate the extruder moving along its rails. These velocities are prescribed to match the target speed that Ultra-Span aims to achieve with the optimized extruder. Additionally, the top face of the hopper has a stagnation inlet condition applied to it, which allows for flow to be pulled into the domain in order to reach equilibrium.

5.1.4. Solving

The segregated solver within STAR-CCM+ is used for its low computational cost and high stability. The solver is used with a convergence criterion of 1.0×10^{-5} on the RMS of the X, Y, and Z momentum residuals throughout the domain for the design concepts. This criterion resulted in solutions converging in 500-700 iterations.

5.1.5. Post-Processing

For the analysis of the results, Ultra-Span has requested images demonstrating the changes in pressure, viscosity, and velocity throughout the extruder, both in 2D and 3D renders. These plots guide the team at WWC in the optimization of the concepts and in determining the effectiveness of the final design.

Due to the limitations of modern commercial CFD packages, multiple physics effects such as the extruder vibration or the concrete thickening are ignored for the CFD. As a result, it is not known if the final simulation results are accurate on an absolute level. Knowing this, Ultra-Span requested the team take two sets of solution data and subtract the baseline flow field from the concept flow field. This method will show the difference between designs, allowing for positive or negative trends to be compared.

5.2. Presentation of CFD Results

The most important parameters to consider are pressure and viscosity, specifically, reduction in pressure and increase in viscosity at the outlet. These flow properties are desired because a decrease in pressure near the outlet promotes concrete flow towards the outlet, leading to more coverage of the desired slab geometry. Additionally, higher viscosity (more solidity) of the slab before the outlet results in having more material for the upstream concrete to push against, increasing the extrusion speed. The following list shows the four methods that WWC uses to show the pressure and viscosity results:

- Pressure contour plots at various cut planes
- Kinematic viscosity contour plots at various cut planes
- Pressure volume renderings
- Kinematic viscosity volume renderings

The location of the various cut planes Ultra-Span considers are shown in Figure 24 to Figure 26. Plane F4 is used within the body of the report because it represents the outlet of the extruder cassette and dictates the final slab geometry. All planes are shown in this section and their purpose explained in order to show the detail and work the team at WWC has done to arrive at the results presented within this report. Plots showing planes other than Plane F4 are shown in Appendix C where detailed final CFD results are located.

The cut planes are labeled according to the direction that the viewer is looking at the results. F-planes are planes that are viewed from the front of the extruder, T-planes are viewed from the top of the extruder, and S-planes are when viewing from the side of the extruder.

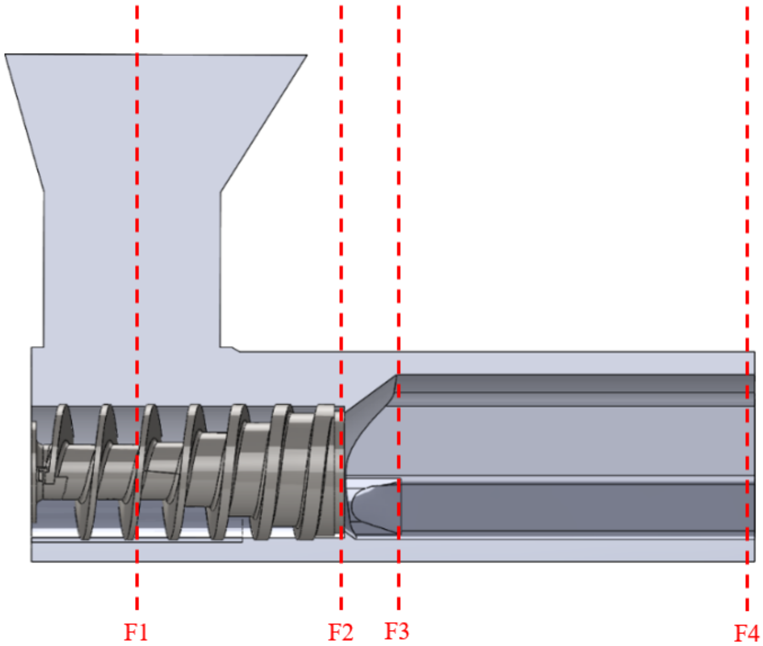

Figure 24. Side view of the extruder (front view cut planes)

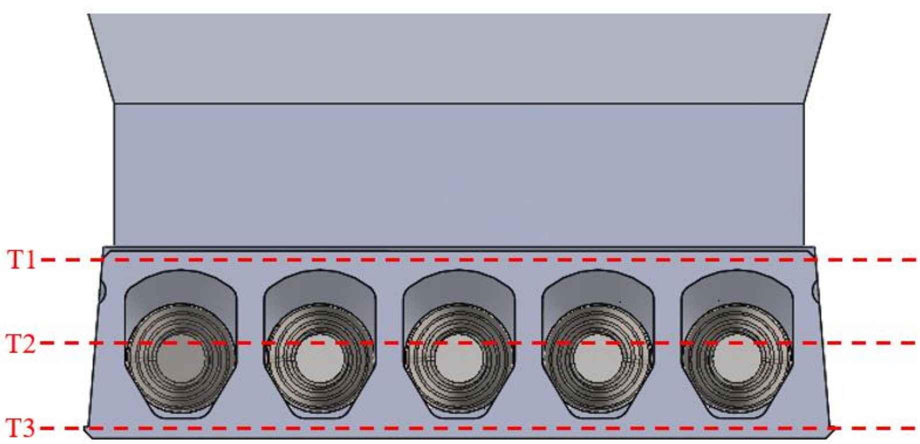

Figure 25. Front view of the extruder cassette (top view cut planes)

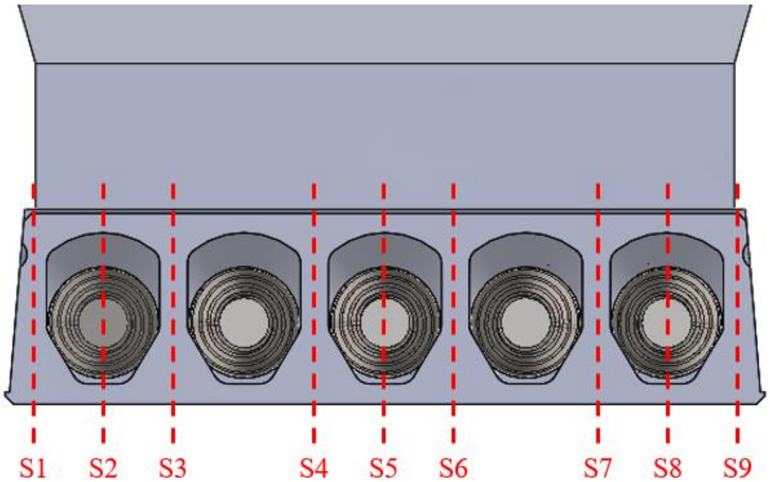

Figure 26. Front view of the extruder cassette (side view cut planes)

A detailed explanation of the cut planes used for analysis of the CFD results is as follows:

Front Plane

- The purpose of F1 is to show the impact of the design on the inlet concrete flow and interaction of the concrete with the augers.
- F2 and F3 are selected because they represent the start and end of the mandrel shape change and are locations where the most concrete blockage is observed.
- F4 is placed near the outlet because it provides an understanding of the quality and geometry of the final concrete slabs produced.

Top Plane

- The purpose of T1, T2 and T3 are to show the amount of solidity penetration into the extruder. In other words, the top planes allow for easy visualization of the viscosity variation form the inlet to the outlet, capturing the effects of the auger, mandrel, and follower tubes.

Side Plane

- The purpose of S1, S3, S4, S6, S7, and S9 is to show the variation in concrete properties from top to bottom of the slab, in between and around the auger, mandrel, and follower tube assemblies.

- Conversely, S2, S5, and S8 cut through the auger, mandrel, and follower tube assemblies, thus showing the properties of the concrete above and below the auger, mandrel and follower tube assembly.

Although flow lines show where concrete is moving within the extruder, they do not provide any meaningful data into the improvement of the concrete slabs produced. Therefore, other than for qualitative understanding of the flow field, flow lines are not considered as a result needed for comparison. Moreover, the flow line results are evaluated with caution because the CFD analysis is for a simplified flow domain that does not consider the vibration of the mandrels which may change the flow velocity magnitude and direction. The CFD setup also specifies an outlet velocity and therefore the velocity at the outlet will always be the same for each case.

Finally, all quantitative results are based on trends. The success or failure of a design is based on the relative percent difference between the modified design and the base case. Absolute values are not considered because the values resulting from CFD analysis are for the simplified analysis domain and do not accurately represent the real situation.

6. Concept Evaluation

The four advancing concepts were not evaluated in the CDR because at that time the CFD analysis and design features were not fully defined. Using the methodology developed by the team at WWC from Section 4, the CFD analysis on the four advancing designs is now shown.

To quantitatively analyze the concepts, each of the advancing concepts (Concept B, Concept D, Concept H, and Concept O), are compared to the base case (current NCV design). Using the CFD results, the parameters evaluated are outlet pressure, outlet viscosity and overall flow uniformity. Results are shown as contour plots, iso-surfaces, or relative percent differences. The other design parameters (compatibility for manufacture, minimal number of parts, and maintenance/cleaning ease) were considered in the CDR and summarized in Section 4 because they were purely qualitative assessments and did not rely on the comprehensive CFD.

6.1. Outlet Viscosity Performance

Contour plots of the kinematic viscosity at the outlet of the extruder (plane F4) are shown in Figure 28 to Figure 32. The viscosity penetration into the extruder cassette is illustrated by 3D volume renderings in Figure 33 to Figure 37. Additionally, average outlet viscosity and the percent deviation from the reference concept is indicated to provide a quantitative assessment of the results. The quantitative results are tabulated in Table V.

The ideal viscosity contour plot is uniform and all red. The ideal viscosity contour plot is shown in Figure 27.

Figure 27. Ideal viscosity contour plot

Following the presentation of the results, discussion is provided to explain what the results indicate. Based on the viscosity performance of each concept, the concepts are ranked, and a brief justification is provided.

Current Design

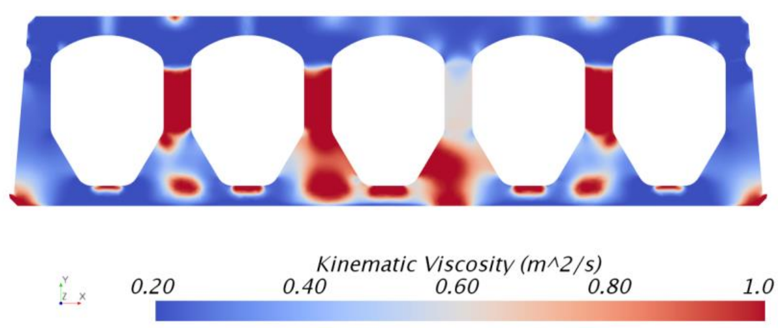

Figure 32. Viscosity distribution at plane F4 for Concept A: Reference Concept (Current Design)

Concepts

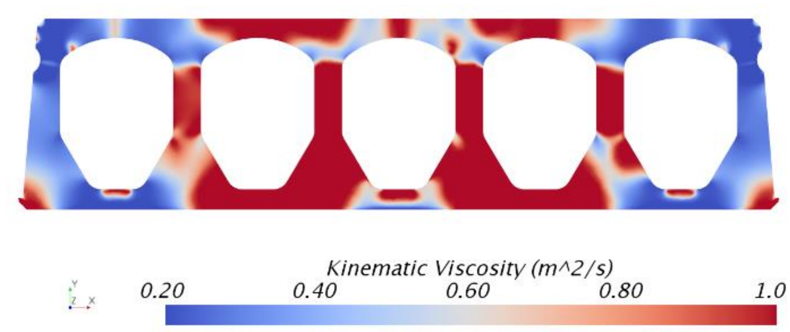

Figure 28. Viscosity distribution at plane F4 for Concept B: Alternating Auger Rotation

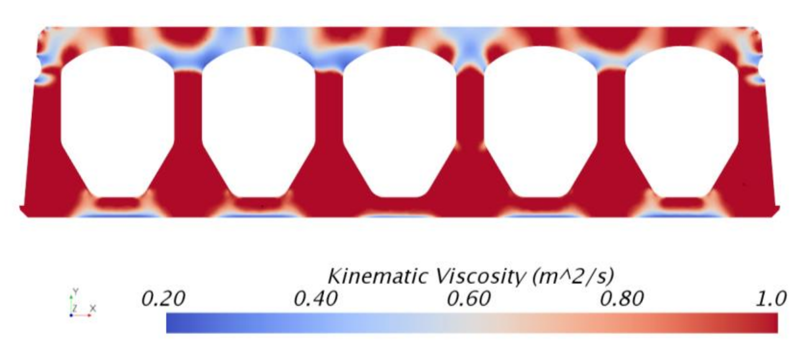

Figure 29. Viscosity distribution at plane F4 for Concept D: Sealed and Elongated Material Shields

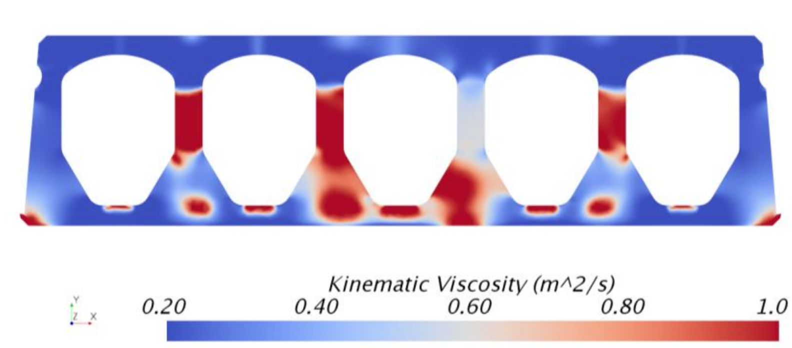

Figure 30. Viscosity distribution at plane F4 for Concept H: Mandrel Vanes

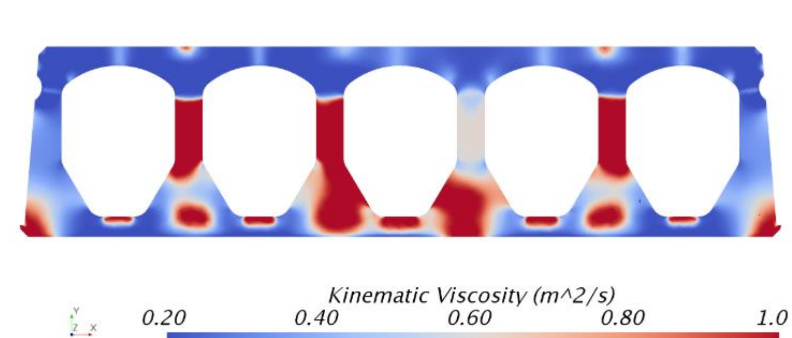

Figure 31. Viscosity distribution at plane F4 for Concept O: Sidewall Vanes

Current Design

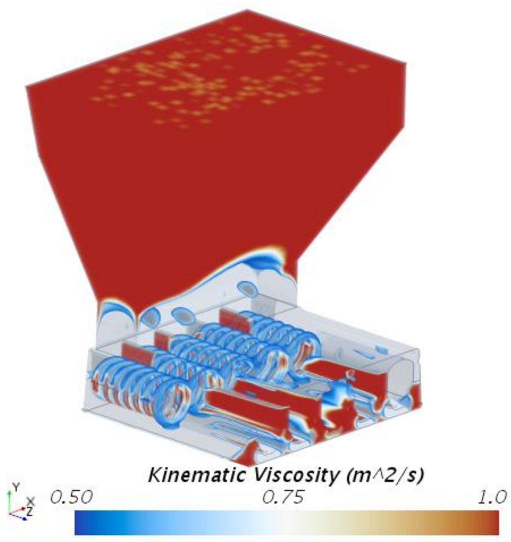

Figure 37. Viscosity volume rendering for Concept A: Reference Concept (Current Design)

Concepts

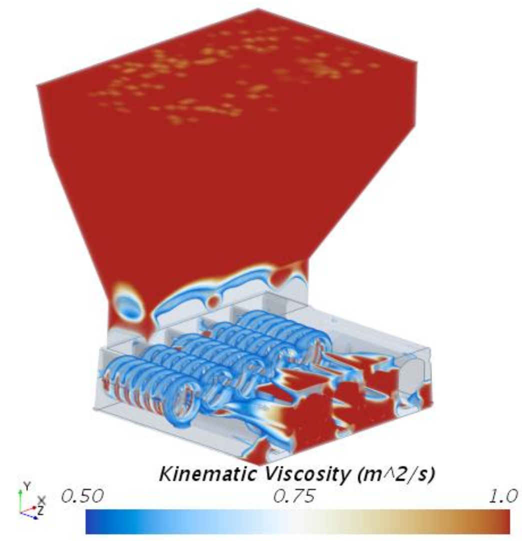

Figure 33. Viscosity volume rendering for Concept B: Alternating Auger Rotation

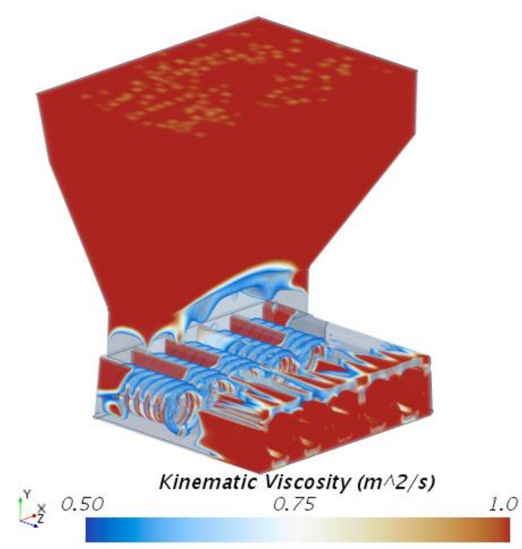

Figure 35. Viscosity volume rendering for Concept D: Sealed and Elongated Material Shields

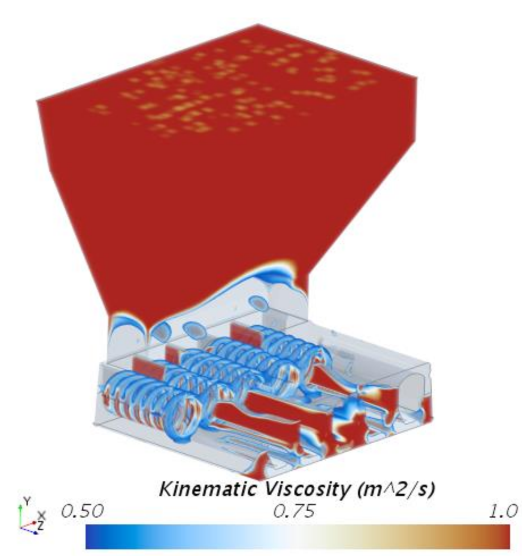

Figure 34. Viscosity volume rendering for Concept H: Mandrel Vanes

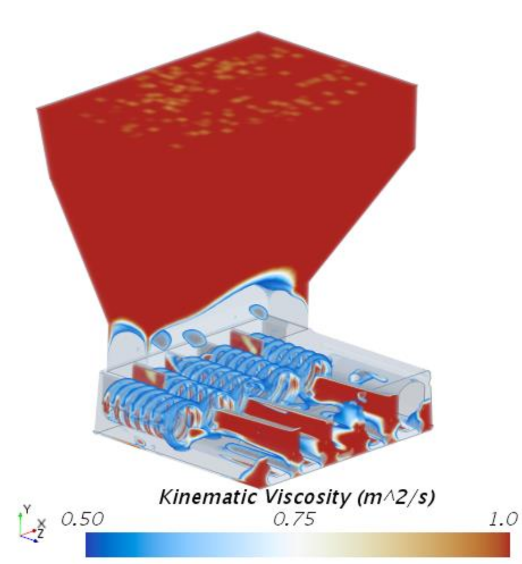

Figure 36. Viscosity volume rendering for Concept O: Sidewall Vanes

TABLE V. VISCOSITY COMPARISON

Concept	Average Outlet Viscosity [m^2/s]	Deviation from Reference Concept
Reference Concept: Current Design	0.53758	-
Concept B: Alternating Auger Rotation	0.67191	24.99%
Concept D: Sealed and Elongated Material Shields	0.76720	42.71%
Concept H: Mandrel Vanes	0.52587	-2.18%
Concept O: Sidewall Vanes	0.56675	5.43%

For both the contour plots and the volume renderings, the color configuration used within this report has been selected to match the colors used in Ultra-Span's existing CFD analysis results. The color blue indicates low viscosity and red indicates high viscosity.

Previous CFD analysis at Ultra-Span has indicated a correlation between higher viscosity and improved field results when testing the actual NCV extruder. Therefore, a higher viscosity is desired at the outlet, with high viscosity penetrating as far upstream as possible. High viscosity is desired at the outlet due to the nature of the Herschel-Bulkley model. According to the Herschel-Bulkley model, if the flow exiting the extruder is uniform then there will be low shear rates at the outlet and thus high viscosity at the outlet. For this reason, viscosity is used as a representation of flow evenness near the extruder outlet showing that the concrete flow will be in the shape of the desired slab geometry.

Concept D: Sealed and Elongated Material Shields performs best when comparing the average viscosity and evenness of viscosity distribution. This is seen in Figure 29 where the viscosity contour plot has the most red and in Table V where an increase in outlet viscosity of 42.71% is shown. Furthermore, the volume rendering in Figure 35 shows high viscosity penetrating down the center and along the sides of the extruder cassette. Concept B: Alternating Auger Rotations also performed well, increasing the average outlet viscosity by 24.99%, however, the viscosity near the wall remained low as seen in Figure 28 and Figure 33. Concept H: Mandrel Vanes and Concept O: Sidewall Vanes performed the worst, with no improvement relative to the current design in evenness of viscosity, and in the case of Concept O: Mandrel Vanes even decreased the average viscosity at the outlet by 2.18%.

6.2. Outlet Pressure Performance

Contour plots of the pressure at the outlet of the extruder (plane F4) are shown in Figure 39 to Figure 43. Additionally, average outlet pressure and the percent deviation from the reference concept is indicated to provide a quantitative assessment of the results. The quantitative results are tabulated in Table VI.

Following the presentation of the results, discussion is provided to explain what the results indicate. Based on the pressure performance of each concept, the concepts are ranked, and a brief justification is provided.

The ideal pressure contour plot is uniform and all light blue. The ideal pressure contour plot is shown in Figure 38.

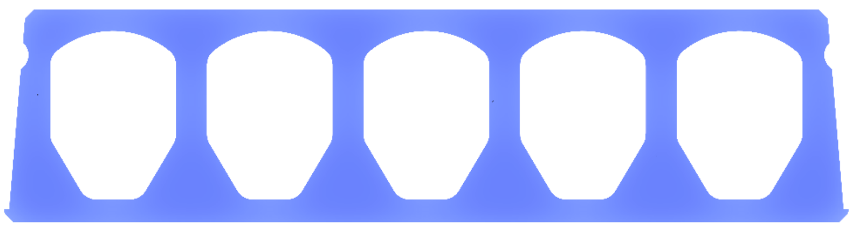

Figure 38. Ideal pressure contour plot

Reference

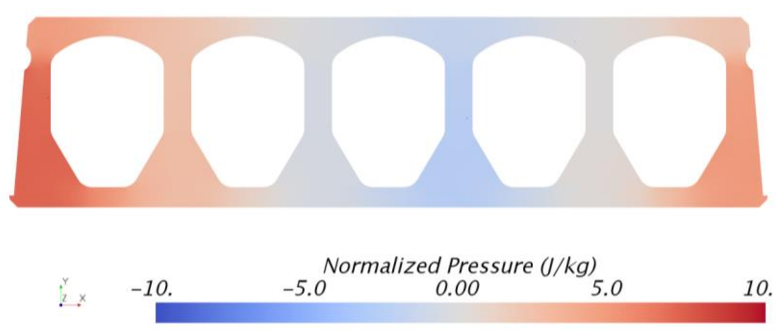

Figure 43. Pressure distribution at plane F4 for Concept A: Reference Concept (Current Design)

Concepts

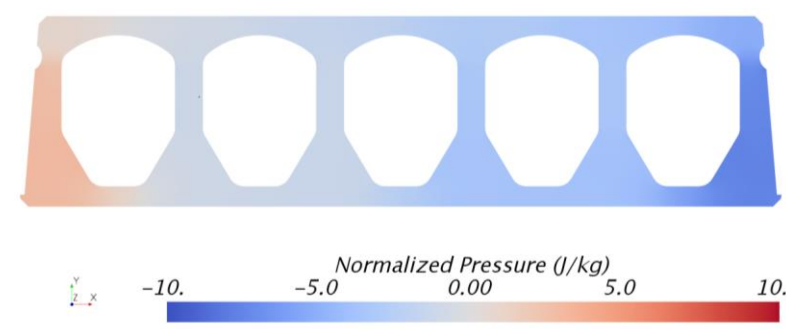

Figure 39. Pressure distribution at plane F4 for Concept B: Alternating Auger Rotation

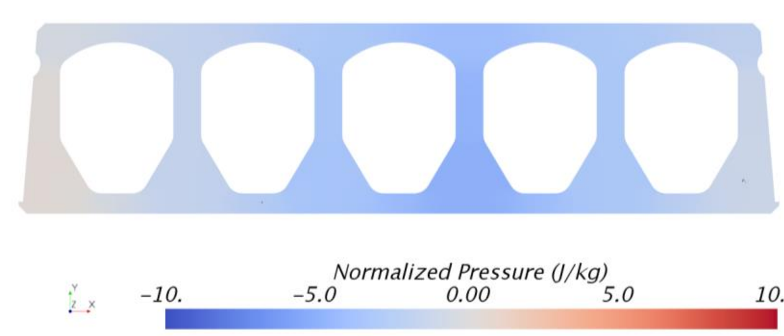

Figure 40. Pressure distribution at plane F4 for Concept D: Sealed and Elongated Material Shields

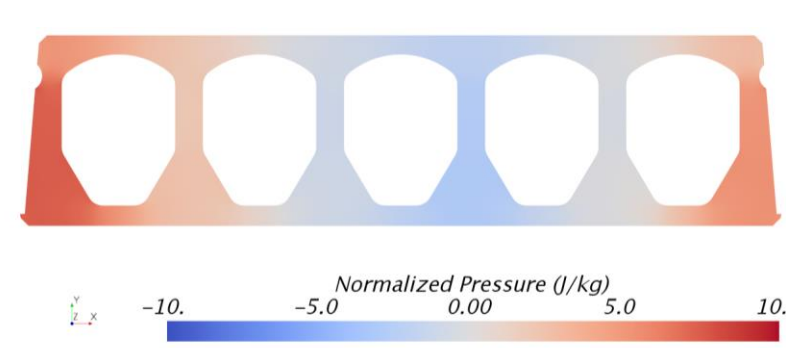

Figure 41. Pressure distribution at plane F4 for Concept H: Mandrel Vanes

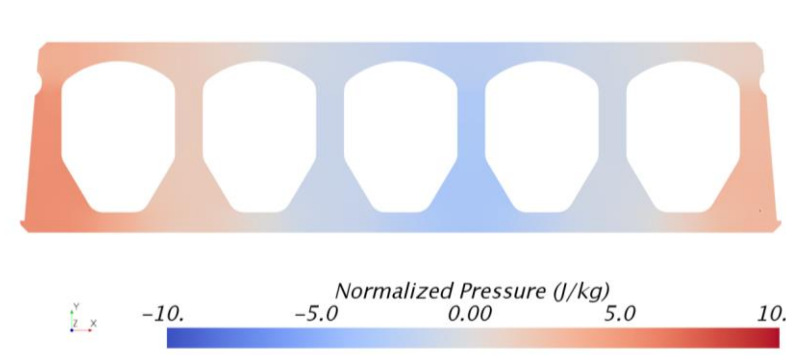

Figure 42. Pressure distribution at plane F4 for Concept O: Sidewall Vanes

TABLE VI. OUTLET PRESSURE COMPARISION

Concept	Average Outlet Pressure [*Pa*]	Percent Deviation from Reference Concept
Reference Concept (Current Design)	31167	-
Concept B: Alternating Auger Rotation	23818	-23.58%
Concept D: Sealed and Elongated Material Shields	23365	-24.98%
Concept H: Mandrel Vanes	30783	-1.23%
Concept O: Sidewall Vanes	29147	-6.48%

A concept that has good pressure performance is one that has a low and even pressure distribution. Similar to viscosity, for the pressure contours blue indicates low pressure and red indicates high pressure. The pressure contour plots show normalized pressure by taking the gauge pressure within the extruder, removing the pressure gradient due to gravity, and dividing by the density of the fluid. The results are presented with normalized pressure for Ultra-Span to compare WWC's results with their current data.

The results show that Concept D: Sealed and Elongated Material Shields performed the best with excellent low pressure distribution as seen in Figure 40 and a 24.98% reduction in pressure at the outlet from the current design. Concept B: Alternating Auger Rotation resulted in an excellent 23.58% reduction in outlet pressure, however Figure 39 shows that the pressure distribution is not uniform across the outlet. Concept O: Sidewall Vanes did not improve or worsen the pressure performance with a pressure distribution similar to the current design. Concept H: Mandrel Vanes performed the worst, with no improvement in pressure uniformity and did not decrease average pressure relative to the reference.

6.3. Flow Uniformity Performance

Streamline plots of the velocity along the top of the extruder cassette are shown in Figure 45 to Figure 48. No average outlet velocity or relative change in velocity has been provided because the CFD setup specifies an outlet velocity; the velocity at the outlet will always be the same for each case.

Reference

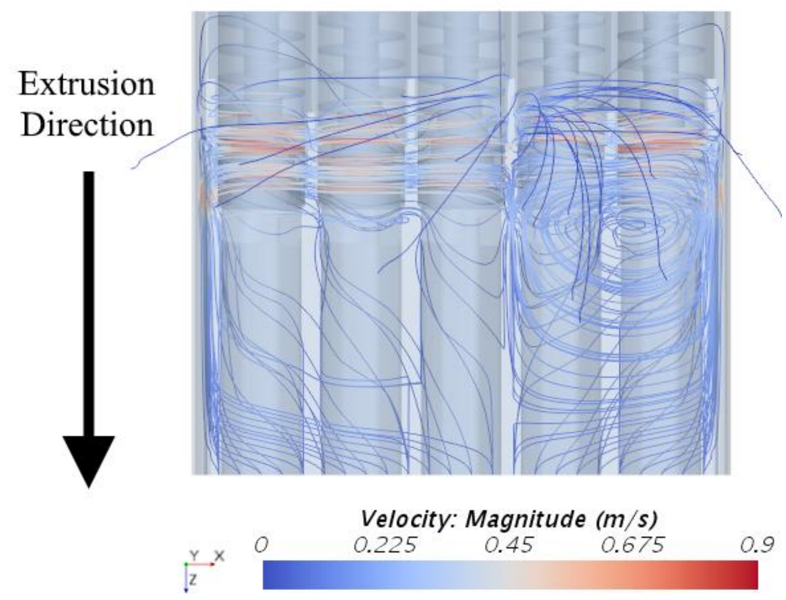

Figure 48. Velocity streamline for Concept A: Reference Concept (Current Design)

Concepts

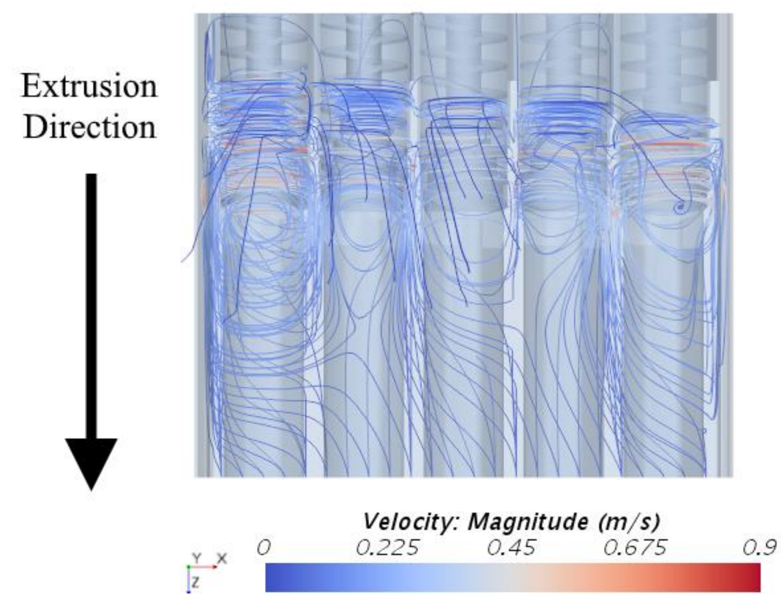

Figure 45. Velocity streamline for Concept B: Alternating Auger Rotation

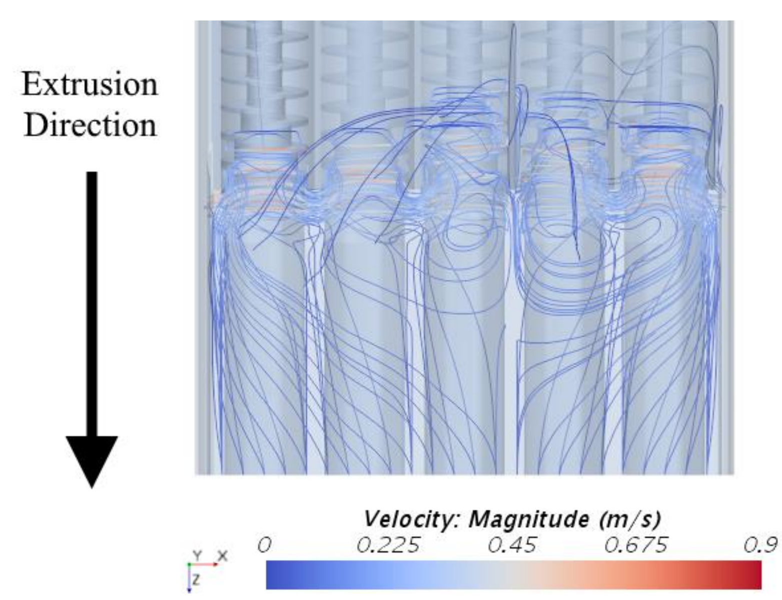

Figure 44. Velocity streamline for Concept D: Sealed and Elongated Material Shields

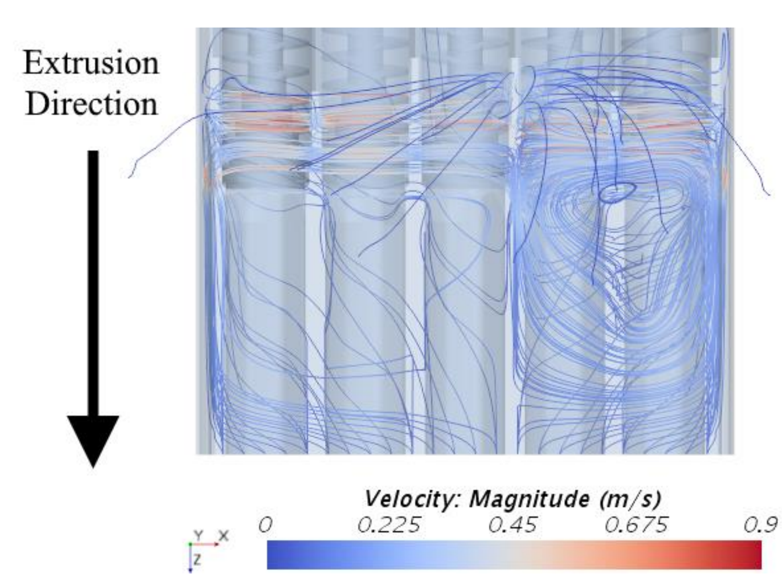

Figure 46. Velocity streamline for Concept H: Mandrel Vanes

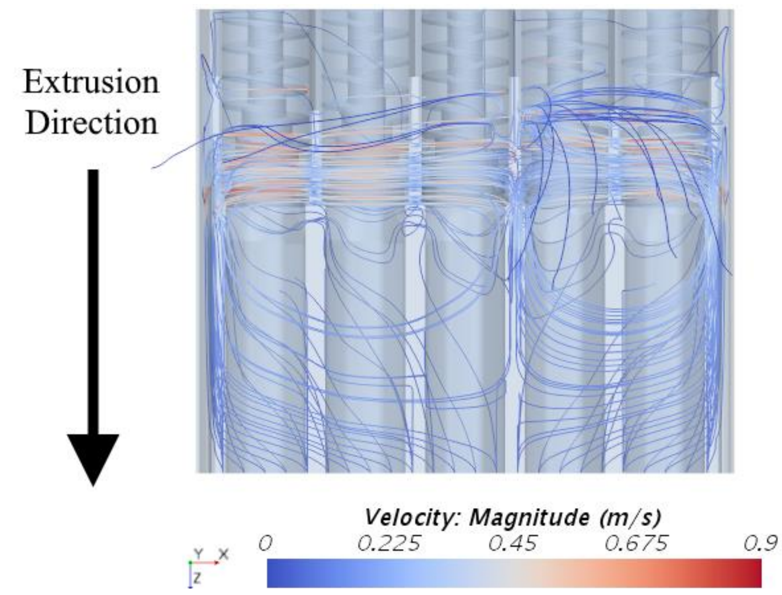

Figure 47. Velocity streamline for Concept O: Sidewall Vanes

A desirable flow pattern is one in which flow is uniform throughout the extruder cassette and is directed downstream towards the outlet. The use of the velocity streamline contour plots are to gain a better understanding of the flow throughout the extruder and to see where concrete wants to flow.

For the reference concept, the results show that a large amount of flow exiting the extruder comes from the sides of the extruder. Additionally, a recirculation zone is seen on the right side of the extruder cassette. These same flow structures are also observed in both the Mandrel and Sidewall Vanes concepts and are not a desirable flow pattern.

Consequently, Concept B: Alternating Auger Rotation is best in terms of flow uniformity, followed by Concept D: Sealed and Elongated Material Shields. Both Concept H: Mandrel Vanes and Concept O: Sidewall Vanes showed no improvement from the current design.

7. Concept Selection

A rigorous concept selection process is followed to select the final concept for detailed design and optimization. A criteria weighting matrix (CWM) is used to determine the appropriate weight for each criterion. A weighted decision matrix (WDM) is then used to compare and assign the winning concept.

7.1. Criteria Weighting Matrix

Based on the needs of the client, several criteria have been developed and are as follows:

Compatibility for manufacture: This criterion measures the feasibility and ease for the modifications to be manufactured. A component that can be reworked or manufactured in-house is generally more time efficient and easier to implement at Ultra-Span.

Minimal number of parts: This criterion measures the number of parts required for the new design. An extruder design that has more parts leads to more maintenance for the user of the extruder and is not desired by Ultra-Span's clients. To maintain a competitive edge in the industry fewer parts is favored by Ultra-Span.

Pressure performance: This criterion measures the overall improvement in concrete flow pressure at the extruder outlet. It is necessary for the final design to have a more even pressure distribution and a lower pressure at the outlet to promote more concrete flow downstream.

Viscosity performance: Similar to the pressure criterion, concrete viscosity is also an important feature of the final design, where high viscosity is favored. Evenly distributed high viscosity at the outlet represents a uniform and stable concrete slab leading to higher quality extrusions.

Flow uniformity: This criterion measures the concrete flow direction within the extruder cassette. A design that moves concrete uniformly throughout the extruder cassette and is directed downstream towards the outlet is desired.

Maintenance/cleaning ease: This criterion measures the amount of labour necessary to maintain the extruder during normal operation. Designs containing complex geometry that could lead to hardened concrete build-up are more difficult to clean and increase maintenance costs. The simpler the design the better it performs for this criterion.

The CWM shown in Table VII assigns the weights for each criterion by first comparing each criterion to one another and giving a “hit” to the criterion deemed more important. The total number of hits for each criterion are then divided by the total number of available hits. This fraction is then converted into a percentage, yielding the weight to be used in the WDM.

TABLE VII. CRITERIA WEIGHTING MATRIX

CRITERIA		Compatibility for manufacture	Minimal number of parts	Pressure performance	Viscosity performance	Flow uniformity	Maintenance/ cleaning ease
		A	B	C	D	E	F
Compatibility for manufacture	A	A	A	C	D	E	A
Minimal number of parts	B		B	C	D	E	B
Pressure performance	C			C	C	C	C
Viscosity performance	D				D	D	D
Flow uniformity	E					E	E
Maintenance/ cleaning ease	F						F
Total hits		3	2	6	5	4	1
Weighting		14.29%	9.52%	28.57%	23.81%	19.05%	4.76%

7.2. Weighted Decision Matrix

In the WDM, a rating ranging from 1 (poor) to 10 (excellent) is assigned to each concept based on its performance for each metric. A concept that performs equally as well as the reference design scores a 5 (no change). Considering each concept's performance for the given design criteria, each concept is rated accordingly. The rating is then multiplied by the weight assigned by the CWM to determine the score for that particular metric. Summing all of the weighted scores, a final design is selected as the design with the largest total score. Concepts B: Alternating Auger Rotation and D: Sealed and Elongated Material shield are the two highest performing concepts. A completed WDM for the four advancing concepts is shown in Table VIII.

TABLE VIII. WEIGHTED DECISION MATRIX

		CONCEPTS							
		B: Alternating Auger Rotation		D: Sealed and Elongated Material Shields		H: Mandrel Vanes		O: Sidewall Vanes	
SELECTION CRITERIA	Weight	Rating	Weighted Score	Rating	Weighted Score	Rating	Weighted Score	Rating	Weighted Score
Compatibility for manufacture	14.29%	10	1.429	8	1.143	6	0.857	6	0.857
Minimal number of parts	9.52%	5	0.476	5	0.476	4	0.381	2	0.190
Pressure performance	28.57%	7	2.000	9	2.571	5	1.429	6	1.714
Viscosity performance	23.81%	7	1.667	9	2.143	4	0.952	5	1.190
Flow uniformity	19.05%	8	1.524	7	1.333	5	0.952	4	0.762
Maintenance/cleaning ease	4.76%	5	0.238	8	0.381	4	0.190	4	0.190
Total Score		7.334		8.047		4.761		4.903	
Rank		2		1		4		3	
Final Selected Concept		**Yes**		**Yes**		No		No	

8. Final Design Optimization

Concept B: Alternating Auger Rotation and Concept D: Sealed and Elongated Material Shields are the two highest performing concepts with their final scores differing by less than one point. Both designs have therefore been selected to proceed to the final design optimization phase. Multiple combinations of auger rotation directions are then analyzed for the final design optimization and the best auger rotation is combined with the elongated material shield. This combination of the auger rotation and elongated material shield will be selected as the final design, provided it improves the extruder performance. If the combined concept is not an improvement, the elongated material shield is selected as the final design since the WDM demonstrated that it is superior to the other three concepts.

Three auger configurations B2, B3 and B4 are shown in Figure 49. For reference, B1 is the auger rotation configuration that was analyzed in Section 5 Concept Evaluation. The analysis of the additional configurations follows the same CFD methodology described in Section 4. Results are also presented similarly to the concept evaluation in Section 5.

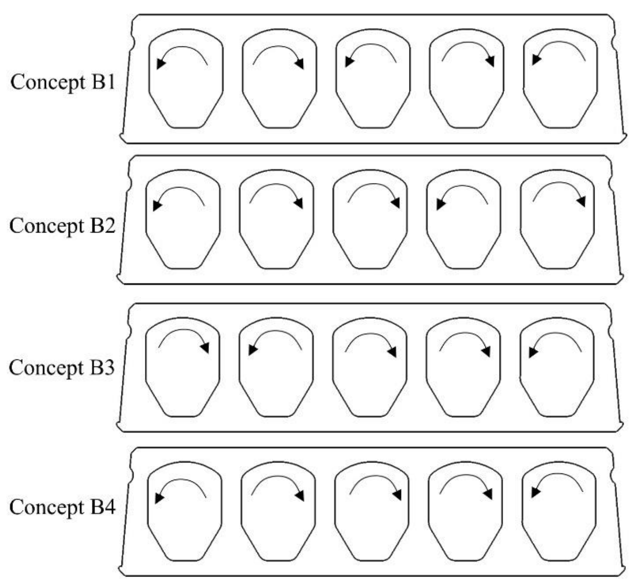

Figure 49. Additional auger configurations

8.1. Auger Rotation Viscosity Comparison

Contour plots of the pressure at the outlet of the extruder (plane F4) are shown in Figure 50 to Figure 53 and volume renderings are shown in Figure 54 to Figure 57. The average outlet pressure and the percent deviation from the reference concept are tabulated in Table IX.

Reference Configuration

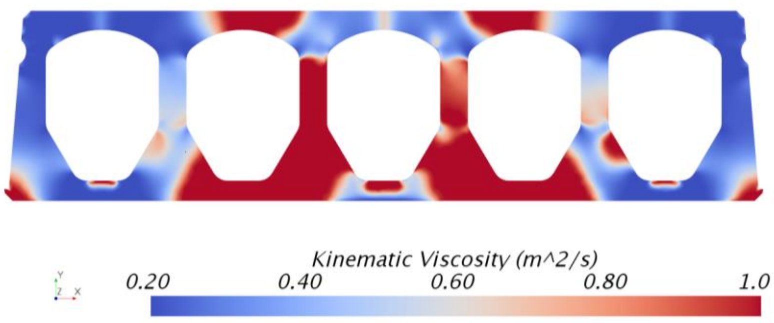

Figure 53. Viscosity distribution at plane F4 for Auger Configuration B1

Additional Configurations

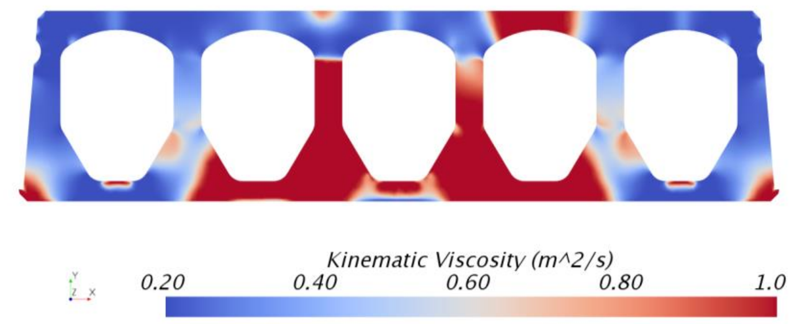

Figure 50. Viscosity distribution at plane F4 for Auger Configuration B2

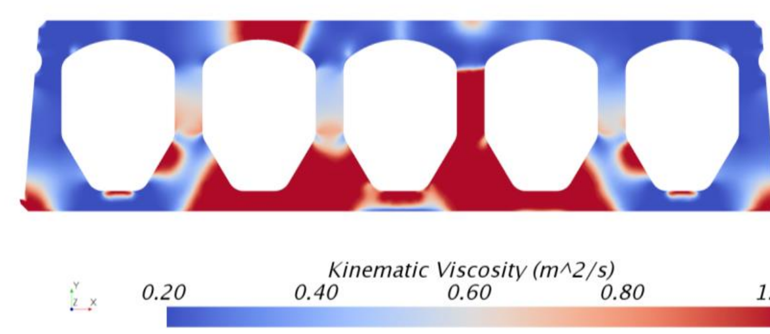

Figure 51. Viscosity distribution at plane F4 for Auger Configuration B3

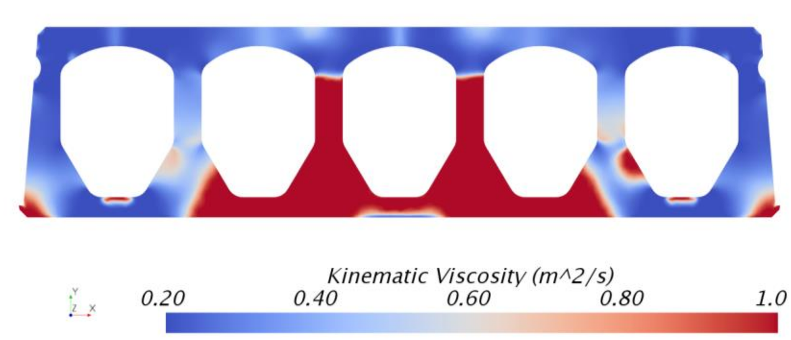

Figure 52. Viscosity distribution at plane F4 for Auger Configuration B4

Reference Configuration

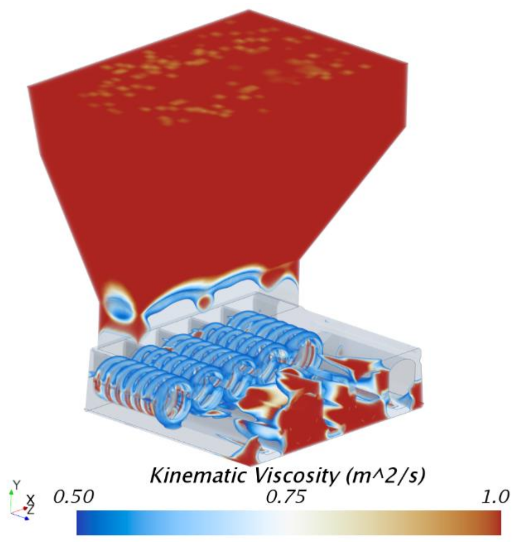

Figure 57. Viscosity volume rendering for Auger Configuration B1

Additional Configuration

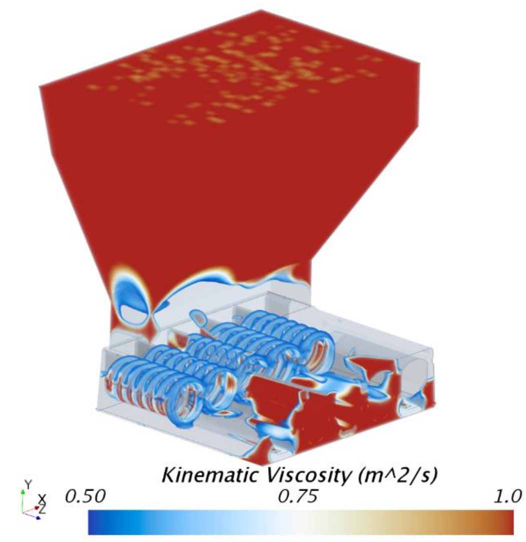

Figure 54. Viscosity volume rendering Auger Configuration B2

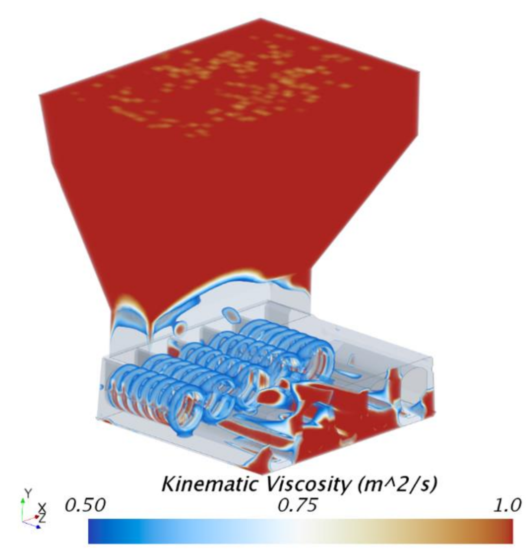

Figure 55. Viscosity volume rendering for Auger Configuration B3

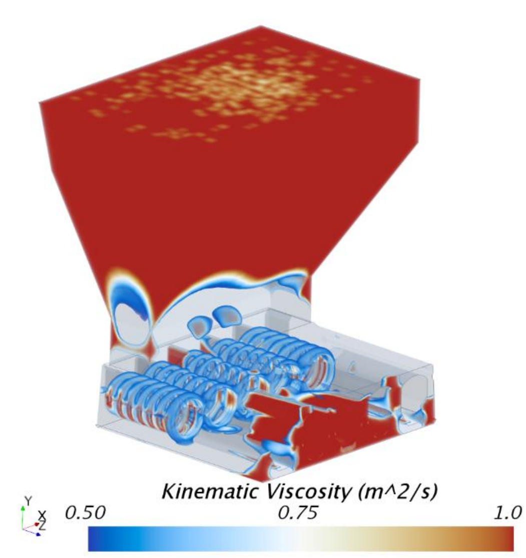

Figure 56. Viscosity volume rendering for Auger Configuration B4

TABLE IX. OUTLET VISCOSITY COMPARISION OF DIFFERENT AUGER CONFIGURATIONS

Auger Rotation Configuration	**Average Outlet Pressure [*Pa*]**	**Percent Deviation from Reference Concept**
Configuration B1 (reference)	0.66923	-
Configuration B2	0.67722	1.19%
Configuration B3	0.66345	-0.86%
Configuration B4	0.66314	-0.91%

The results show no notable changes in viscosity magnitude or distribution when comparing the average viscosity and evenness of the viscosity distribution. Furthermore, referring to quantitative values in Table IX, the deviations are generally within ±2% which is negligible since no clear trend can be identified. No configuration performed better or worse than the other in terms of viscosity performance.

8.2. Auger Rotation Pressure Comparison

Contour plots of the pressure at the outlet of the extruder (plane F4) are shown in Figure 58 to Figure 61. The average outlet pressure and the percent deviation from the reference configuration are tabulated in Table X.

Reference Configuration

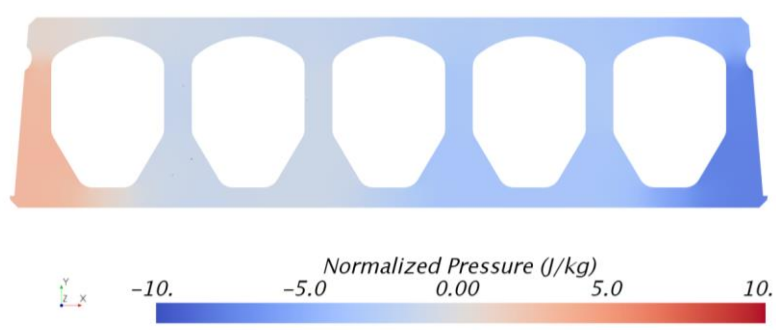

Figure 61. Pressure distribution at plane F4 for Auger Configuration B1

Additional Configurations

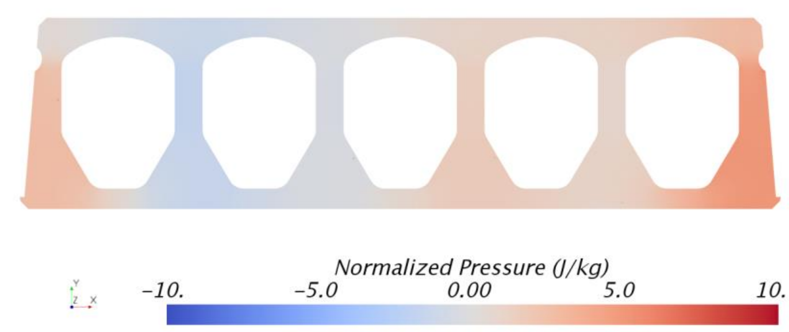

Figure 58. Pressure distribution at plane F4 for Auger Configuration B2

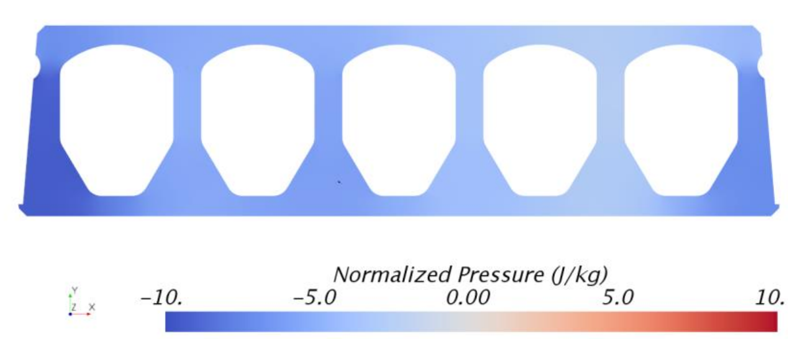

Figure 59. Pressure distribution at plane F4 for Auger Configuration B3

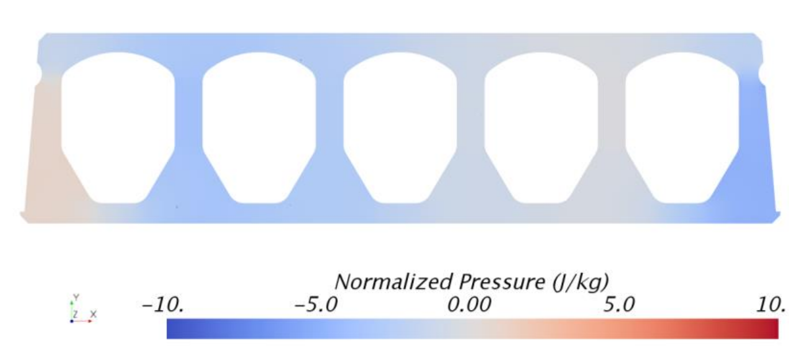

Figure 60. Pressure distribution at plane F4 for Auger Configuration B4

TABLE X. OUTLET PRESSURE COMPARISION OF DIFFERENT AUGER CONFIGURATIONS

Auger Rotation Configuration	**Average Outlet Pressure [*Pa*]**	**Percent Deviation from Reference Concept**
Configuration B1 (reference)	23,907	-
Configuration B2	30,310	26.78%
Configuration B3	18,069	-24.42%
Configuration B4	24,534	2.62%

Configuration B3 performs best when comparing the average pressure and evenness of pressure distribution. Configuration B4 has no difference from the reference and Configuration B2 performs the worst of all the configurations.

8.3. Auger Rotation Velocity Streamline Comparison

Streamline plots of the velocity along the top of the extruder cassette are shown in Figure 62 to Figure 65. The velocity at the outlet will always be the same for each configuration because the CFD setup specifies an outlet velocity. Therefore, no average outlet velocity or change in absolute velocity values have been provided. For clarity some simple arrows are overlaid on the plot indicating the general flow direction.

Reference Configuration

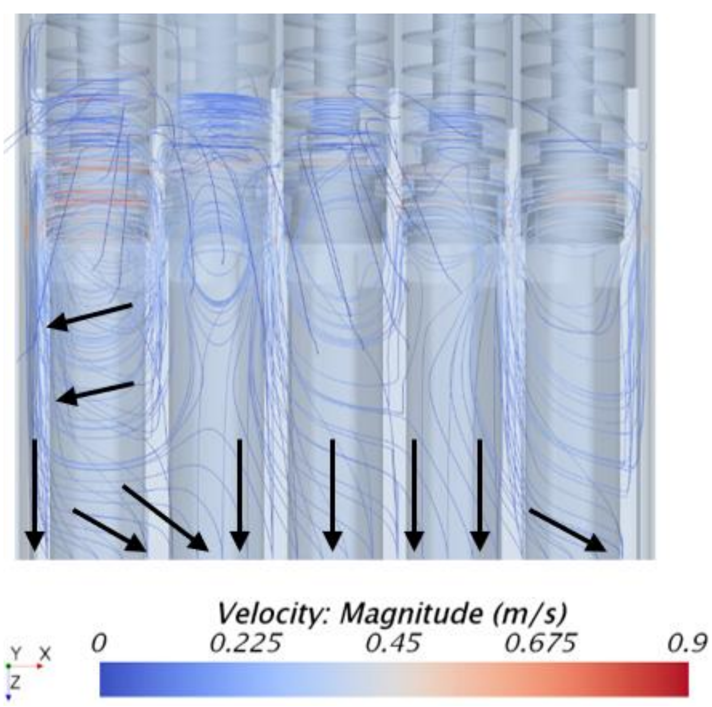

Figure 65. Velocity streamlines for Auger Configuration B1

Additional Configuration

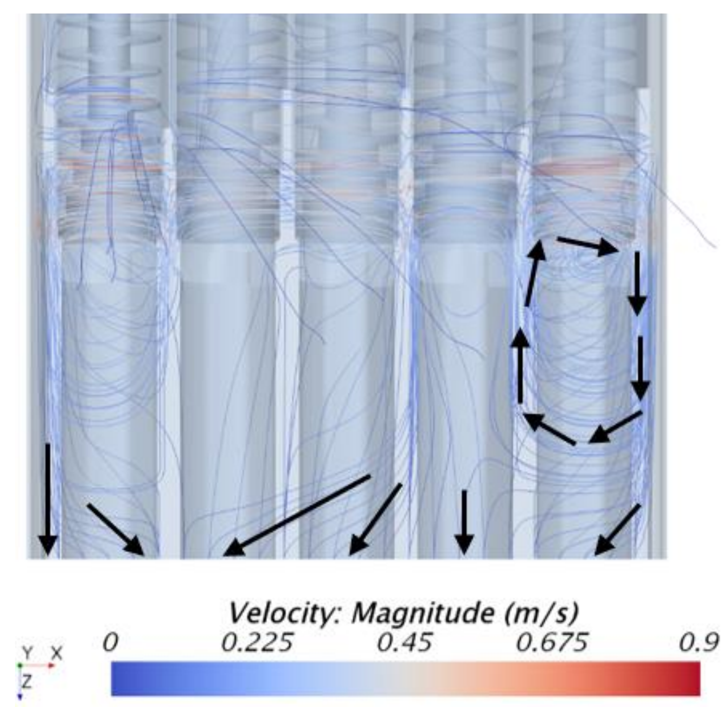

Figure 62. Velocity streamlines for Auger Configuration B2

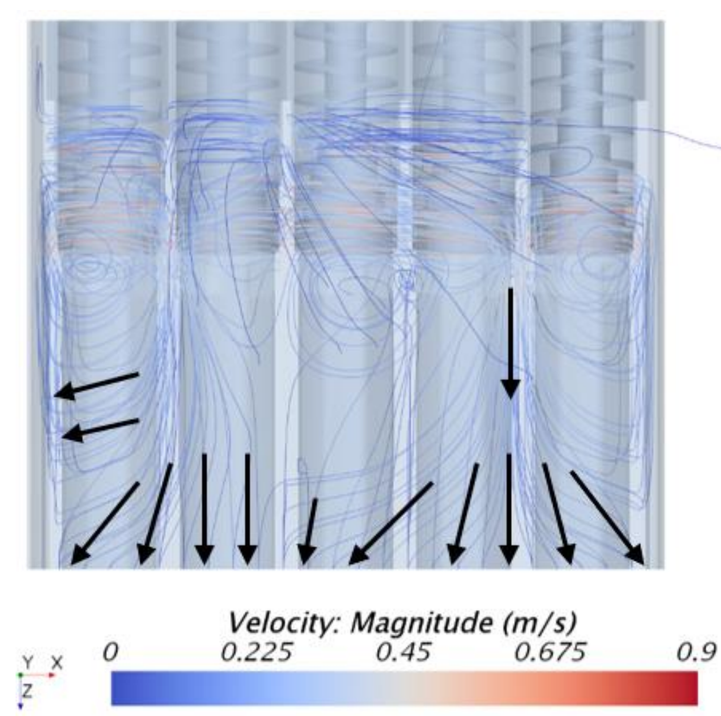

Figure 63. Velocity streamlines for Auger Configuration B3

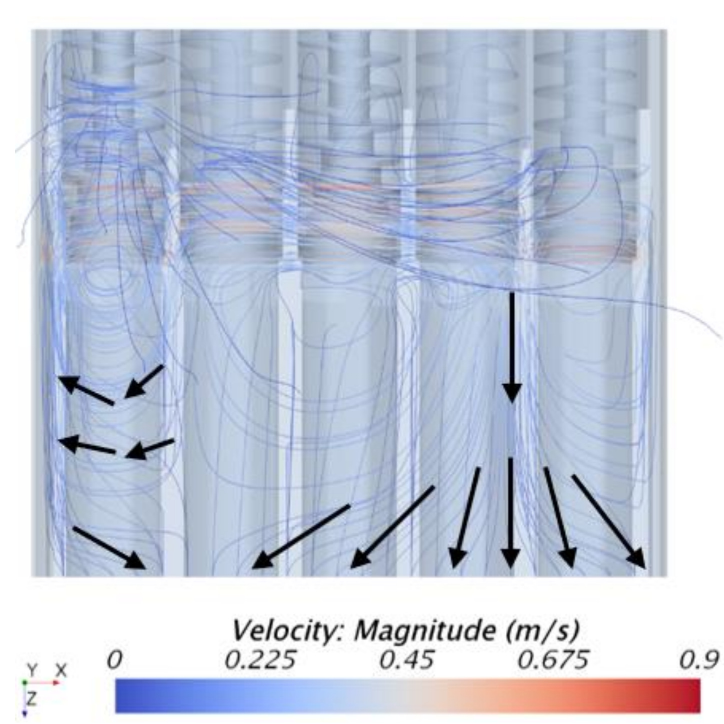

Figure 64. Velocity streamlines for Auger Configuration B4

Configuration B3 has the best flow. The flow is uniformly distributed across the cassette while also feeding concrete toward the top corners. Configuration B4 is not as uniform as the reference configuration and does not have concrete flow toward the left most outlet corner. Configuration B2 performs poorly in terms of both flow toward the corners and flow uniformity.

8.4. Performance of Auger Rotation with Elongated Material Shield

For the comparison of the additional auger configurations, no decision matrix is required since each concept performed nearly identical in the pressure and viscosity parameters and only differed slightly in the velocity streamline plots. For these reasons, Auger Configuration B3 is chosen as the ideal auger direction configuration.

To further optimize the design, Auger Configuration B3 is combined with Concept D: Sealed and Elongated Material Shield. Again, CFD analysis is performed on the new design. Figure 66 and Figure 67 show the pressure distribution with or without the sealed and elongated material shield.

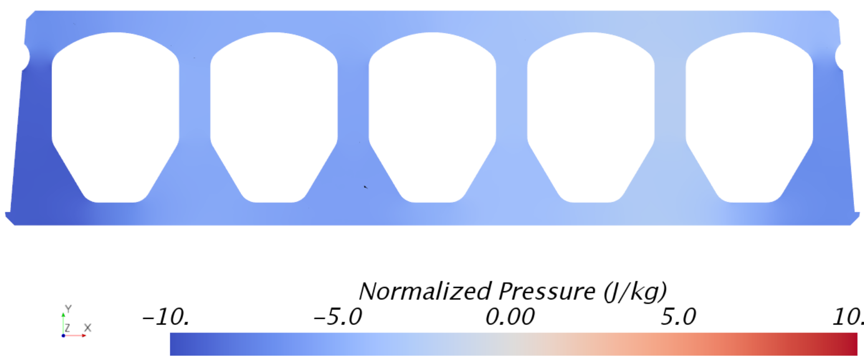

Figure 66. Pressure distribution at plane F4 for Auger Configuration B3

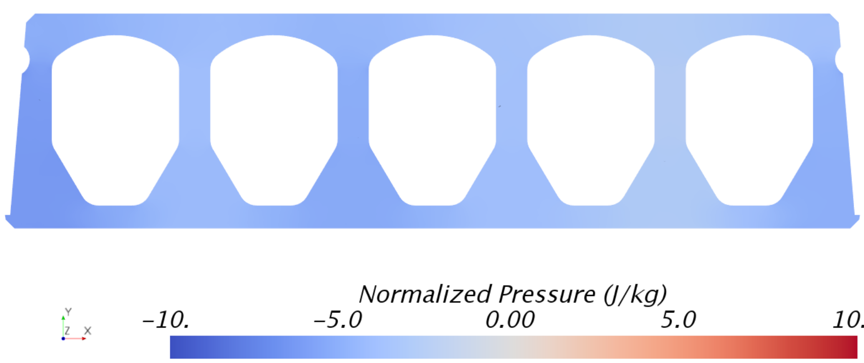

Figure 67. Pressure distribution at plane F4 for Auger Configuration B3 with Concept D: Sealed and Elongated Material Shields

Sealed and elongated material shields cause a significant decrease in pressure deviation across the outlet as seen in Figure 67 with the light blue colour spread consistently across the outlet region. The light blue colour shows low and uniform pressure at the outlet when combing Auger Configuration B3 and Concept D: Sealed and Elongated Material Shields. Similarly, comparing Figure 68 and Figure 69 an increase in viscosity performance also results from combing Auger Configuration B3 and Concept D: Sealed and Elongated Material Shields.

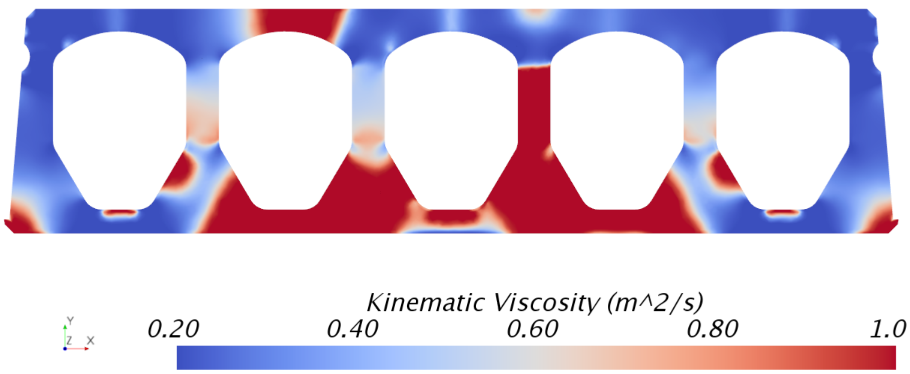

Figure 68. Kinematic viscosity distribution at plane F4 for Auger Configuration B3

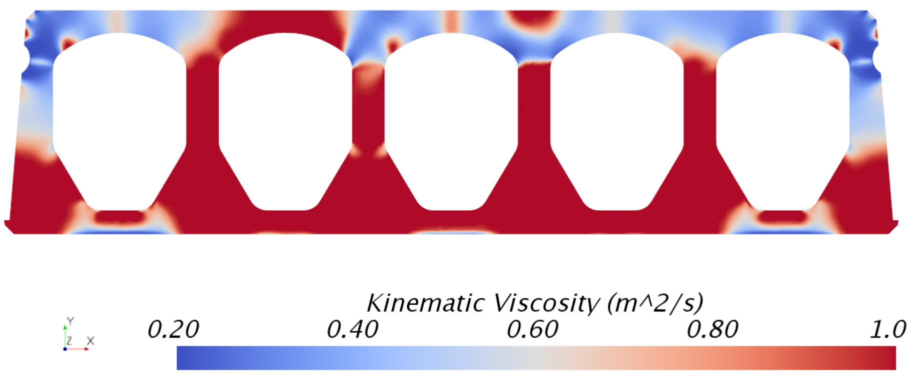

Figure 69. Kinematic viscosity distribution at plane F4 for Auger Configuration B3 with Concept D: Sealed and Elongated Material Shields

Referring to Figure 68 and Figure 69, it is noticeable that with the added sealed and elongated material shields, higher viscosity regions (coloured red) are obtained. This phenomenon is also observed in the two volume renderings in Figure 70 and Figure 71. Since a high kinematic viscosity is desired to increase extrusion speed and flow uniformity, the results suggest higher concrete slab quality when combining Auger Configuration B3 and Concept D: Sealed and Elongated Material Shields.

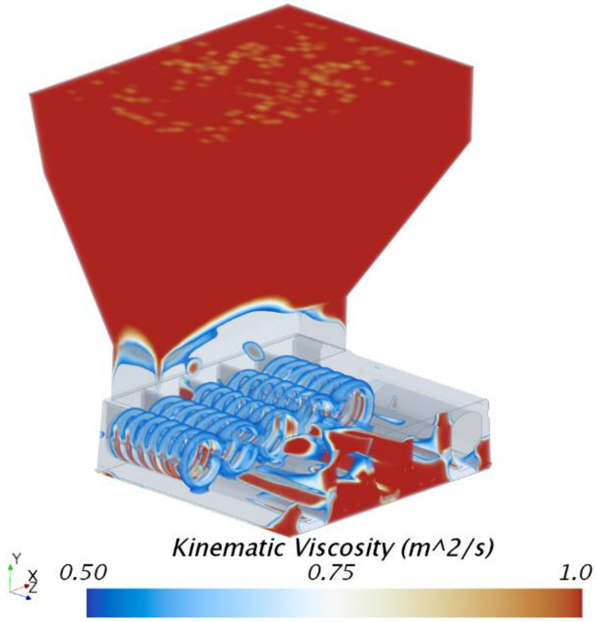

Figure 70. Viscosity volume rendering for Auger Configuration B3

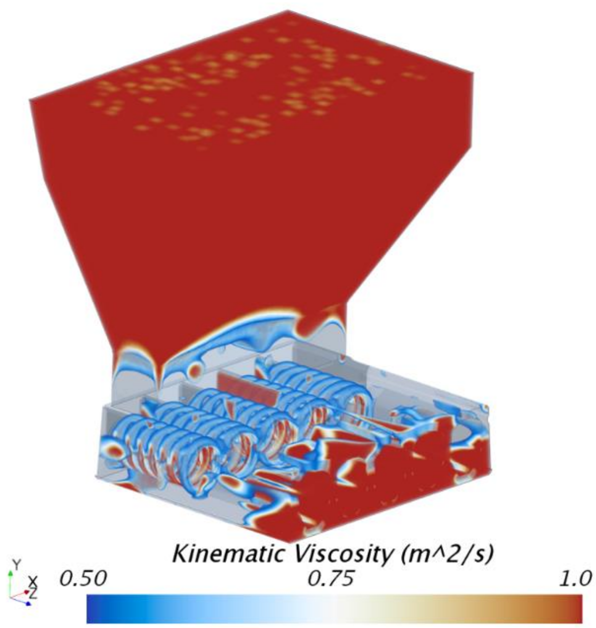

Figure 71. Viscosity volume rendering for Auger Configuration B3 with Concept D: Sealed and Elongated Material Shields

A recirculation zone is observed in Figure 72 for auger rotation Configuration B3, particularly around the left most auger. When adding the Sealed and Elongated Material Shields the recirculation is greatly reduced. Slight improvement in flow uniformity is seen in Figure 73.

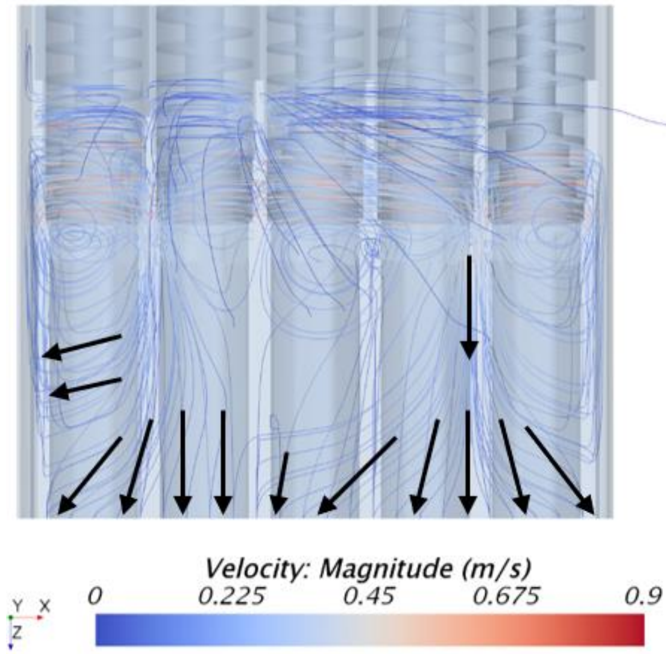

Figure 72. Velocity streamlines for Auger Configuration B3

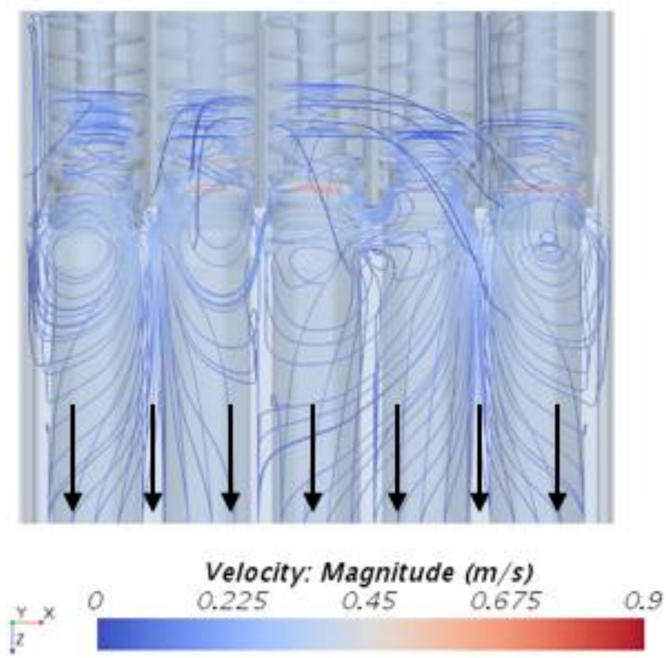

Figure 73. Velocity streamlines for Auger Configuration B3 with Concept D: Sealed and Elongated Material Shields

Table XI qualitatively compares the results between the combined Auger Configuration B3 and Concept D: Sealed and Elongated Material Shields against only the Auger Configuration B3.

TABLE XI. NUMERICAL COMPARISON BETWEEN AUGER CONFIGURATION B3 WITH AND WITHOUT SEALED AND ELONGATED MATERIAL SHIELDS

Metric	**Configuration B3**	**Configuration B3 with Sealed and Elongated Material Shields**	**Relative Difference Between Designs**
Outlet Pressure Standard Deviation	3,749.9	2,462.7	-34.06%
Average Outlet Pressure [*Pa*]	18,069	19,766	+9.39%
Average Outlet Viscosity [m^2/s]	0.66345	0.81243	+22.45%

By combining Auger Configuration B3 and Concept D: Sealed and Elongated Material Shields, a moderate increase in average outlet pressure is observed. Increasing the outlet pressure is not ideal because it serves to promote flow to go upstream instead of downstream, leading to stagnation of the concrete flow within the extruder. However, major performance gains are seen in the average outlet viscosity and outlet pressure standard deviation. By increasing the viscosity at the outlet there is less shearing. Less shearing along with uniform pressure at the outlet shows that the combined design helps to make the flow uniform across the outlet and within the extruder. Considering the increased viscosity and uniformity of the pressure, combing Auger Configuration B3 and Concept D: Sealed and Elongated Material Shields is selected as the final design.

9. Detailed Final Design

The objectives of this project are to optimize Ultra-Span's NCV concrete extruder, improve the quality of the concrete slabs produced and increase the extrusion speed, all while maintaining the outlet geometry of the concrete slab prescribed by structural engineers. The features of Ultra-Span's current design that were permitted to be optimized are the speed and direction of the augers, the mandrel shape and length, the material shields, and the addition of minor components such as vanes or pushing plates to re-direct the flow.

WWC developed CFD models that analyzed the concrete flow coming from Ultra-Span's NCV extruder. After thorough concept generation, evaluation and optimization, a final optimized design has been proposed by WWC.

9.1. Overview of the Final Design

The final design combines the following two features:

- Sealing the gaps between material shields and increasing the material shields to be the full length of the augers (15.75 [*in*]), as seen in Figure 75.
- Changing the direction of the auger rotations to be CW CCW CW CW CCW, as seen in Figure 77.

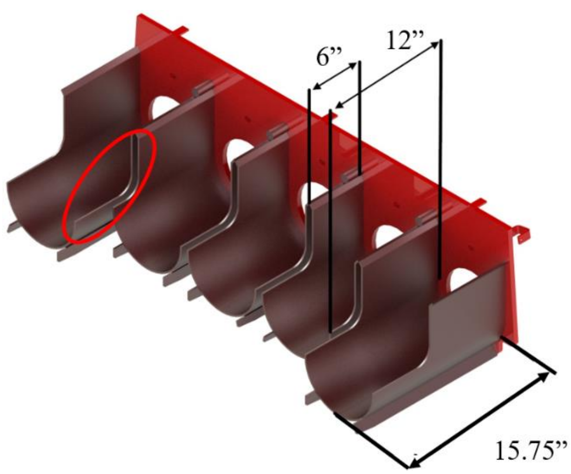

Figure 74. Current material shields with gaps between material shield circled in red

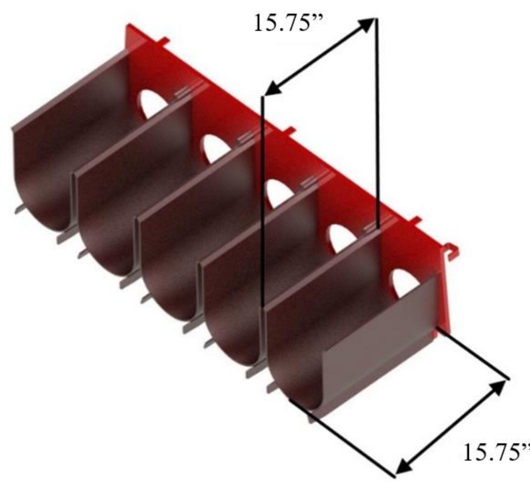

Figure 75. Final sealed and elongated material shields

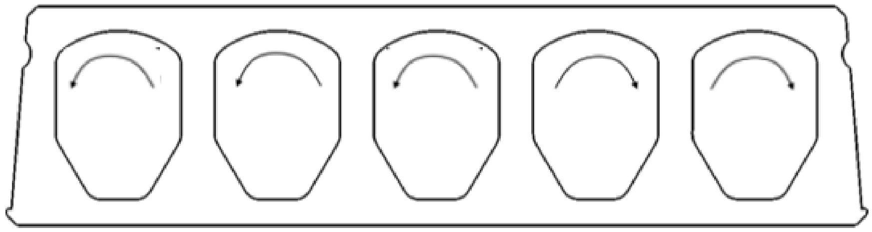

Figure 76. Current auger rotation configuration

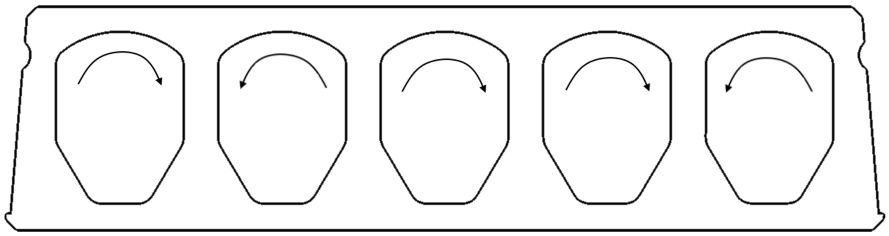

Figure 77. Optimized auger rotation configuration

A more uniform concrete flow was demonstrated in the final optimized design when sealing and elongating the material shields to be 15.75 [*in*], combined with changing the auger rotational directions to be CW CCW CW CW CCW. This optimization lowers the flow pressure at the outlet, extruding the concrete more easily. This optimization also increases the viscosity which indicates less shearing as the concrete exits the extruder. By optimizing the NCV extruder, the flow path that the concrete follows from the entry point of the extruder at the hopper to the exit at the outlet of the extruder cassette improved overall.

9.2. Needs Satisfied by the Final Design

Of the 17 needs identified in Section 1.3, there are five key specifications developed in consultation with Ultra-Span that determine the success of the final design. The following discussion explains how the design satisfies the user requirements and project objectives:

The extruder design needs to use Ultra-Span's existing platform

- The new extruder design integrates perfectly into Ultra-Span's existing platform. The optimized design effectively takes components for the current NCV concrete extruder and simply resizes or re-arranges them. Thus, the optimized design is perfectly suited to be integrated into Ultra-Span's existing platform.

The concrete needs to be extruded at a minimum rate of over 60 [*in/min*]

- According to the boundary conditions specified by WWC's CFD analysis, the results presented in Section 6 and 8 are all for an extrusion speed of 60 [*in/min*]. Therefore, the CFD optimization suggests that the results presented in this report will apply for the desired extrusion speed on 60 [*in/min*].

The extruder needs to operate normally for Ultra-Span's recommended aggregate/cement mixes

- The optimized design features guarantee that the extruder will operate normally for any of Ultra-Span's recommended aggregate/cement mixes. By using the same augers that Ultra-Span currently uses and simply re-ordering them within the extruder cassette, no new auger castings need to be made. Additionally, the current design's augers already function with the recommended aggregate/cement mix, therefore the new design using the same augers will also satisfy this requirement.

Any suggested design changes need to be possible within Ultra-Span's existing infrastructure

- By only modifying the material shield to be longer, no new components need to be manufactured. The elongated material shields reduce the amount of machining that is necessary since they do not need to be machined down to size or to a specific curvature.

The location of all the voids as well as the overall dimension of the extruded concrete slabs must remain unchanged and comply with the technical drawing shown in Figure 78

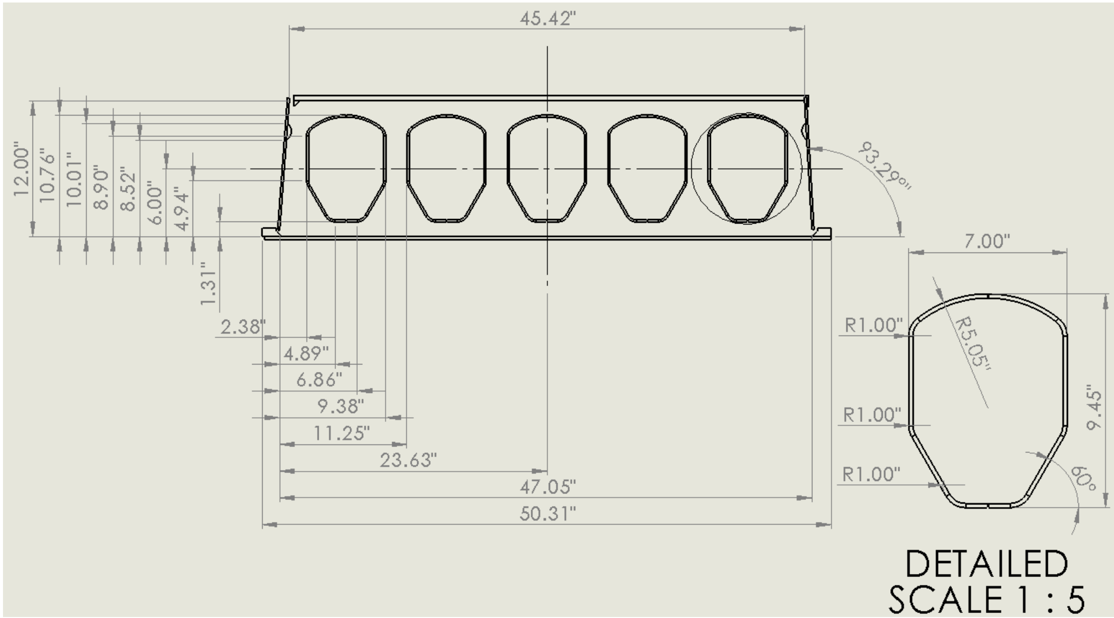

Figure 78. Required concrete slab geometry produced by the NCV extruder

- In the final design, the locations of the voids remain unchanged. According to the CFD results, the optimized design should produce concrete slabs with a tighter tolerance to the dimensions specified by the structural engineers. The overall dimensions of the extruded concrete slabs will therefore satisfy the prescribed outlet geometry.

9.3. Final Design Features

The final design developed by WWC integrates perfectly into Ultra-Span's existing NCV extruder cassette with no additional components necessary. The simple yet effective final design extends Ultra-Span's original material shields from 6 [*in*] on the top and 15.75 [*in*] on the bottom to 15.75 [*in*] at the top and at the bottom as shown in Figure 79. The final design also re-configures Ultra-Spans current auger rotation directions to the optimized rotation configuration shown in Figure 80 and Table XII.

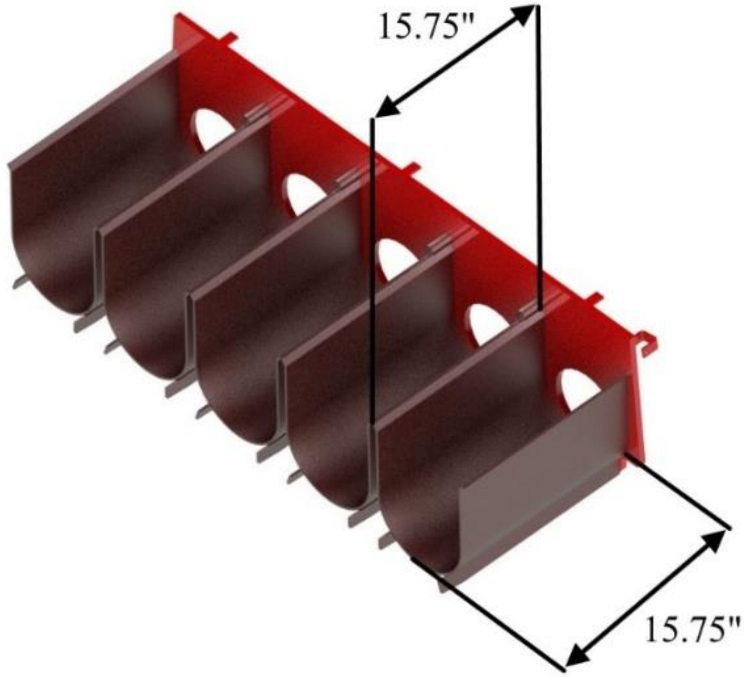

Figure 79. Sealed and elongated material shields (isometric view)

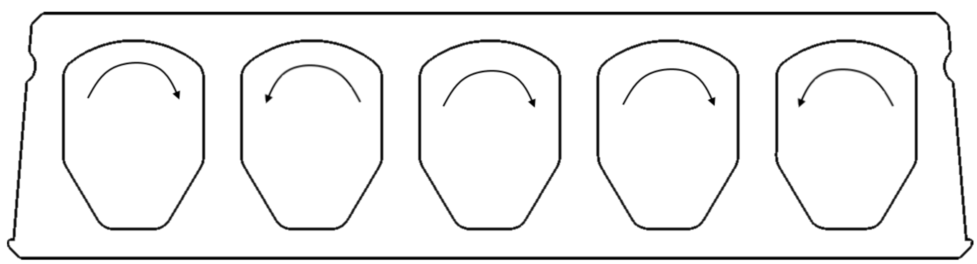

Figure 80. Optimized auger rotation configuration

TABLE XII. FINAL AUGER SPEED AND ROTATION

Auger	**1**	**2**	**3**	**4**	**5**
Speed [*rpm*]	83	74	74	74	83
Rotation	CW	CCW	CW	CW	CCW

With the optimized design there are no modifications to the current operation of the NCV extruder. The other components of the NCV extruder such as the mandrels, follower tubes, compaction plates, and drive motors remain as current. Operator usage is also unaffected. The integration of the optimized material shield and auger configurations are shown in Figure 81.

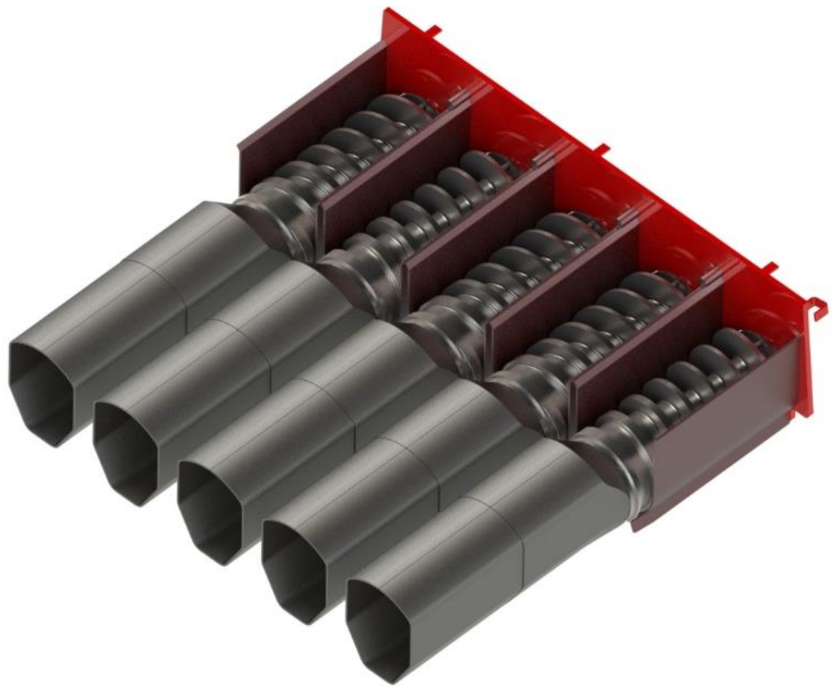

Figure 81. Integration of final design into existing NCV extruder cassette

9.4. CFD Performance of Final Design

To show the efficacy of the changes WWC has proposed, WWC has performed CFD analysis on both Ultra-Span's current design and the final optimized design. As mentioned throughout this report, the slab quality will be improved when the pressure near the outlet is decreased. This decrease in pressure promotes concrete flow towards the outlet, leading to more coverage of the desired slab geometry. The proposed optimization also promotes higher viscosity which means there is more material upstream to push against and increases the extrusion speed. Uniformity of the velocity streamlines also indicates consistency of the concrete extrusion process. Viscosity, pressure, and velocity streamline plots are shown in Figure 82 to Figure 89. Additional detailed CFD results are shown in Appendix C.

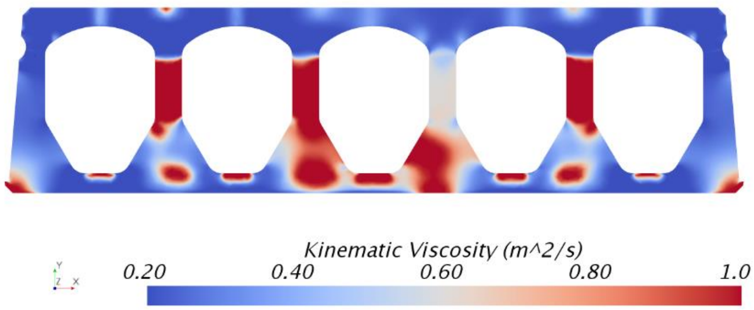

Figure 82. Viscosity distribution at plane F4 for the current design

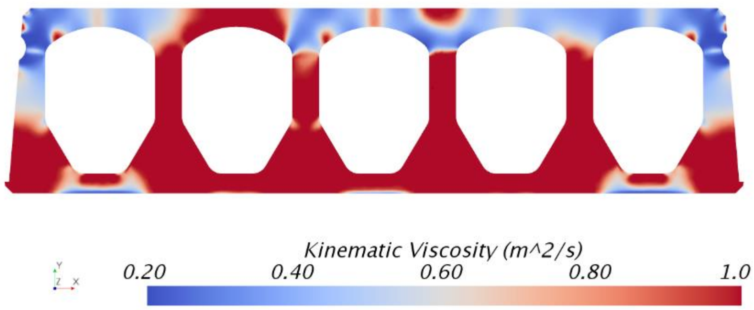

Figure 83. Viscosity distribution at plane F4 for the final design

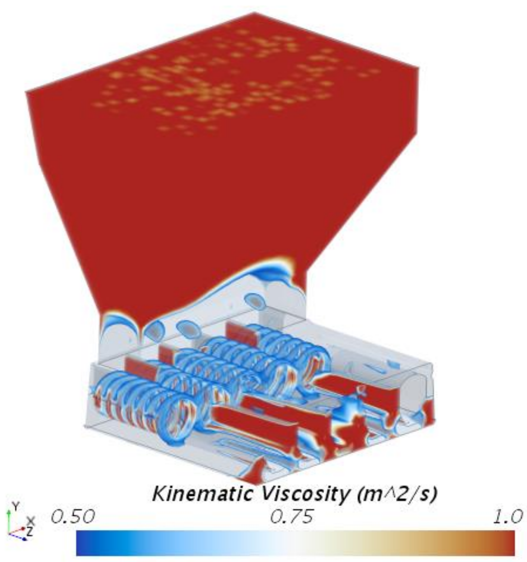

Figure 84. Viscosity volume rendering for the current design

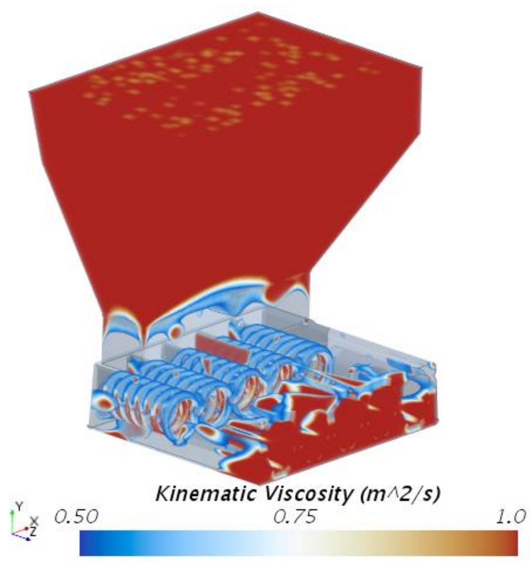

Figure 85. Viscosity volume rendering for the final design

The viscosity plots show that the final optimized design results in regions of higher viscosity (in red) penetrating deep into the extruder cassette. High viscosity also extends all the way to the sidewall of the extruder cassette. Due to the nature of the Herschel-Bulkley model high viscosity is desired at the outlet because it indicates low shearing of the concrete. Therefore, sealing and elongating the material shields along with alternating the auger rotation has led to high viscosity and low shear rates at the outlet.

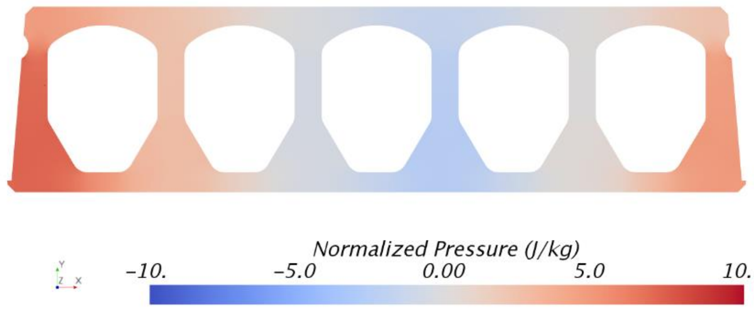

Figure 86. Pressure distribution at plane F4 for the current design

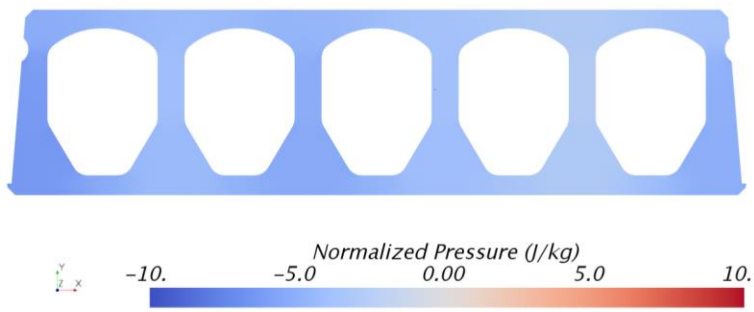

Figure 87. Pressure distribution at plane F4 for the final design

The improvement of the final design is abundantly clear when comparing Figure 86 to Figure 87. In Figure 87, the optimized design, the pressure contour plot is uniformly blue. The blue indicates low pressure and the uniform color means that the pressure at the outlet is consistent across the face of the outlet. Given this pressure behavior, uniform flow following the prescribed geometry is expected to exit the extruder.

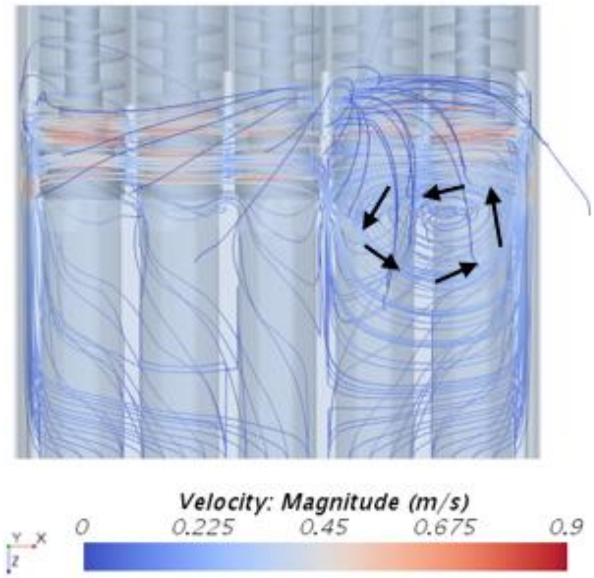

Figure 88. Velocity streamlines for the current design

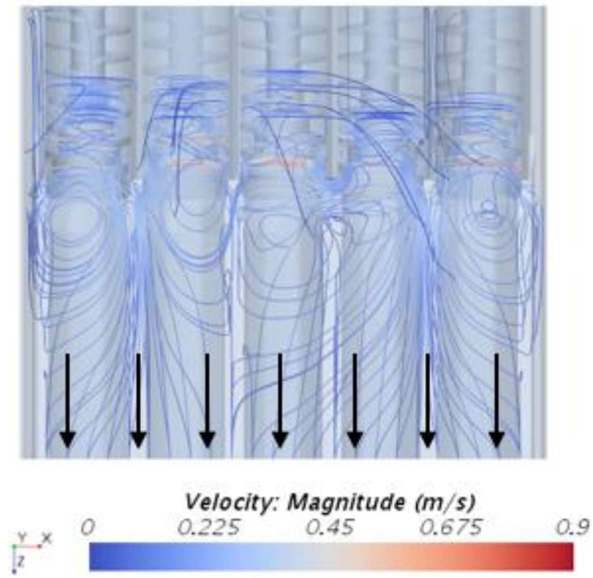

Figure 89. Velocity streamlines for the final design

The velocity streamlines in Figure 89 also show uniform flow exiting the extruder. Conversely, the current design shows a zone of recirculation and locations where concrete can stagnate around the mandrels and follower tubes.

Table XIII provides a quantitative demonstration of the pressure and viscosity performance illustrated in the above figures suggests that the optimized design can decrease the average outlet pressure by 39.31% from the current design and reduce shearing at the outlet (increase viscosity) by 53.91%. Ultimately WWC has proposed a simple design that does not require any additional components beyond what Ultra-Span already uses and achieves all of their needs.

TABLE XIII. QUANTITIATIVE COMPARISON OF CURRENT AND FINAL DESIGN

Metric	**Current Design**	**Final Design**	**Relative Difference from Current Design**
Average Outlet Pressure [*Pa*]	5517.41	3343.12	-39.31%
Average Outlet Viscosity [m^2/s]	0.54712	0.84209	+53.91%

10. Recommendations

The scope of this project involved extensive CFD analysis with very positive results. However, the CFD model is a theoretical model and it is recommended that Ultra-Span verify the final design with an internal analysis before producing any corresponding technical drawings. The dimensions provided are applicable to computer modeling and do not reflect any geometric dimensioning or tolerancing for manufacture. Although the CFD model suggests an optimal design that extends the material shields and reconfigures the auger rotational direction, for the design to go forward Ultra-Span needs to prototype the modified components for field testing and obtain physical data to validate the project's numerical analysis. It is necessary for Ultra-Span to acknowledge that the final design should be implemented under the prescribed constraints and assumptions of the project definition as failure to do so could compromise the functionality of the modified components.

Ultra-Span may also benefit from additional research to refine the viscosity model for concrete. As this is a developing field, it is recommended that Ultra-Span contact an academic institution or work closely with a research group involved in the field of numerically simulating non-Newtonian fluid flows. Refining the numerical simulations will permit a more accurate representation of the concrete being used, thus expanding the results to provide usable absolute values.

11. Conclusion

Ultra-Span is a well-established company that designs and manufactures concrete extruders worldwide. One of Ultra-Span's specialties is in the development of hollow core precast concrete extruders. More specifically, Ultra-Span has developed an extruder that produces non-circular void (NCV) concrete slabs. The current model of the NCV extruder produces uneven concrete slabs and its extrusion speed is slow. Due to the uneven compaction, the extruded concrete slabs are experiencing concrete starvation at the two top edges of the slab, making it not suitable for its structural use. The NCV extruder is also extruding at roughly half the speed of its circular void counterpart (30 [*in/min*] versus 60 [*in/min*]). The lower speed extrusion means lower productivity and is less efficient for Ultra-Span's clients.

The team at World Wide Convergence (WWC) undertook the project to optimize Ultra-Span's NCV concrete extruder. WWC's primary objectives for the project were to research other concrete extruders, optimize the existing design, and analyze the concrete fluid flow exiting from Ultra-Span's NCV extruder. WWC's role in this project was to serve as Computational Fluid Dynamics (CFD) specialists. The goal was to equip Ultra-Span with the knowledge necessary to better understand their NCV extruder so they may implement modifications to the NCV extruder themselves.

The scope of work that WWC undertook at the onset of this project included performing CFD analysis, giving detailed design optimization, creating 3D models of the optimized final design, and producing technical drawing of the optimized design. However, a modification to the project scope was made. Due to the complex, technical, and specialized nature of CFD, technical drawings for the final design were no longer required and were beyond the scope of this project. The client deemed rigorous CFD analysis as WWC's primary focus. Therefore, the final deliverables included CFD analysis, detailed design optimization, 3D models of the optimized final design, a poster of the final design, and a final design report. The implications of this are that upon completion of WWC's work, there is not a ready-to-implement design. The CFD results and corresponding designs provided by WWC will need to be verified with experiments, made into technical drawings, and be subject to an engineering economic analysis before they are implemented.

Following an engineering design methodology, the four design concepts chosen for rigorous CFD analysis were:

- Alternate the direction of rotation between the five augers
- Close off gaps between material shields and increase material shield length
- Attach vanes on top of the mandrel to manipulate the flow direction
- Add vanes to the sidewalls to redirect flow downstream

All CFD simulations were performed using Siemens STAR-CCM+. The CFD workflow was split up into the sections of geometry, meshing, setup, solving, and post-processing. A rigorous concept selection process was followed to select the final concept for detailed design and optimization. A weighted decision matrix (WDM) was then used to compare and assign the winning concepts. Alternating the auger rotation and sealed and elongated material shields were the two highest performing concepts. Both designs were therefore selected to proceed to the final design optimization phase. Multiple combinations of auger rotation directions were then analyzed to see if the final design could be optimized further. After considering the possible auger rotation direction permutations, Auger Configuration B3 was selected as the ideal auger configuration.

The simple yet effective final design extends Ultra-Span's original material shields from 6 [in] on the top and 15.75 [in] on the bottom to 15.75 [in] at the top and at the bottom. The final design also re-configures Ultra-Span's current auger rotation directions to be Clockwise – Counter clockwise – Clockwise – Clockwise – Counter clockwise. The optimized design decreases the average outlet pressure by 39.31% from the current design and reduces shearing at the outlet (increase viscosity) by 53.91%. Less shearing along with uniform pressure at the outlet shows that WWC's design makes the flow uniform across the extruder, increasing the extrusion speed and satisfying the required slab geometry specified by Ultra-Span's structural engineers. By taking components from the current NCV concrete extruder and simply resizing or re-arranging them, the final design developed by WWC integrates perfectly into Ultra-Span's existing NCV extruder with no additional components or new procedures. In brief, WWC's optimized design will lead to higher productivity, better accuracy, and improved efficiency for Ultra-Span's NCV concrete extruder.

Ultimately, WWC has diligently worked on this project to satisfy all the needs and expectations of the client. All objectives have been met and the project is completed on time. In conclusion of the project WWC confidently presents a written report, a final design poster and a final oral presentation to Ultra-Span.

12. References

[1] S. d'Auteuil. (2019). “Optimization of Non-Circular Void Extruder,” in *Ultra-Span Optimization of Non-Circular Void Extruder Power Point presentation*, unpublished. [September 11, 2019].

[2] S. d'Auteuil (private communication), September 11, 2019.

[3] Siemens PLM. (2019). *Viscoplastic Fluid* [Online]. Available: https://documentation.thesteveportal.plm.automation.siemens.com/starccmplus_latest_en/index.html [October 24, 2019].

Appendix A

Mesh Independence Study

List of Tables

Appendix A. Mesh Independence Study

To determine the mesh size being used for the CFD analysis, a mesh refinement study was performed using the baseline geometry of the non-circular void (NCV) extruder, the meshes simulated are summarized below in Table A-I.

TABLE A-I. MESHES USED FOR REFINEMENT STUDY

Global Resolution, [*mm*]	Cell Count
10	7.4 million
8	8.8 million
6	11.3 million
4	16.2 million

For these mesh sizes simulations, the outlet pressure standard deviation and the average outlet pressure are shown in Table A-II and Table A-III.

TABLE A-II. MESH INDEPENDENCE FOR AVERAGE OUTLET PRESSURE

Global Resolution, [*mm*]	Average Outlet Pressure, [*Pa*]	Deviation from 4 [*mm*] mesh
10	31217.98	-0.18%
8	31213.52	-0.20%
6	31229.90	-0.15%
4	31258.59	n/a

TABLE A-III. MESH INDEPENDENCE FOR OUTLET PRESSURE STANDARD DEVIATION

Global Resolution, [*mm*]	Outlet Pressure Standard Deviation	Deviation from 4 [*mm*] mesh
10	6521.62	-0.73%
8	6535.44	-0.53%
6	6559.79	-0.16%
4	6569.71	n/a

Due to the low deviation of the results from all meshes in comparison to the finest mesh, a 10 [*mm*] mesh is used for the design process. While the 10 [*mm*] mesh may be sufficient for the design process, the flow structures seen in the results will not be displayed at high resolution. As such, the simulations for the final design comparison use a finer mesh.

Appendix B

Herschel-Bulkley Model

List of Tables

List of Figures

Appendix B. Herschel-Bulkley Model

The Herschel-Bulkley Model is a non-Newtonian fluid model used to describe the shear behavior of certain fluids, such as toothpaste, concrete, or mud. This model has been implemented in several computational fluid dynamics codes, each with their own small modifications from each other. This appendix compares these models and establishes any differences between them. Any plots in this appendix are made using the model coefficients provided by Ultra-Span, which are shown in Table B-I. Graphs are provided in two ranges, those from shear rates in the range of $0<\dot{\gamma}<6$, as tested by de Larrard et al, and those in the range of $0<\dot{\gamma}<50$ as seen in the CFD analysis.

TABLE B-I. PROVIDED HERSCHEL-BULKLEY COEFFICIENTS

Coefficient	**Symbol**	**Value**
Consistency factor	k	132 [$Pa*s$]
Power law exponent	n	1.7
Yield stress threshold	τ_0	385 [Pa]
Yielding viscosity	μ_0	376 [$Pa*s$]

B.1. Sahu et al.

$$\mu(\dot{\gamma}) = \begin{cases} \mu_0, & \dot{\gamma} < \dfrac{\tau_0}{\mu_0} \\ \dfrac{\tau_0 + k(\dot{\gamma})^n}{\dot{\gamma}}, & \dot{\gamma} \geq \dfrac{\tau_0}{\mu_0} \end{cases} \qquad \text{Eq. B-1}$$

Equation B-1 is the standard form of the Herschel-Bulkley model as described by Sahu et al. [1], and serves as the baseline that other versions are compared against.

B.2. STAR-CCM+

$$\mu(\dot{\gamma}) = \begin{cases} \mu_0, & \dot{\gamma} < \dfrac{\tau_0}{\mu_0} \\ \dfrac{\tau_0 + k\left(\dot{\gamma} - \dfrac{\tau_0}{\mu_0}\right)^n}{\dot{\gamma}}, & \dot{\gamma} \geq \dfrac{\tau_0}{\mu_0} \end{cases} \qquad \text{Eq. B-2}$$

Equation B-2 is the form used by Siemens in their software STAR-CCM+ [2], it is the same form as provided by Sahu et al., except for the inclusion of the $\left(-\frac{\tau_0}{\mu_0}\right)$ term inside of the exponent, the purpose of this added term can be seen by plotting the viscosity versus shear rate for the version with the $\left(-\frac{\tau_0}{\mu_0}\right)$ as used in STAR-CCM+, and comparing it against the version without $\left(-\frac{\tau_0}{\mu_0}\right)$ as provided by Sahu et al.

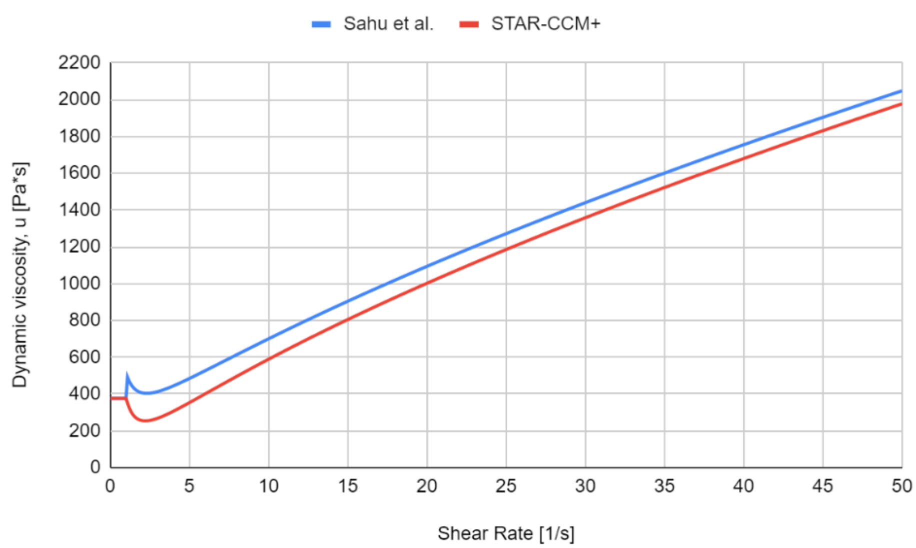

Figure B-1. Viscosity curve from the STAR-CCM+ and Sahu et al. Implementations of the Hershel-Bulkley model, simulated range

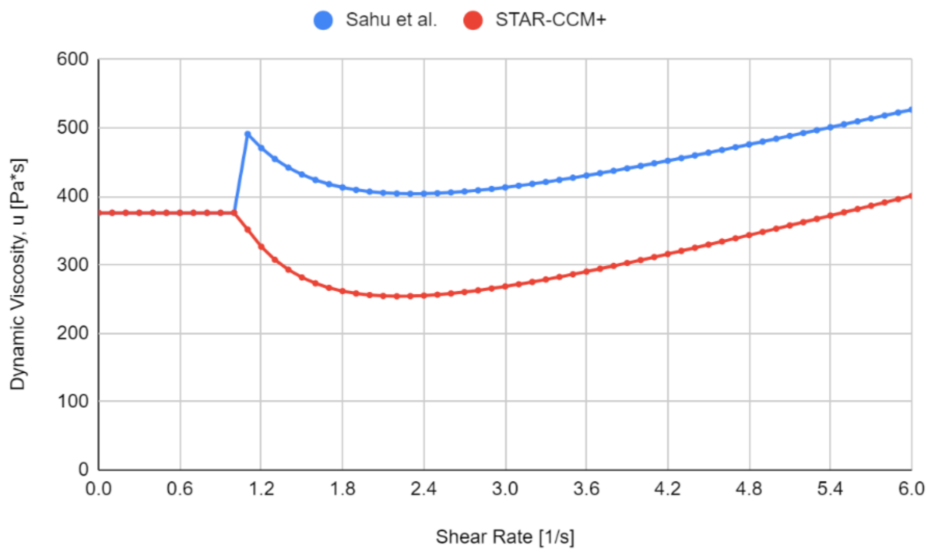

Figure B-2. Viscosity curve from the STAR-CCM+ and Sahu et al. implementations of the Hershel-Bulkley model, tested range

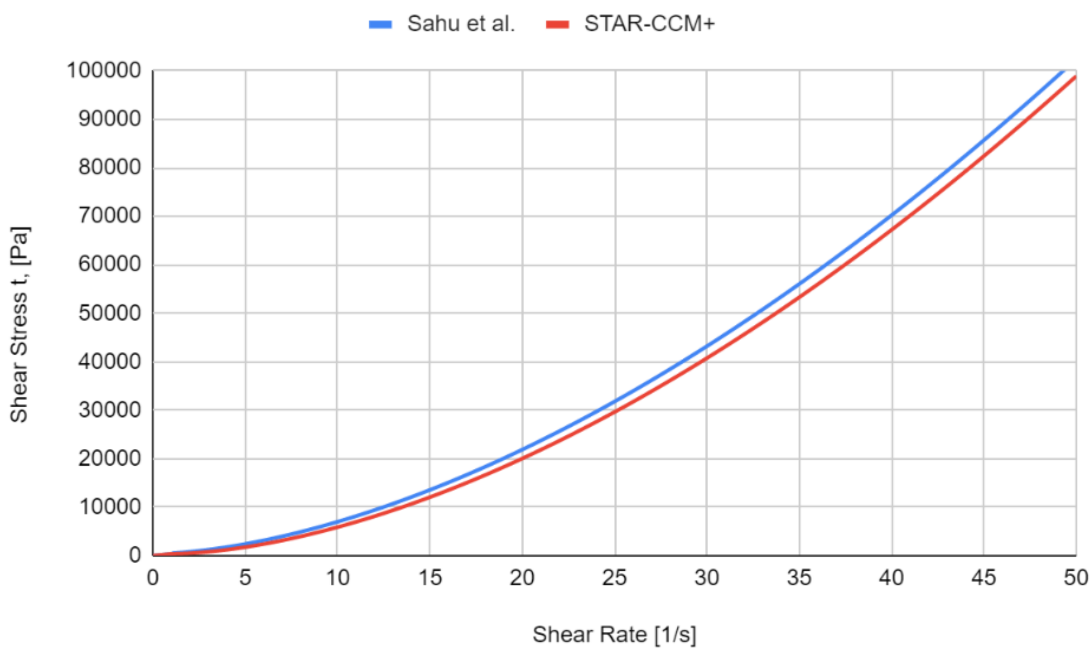

Figure B-3. Shear stress curve from the STAR-CCM+ and Sahu et al. implementations of the Hershel-Bulkley model, simulated Range

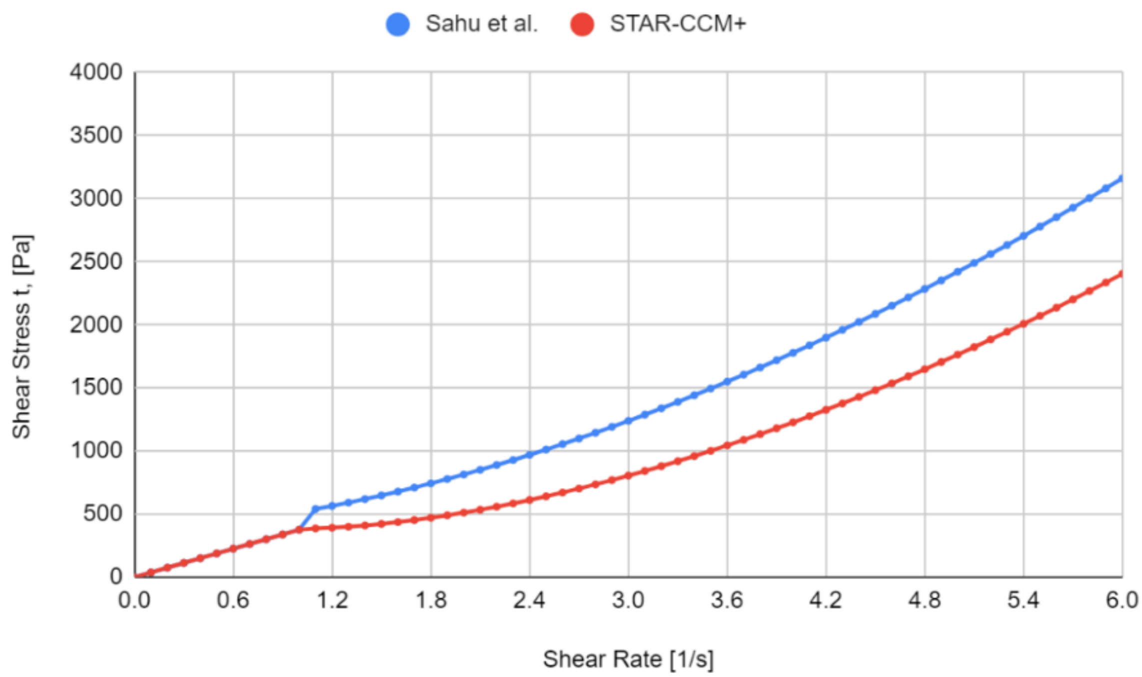

Figure B-4. Shear stress curve from the STAR-CCM+ and Sahu et al. implementations of the Hershel-Bulkley model, tested range

Figures B-3 and B-4 show that once the fluid starts to shear, a jump discontinuity exists in the Sahu et al. implementation, which has been fixed in the STAR-CCM+ implementation. The flaw of the STAR-CCM+ interpretation is that there is a downward shift in viscosity and shear stress. When viewing Figure B-4 it appears that there is a sharp slope for the Sahu et al. interpretation at the transition, this is due to the spacing of the x-coordinates used to create the graph, and that with higher resolution the jump discontinuity will become increasingly apparent.

B.3. OpenFOAM

$$\mu(\dot{\gamma}) = \min\left(\mu_0, \frac{\tau_0 + k(\dot{\gamma})^n}{\dot{\gamma}}\right) \qquad \text{Eq. B-3}$$

Equation B-3 is the form of the Herschel-Bulkley model used within OpenFOAM [3], one issue with this interpretation is that it only allows for a decrease in viscosity relative to the initial viscosity. The reason for this is the ‘min’ operator, in other words, if the right-hand side of the equation is larger than μ_0, the *min* operator will still return μ_0.

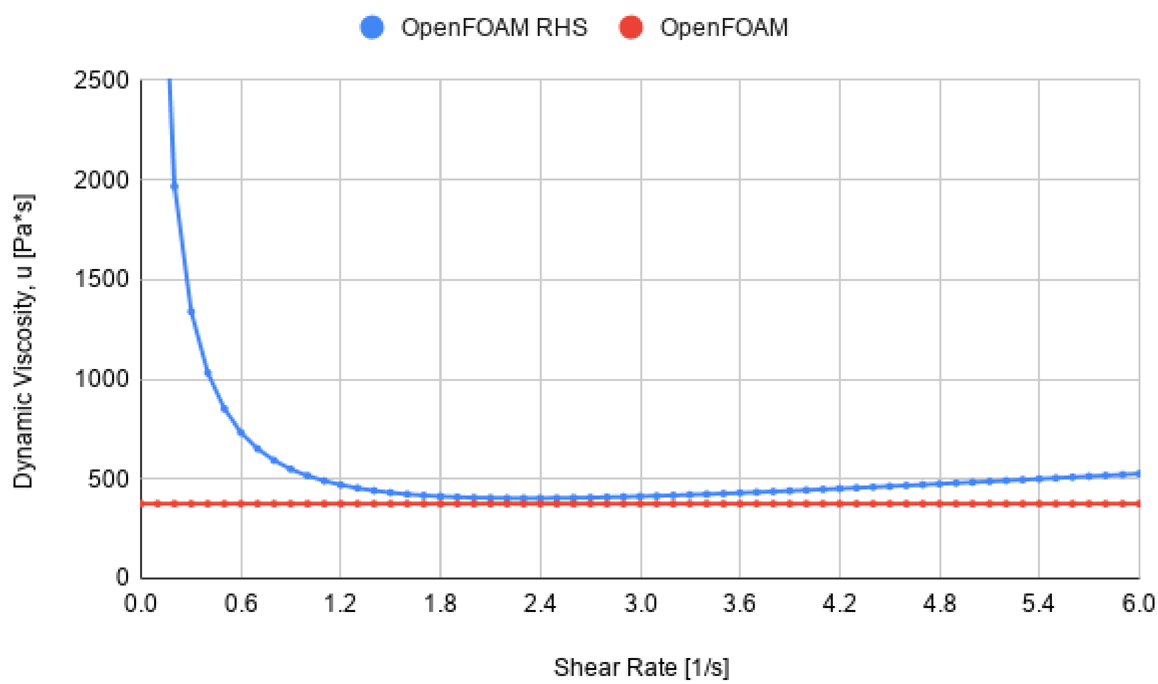

Figure B-5. Viscosity curve from the OpenFOAM implementation of the Hershel-Bulkley model, tested range

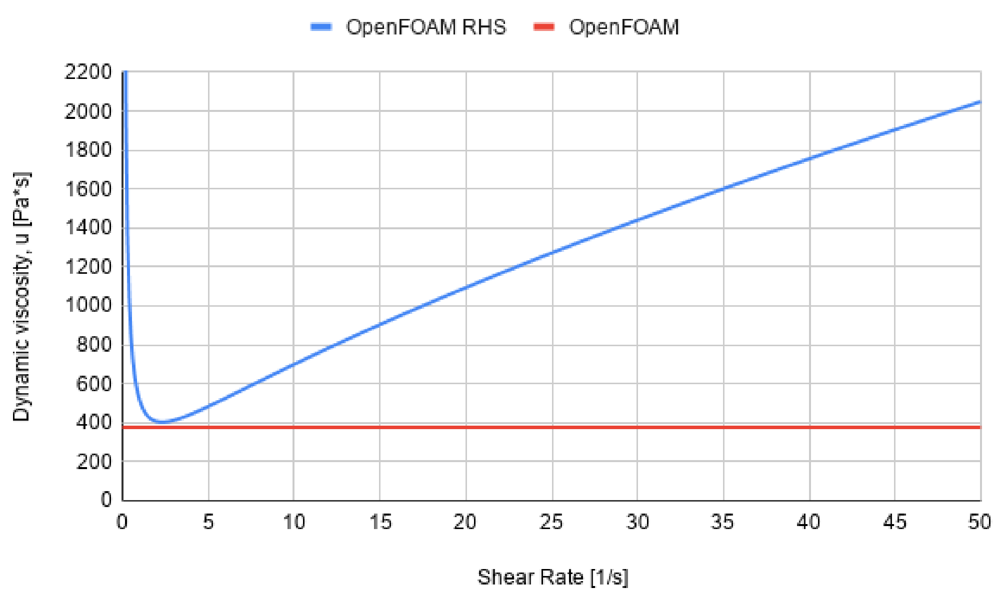

Figure B-6. Viscosity curve from the OpenFOAM implementation of the Hershel-Bulkley model, simulated range

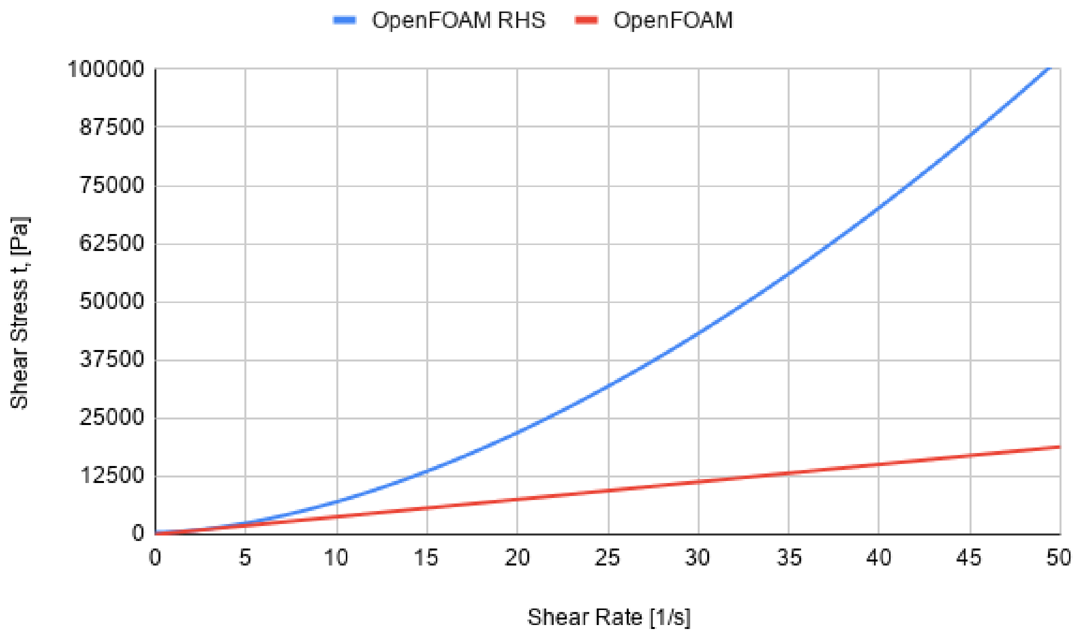

Figure B-7. Shear stress curve from the OpenFOAM implementations of the Hershel-Bulkley model, simulated range

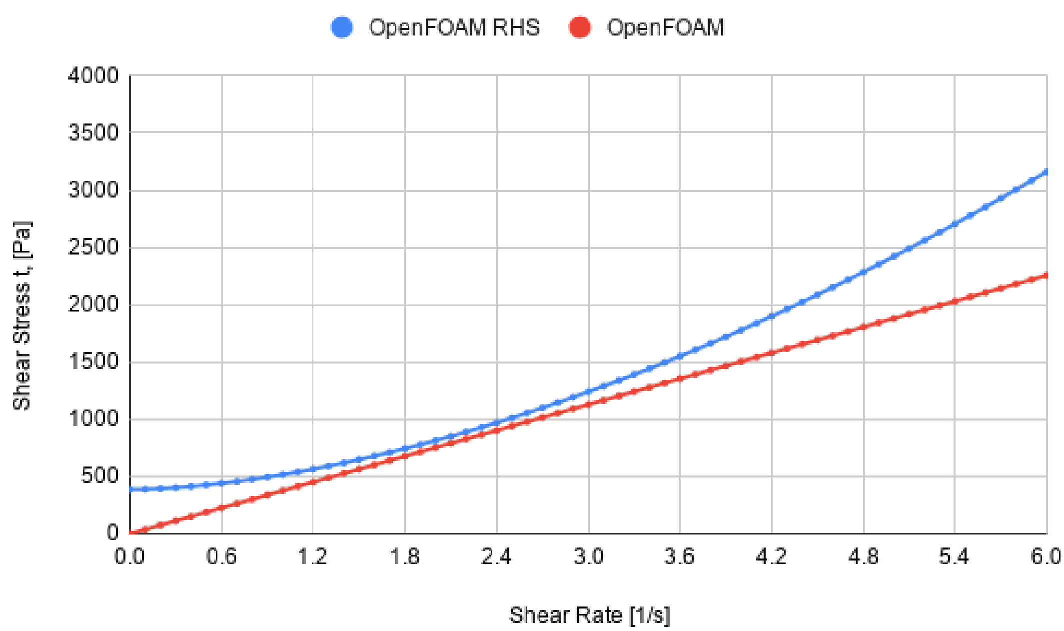

Figure B-8. Shear stress curve from the OpenFOAM implementations of the Hershel-Bulkley model, tested range

B.4. ANSYS

$$\mu(\dot{\gamma}) = \begin{cases} \mu_0\left(2 - \frac{\tau}{\tau_0}\right) + k\left[(2-n) + (n-1)\left(\frac{\tau_0}{\mu_0}\right)\right] & , if\ \dot{\gamma} < \frac{\tau_0}{\mu_0} \\ \frac{\tau_0 + k(\dot{\gamma})^n}{\dot{\gamma}} & , if\ \dot{\gamma} \geq \frac{\tau_0}{\mu_0} \end{cases} \quad \text{Eq. B-4}$$

Equation B-4 if the form of the Herschel-Bulkley used within ANSYS FLUENT [4]. The complex pre-shear term is yet another fix to the jump discontinuity problem, where ANSYS' solution is to continue the upward of viscosity as $\dot{\gamma}$ goes below the shear threshold, this is demonstrated in Figure B-5 and Figure B-6. The flaw with this approach is that the pre-shear viscosity is on average ~70% higher than specified, when using Ultra-Span's provided model coefficients.

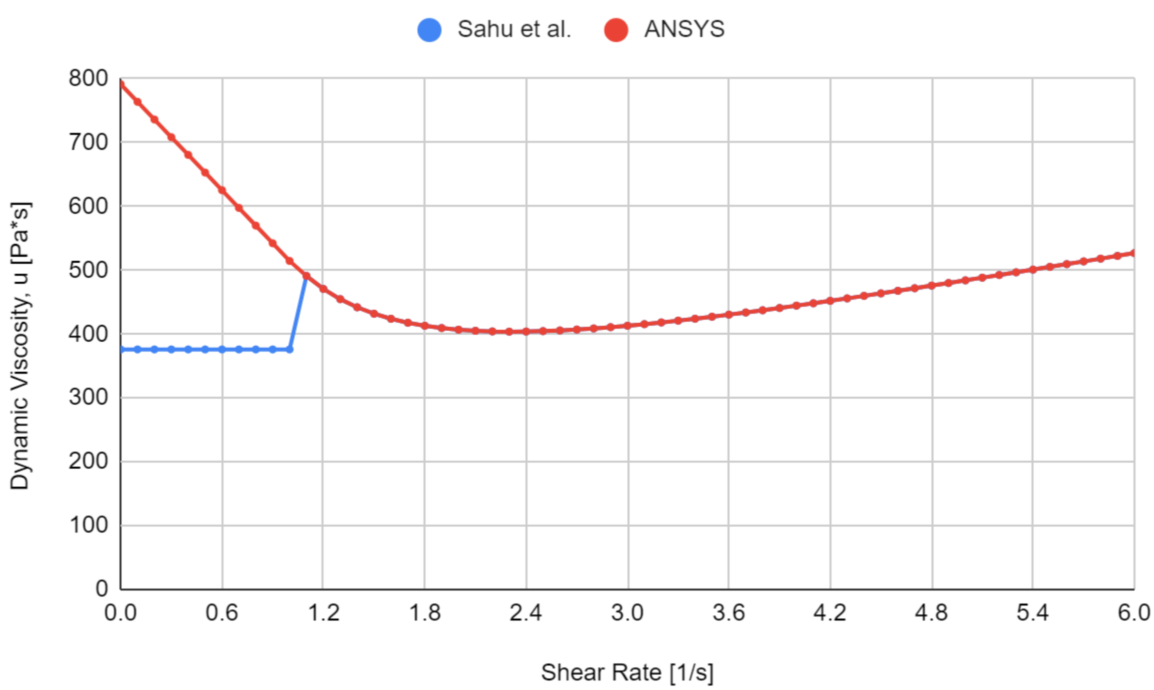

Figure B-9. Viscosity curve from the STAR-CCM+ and Sahu et al. implementations of the Hershel-Bulkley model, tested range

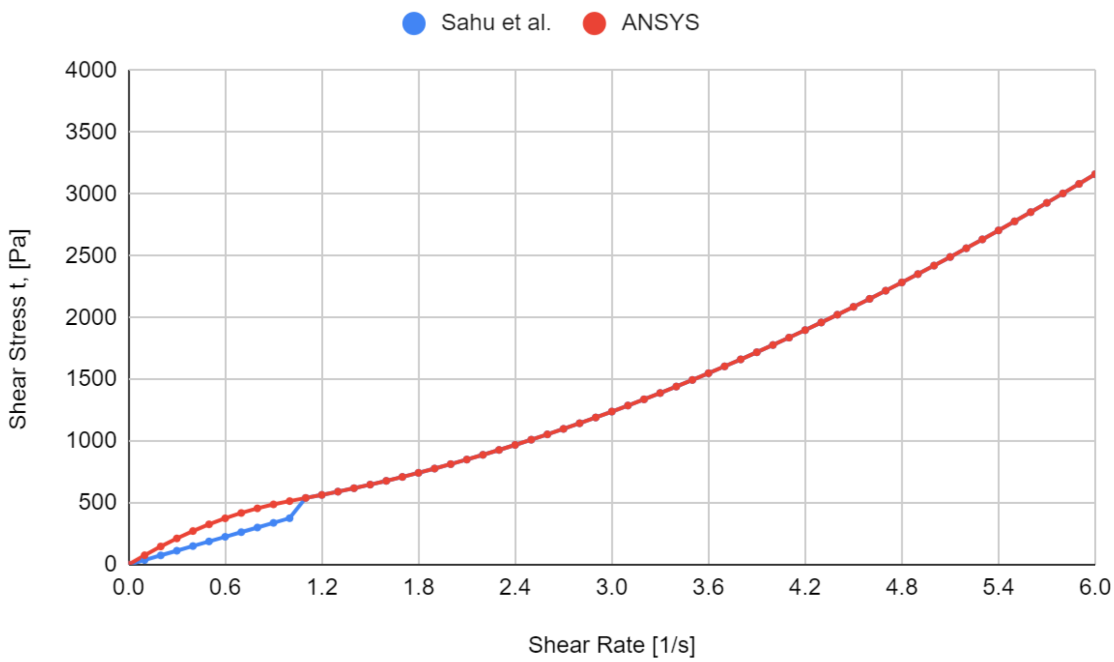

Figure B-10. Shear stress curve from the STAR-CCM+ and Sahu et al. implementations of the Hershel-Bulkley model, tested range

B.5. Usage of Herschel-Bulkley Model in Ultra-Span's Existing CFD Results

Previously, Ultra-Span has had a consultant perform CFD analysis on their Non-Circular Void extruder in order to improve the extruder performance. This consultant uses OpenFOAM, and therefore the OpenFOAM interpretation of the Herschel-Bulkley model shown in Section B.3 was simulated. With their initial simulations using the model coefficients from Table B-I, the fluid flow in these simulations did not experience any change in viscosity, which is consistent with Figure B.5, where the right-hand side of the '*min*' operator does not dip below μ_0, resulting in a constant viscosity of μ_0. Following this, the consultant increased μ_0 to 2000 [kg/m^3] which allowed them to observe the expected shear thinning behavior. The result of this modification can be seen below in Figure B-11 and Figure B-12, with a complete comparison of all models for the new coefficients being seen in Figure B-13 and Figure B-14.

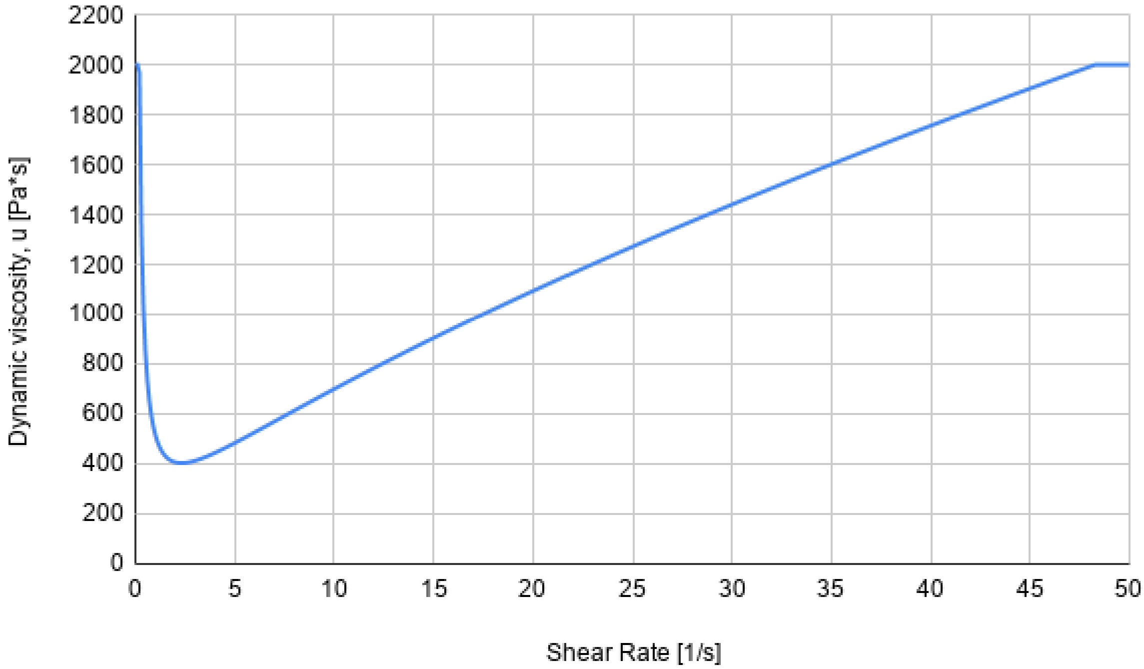

Figure B-11. Viscosity curve for consultant’s modified initial viscosity, simulated range

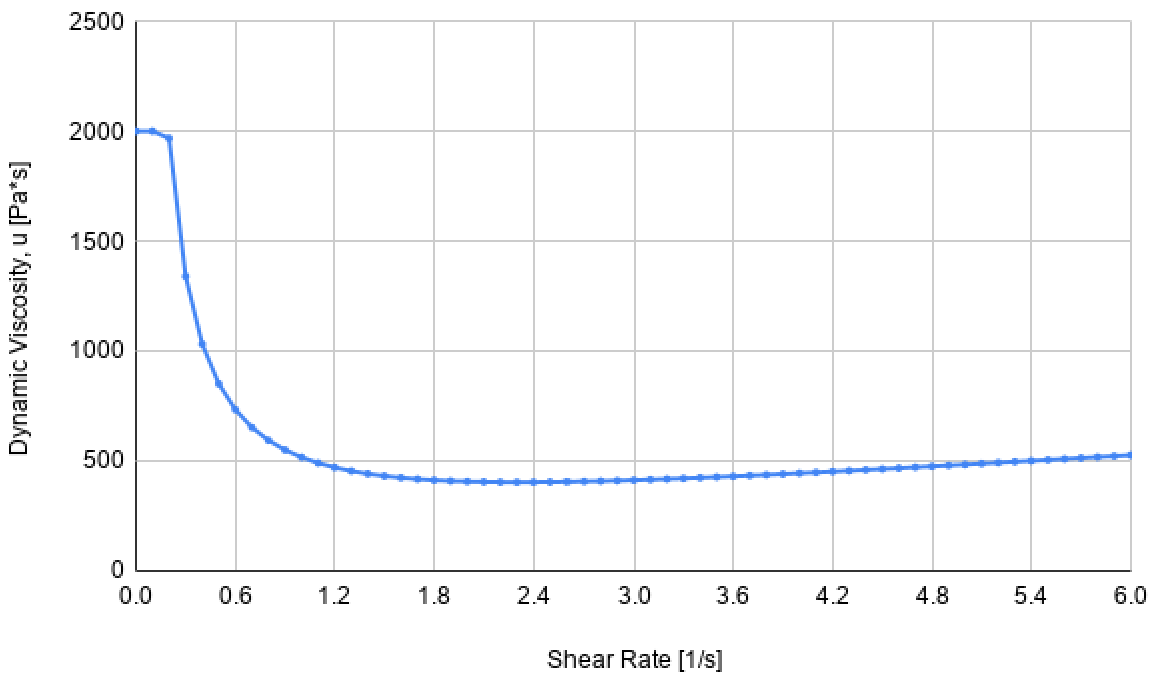

Figure B-12. Viscosity curve for consultant’s modified initial viscosity, tested range

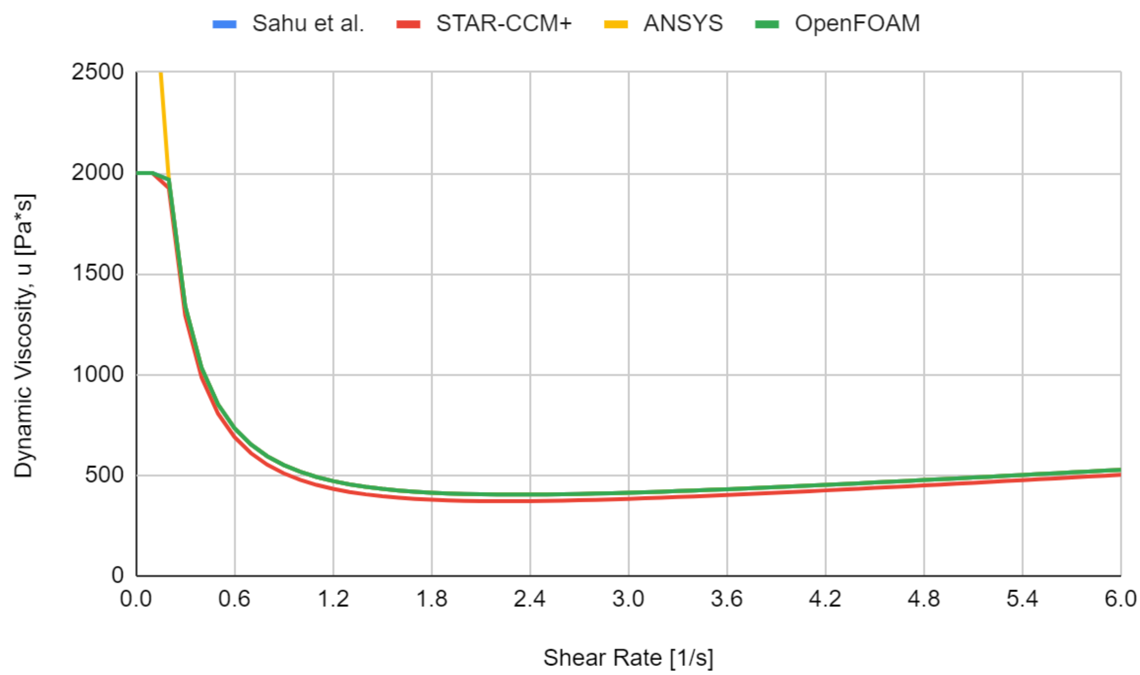

Figure B-13. Viscosity curve comparison for consultant’s modified initial viscosity, tested range

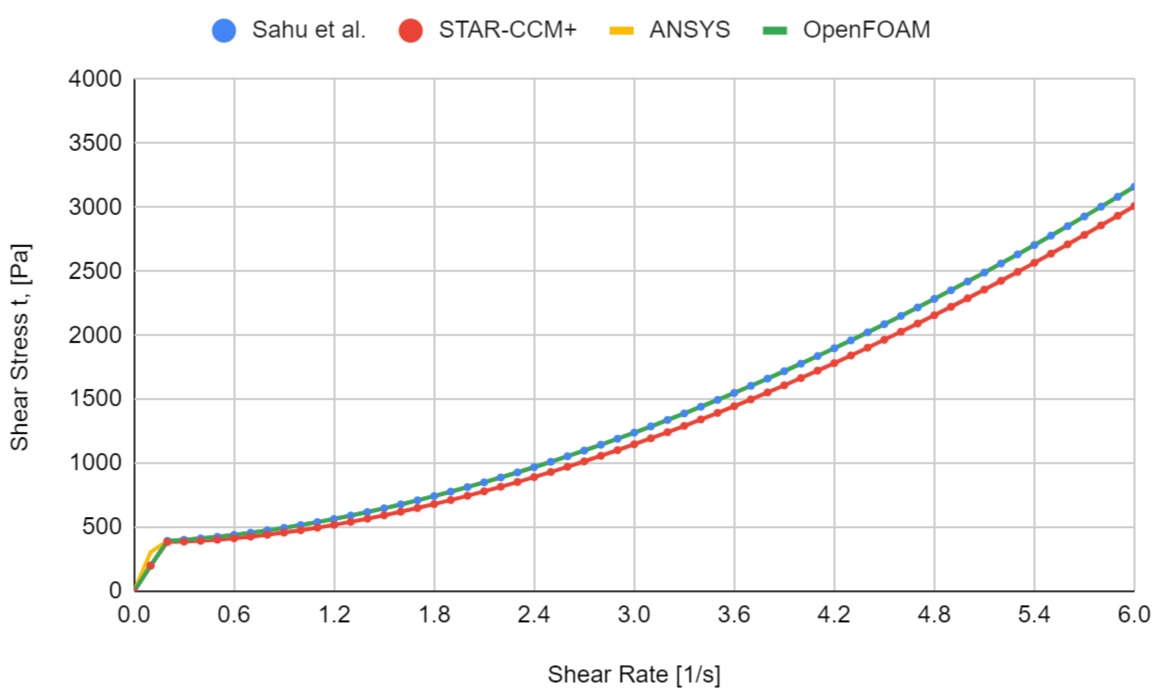

Figure B-14. Shear stress curve comparison for consultant’s modified initial viscosity, tested range

B.6. References

[1] K. Sahu, P. Valluri, P. Spelt and O. Matar, (2007). "Linear instability of pressure-driven channel flow of a Newtonian and a Herschel-Bulkley fluid", in *Physics of Fluids*, vol. 19, no. 12, pp. 122101, 2007. Available: 10.1063/1.2814385 [November 25, 2019].

[2] The Steve Portal. (2019). *Viscoplastic Fluid* [Online]. " Available: https://documentation.thesteveportal.plm.automation.siemens.com/starccmplus_latest_en/index.html [December 2, 2019].

[3] CFD Direct. (2019). *OpenFOAM v6 User Guide: 7.3 Transport/rheology models* [Online]. Available: https://cfd.direct/openfoam/user-guide/v6-transport-rheology/. [December 2, 2019].

[4] Ansys Fluent. (2019). *Herschel-Bulkley Dialog Box* [Online]. Available: https://www.afs.enea.it/project/neptunius/docs/fluent/html/ug/node1072.htm. [December 2, 2019].

Appendix C

Full Post Processing of the Initial and Final Designs

List of Figures

Appendix C. Full Post Processing of the Initial and Final Designs

To assist Ultra-Span Technologies with the optimization of their Non-Circular Void Extruder, a full optimization process was performed with the usage of computational fluid dynamics (CFD), and an improved design was found. For the comparison between the initial and final designs, Ultra-Span has requested images demonstrating the changes in pressure, viscosity, and velocity throughout the extruder, both in 2D and 3D renders.

C.1. Presentation of CFD Results

Upon consultation with the client and confirmation of the client's needs, the most important parameters to consider are pressure and viscosity. Specifically, reduction in pressure and increase in viscosity at the outlet. These flow properties are desired as a decrease in pressure near the outlet promotes concrete flow towards the outlet, leading to more coverage of the desired slab geometry. To demonstrate the improvement in design, Ultra-Span has requested the following post processing results:

- Pressure contour plots at various cut planes
- Kinematic viscosity contour plots at various cut planes
- Kinematic viscosity volume renderings

Figure C-1 to Figure C-3 show the location of the various cut planes considered. The specific location to place cut planes are selected according to the areas of interest identified by the client. The cut planes are labeled according to the direction that the viewer is looking at the results. F-planes are planes that are viewed from the front of the extruder, T-planes are viewed from the top of the extruder, and S-planes are when viewing from the side of the extruder.

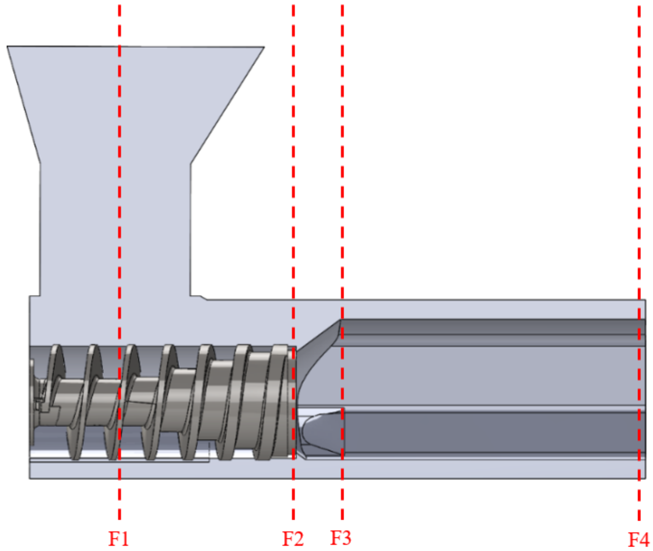

Figure C-1. Side view of the extruder (front view cut planes)

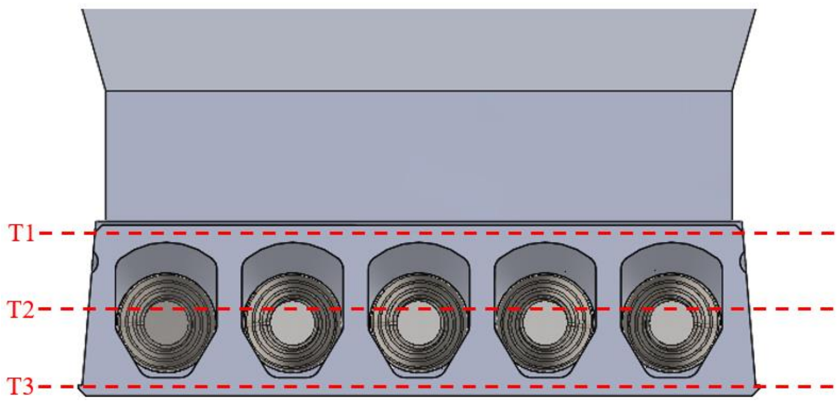

Figure C-2. Front view of the extruder cassette (top view cut planes)

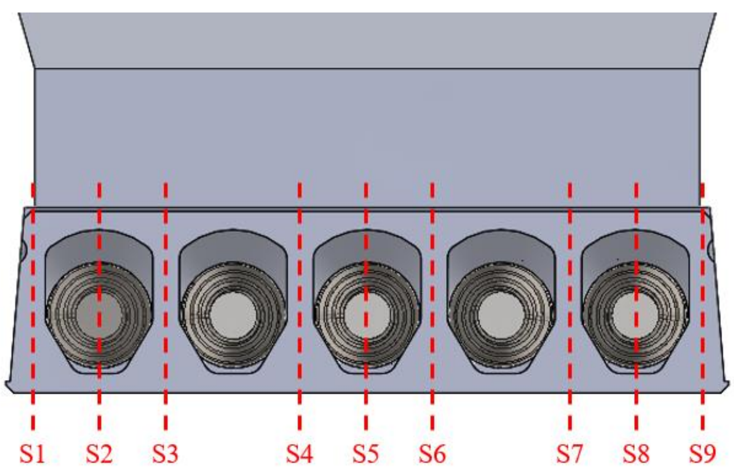

Figure C-3. Front view of the extruder cassette (side view cut planes)

A detailed explanation of the cut planes used for analysis of the CFD results is as follows:

Front Plane

- The purpose of F1 is to show the impact of the design on the inlet concrete flow and interaction of the concrete with the augers.
- F2 and F3 are selected because they represent the start and end of the mandrel shape change and are locations where the most concrete blockage is observed.
- F4 is placed near the outlet because it provides an understanding of the quality and geometry of the final concrete slabs produced.

Top Plane

1. The purpose of T1, T2 and T3 are to show the amount of solidity penetration into the extruder. In other word, the top planes allow for easy visualization of the viscosity variation form the inlet to the outlet. Capturing the effects of the auger, mandrel, and follower tubes.

Side Plane

2. The purpose of S1, S3, S4, S6, S7 and S9 is to show the variation in concrete properties from top to bottom of the slab in between and around the auger, mandrel, and follower tube assemblies.
3. S2, S5, and S8 on the other hand cut through the auger, mandrel, and follower tube assemblies, thus showing the properties of the concrete above and below the auger, mandrel and follower tube assembly.

C.2. CFD Results for Current and Optimized Designs

To provide a set of high-resolution results for comparison between Ultra-Span's current design and the final optimized design, CFD analysis is performed with a 2 [*mm*] mesh comprising of 41.4 million cells. In performing this analysis, a notable difference in results is found compared to the 10 [*mm*] results used for the design process. While this difference is unexpected given the mesh independence study performed, the different was minor in comparison to the differences in between design concepts used to guide the design phase. As such, this mesh dependence is not found to impact the design process detailed in this report. The results of these high resolution simulations are shown below in Figures C-4 to C-101.

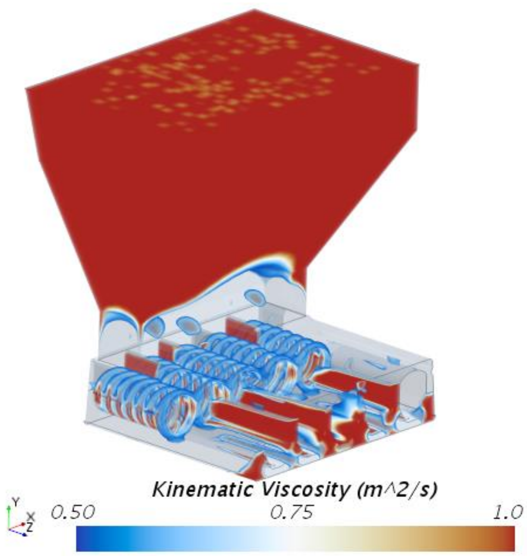

Figure C-4. Viscosity volume rendering for the initial design

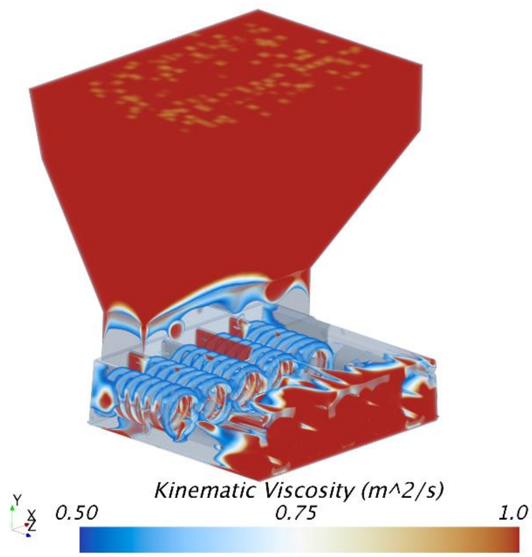

Figure C-5. Viscosity volume rendering for the final design

.

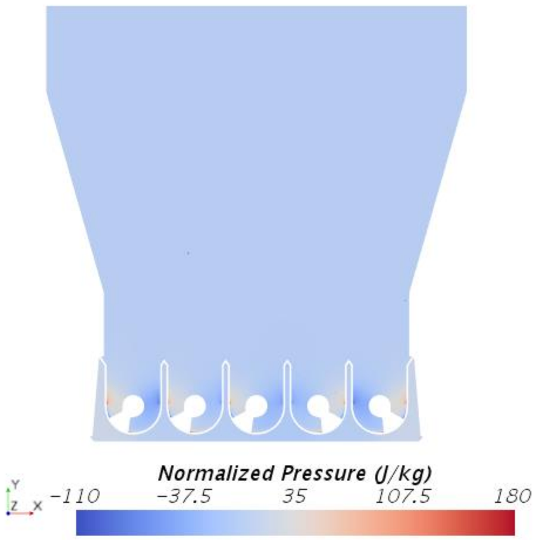

Figure C-6. Normalized pressure at plane F1 for the initial design

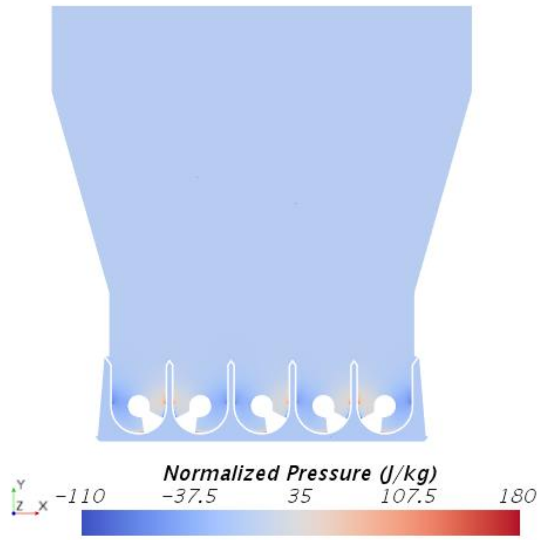

Figure C-8. Normalized pressure at plane F1 for the final design

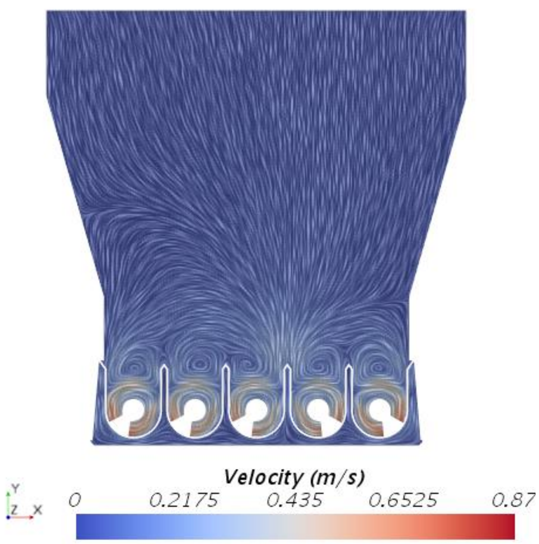

Figure C-7. Velocity profile at plane F1 for the initial design

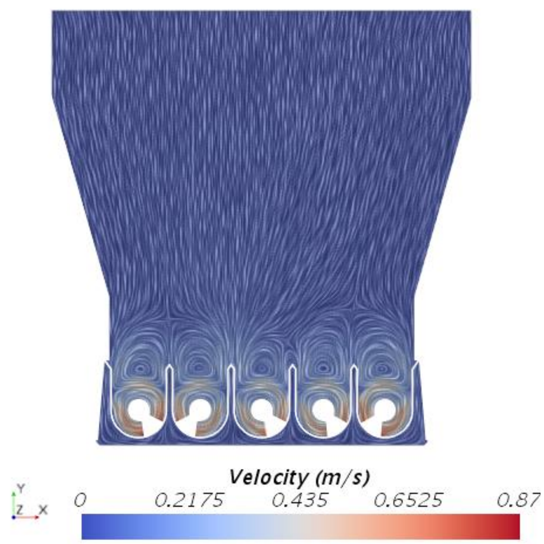

Figure C-9. Velocity profile at plane F1 for the final design

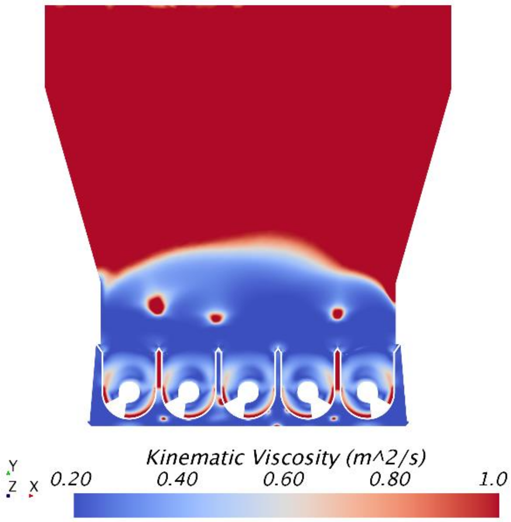

Figure C-10. Viscosity at plane F1 for the initial design

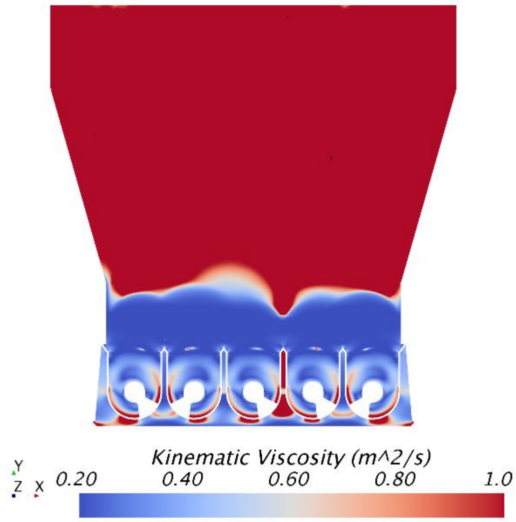

Figure C-11. Viscosity at plane F1 for the final design

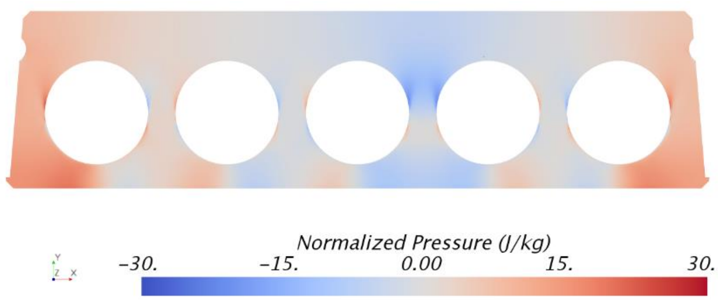

Figure C-12. Normalized pressure at plane F2 for the initial design

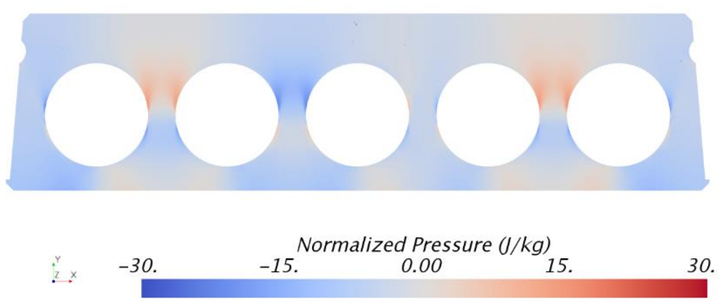

Figure C-13. Normalized pressure at plane F2 for the final design

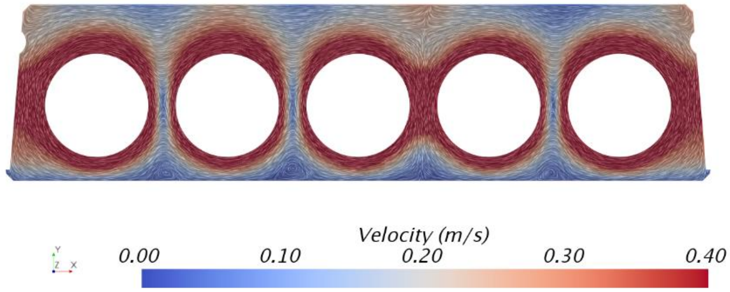

Figure C-14. Velocity profile at plane F2 for the initial design

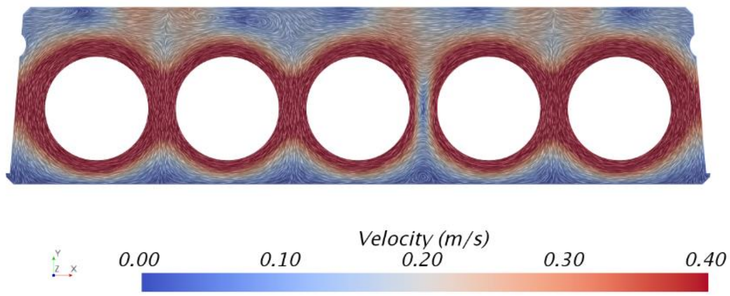

Figure C-15. Velocity profile at plane F2 for the final design

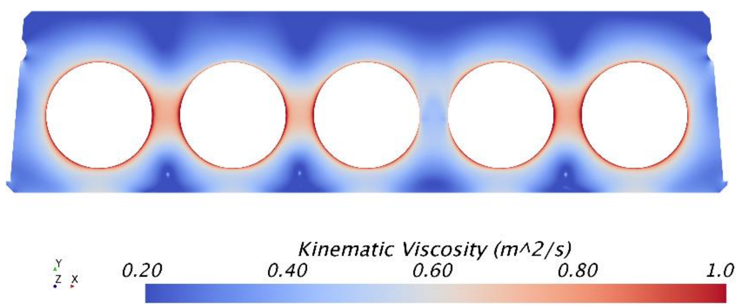

Figure C-16. Viscosity at plane F2 for the initial design

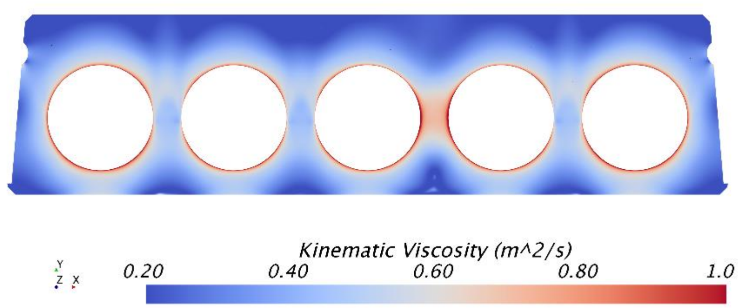

Figure C-17. Viscosity at plane F2 for the final design

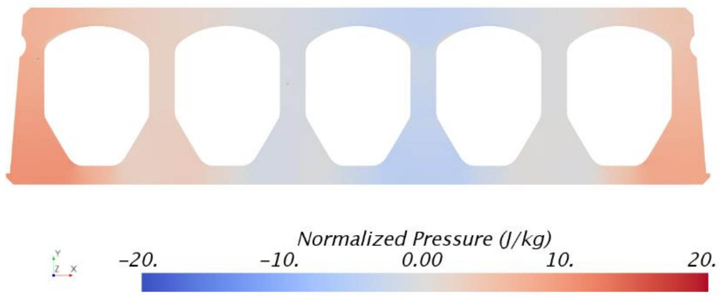

Figure C-18. Normalized pressure at plane F3 for the initial design

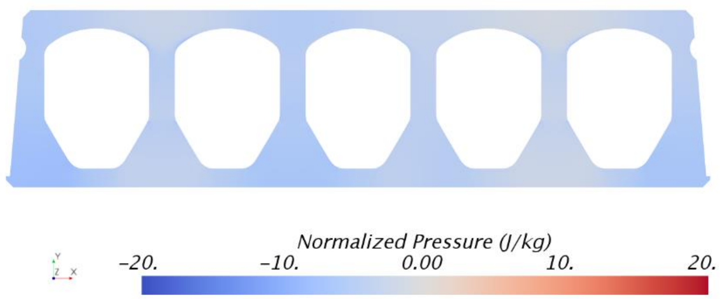

Figure C-19. Normalized pressure at plane F3 for the final design

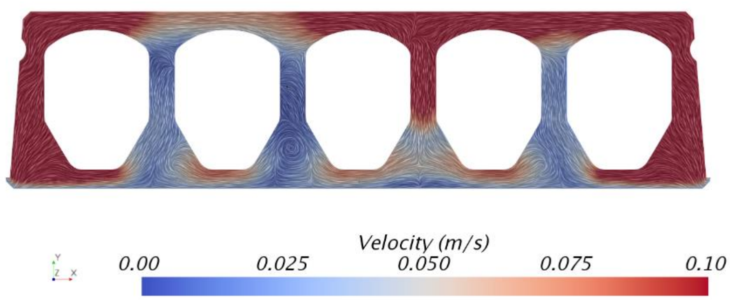

Figure C-20. Velocity profile at plane F3 for the initial design

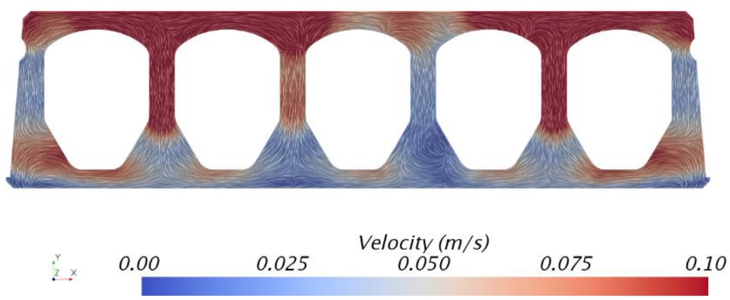

Figure C-21. Velocity profile at plane F3 for the final design

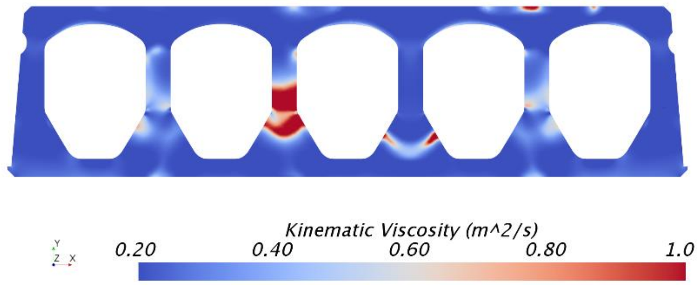

Figure C-22. Viscosity at plane F3 for the initial design

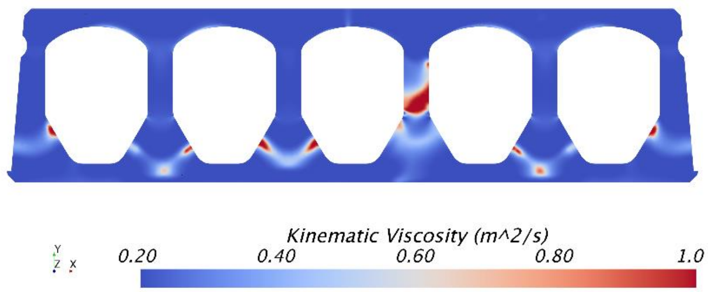

Figure C-23. Viscosity at plane F3 for the final design

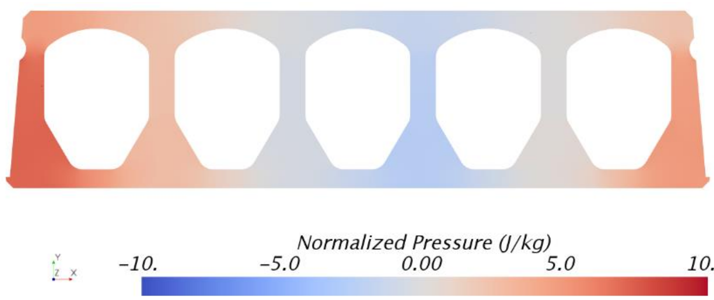

Figure C-24. Normalized pressure at plane F4 for the initial design

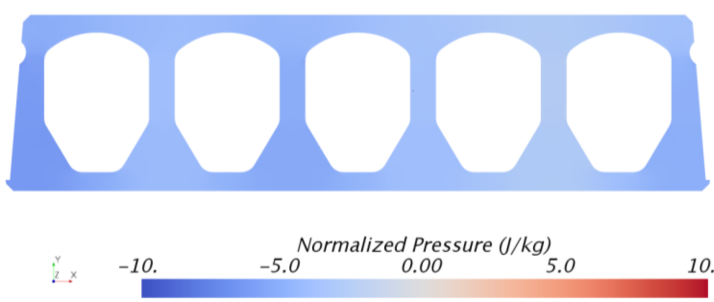

Figure C-25. Normalized pressure at plane F4 for the final design

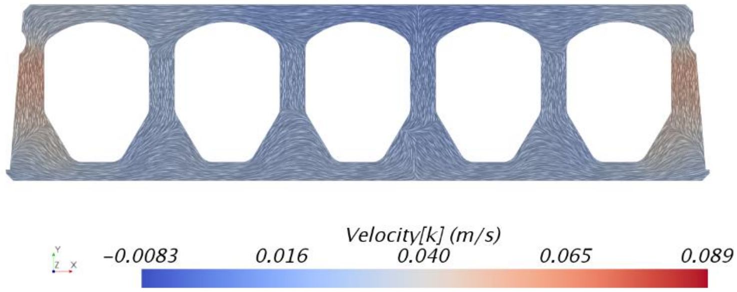

Figure C-26. Velocity profile at plane F4 for the initial design

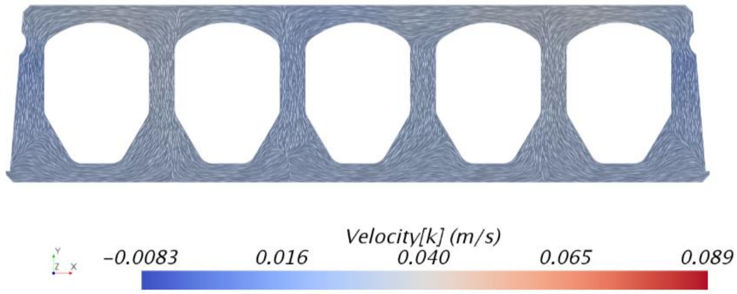

Figure C-27. Velocity profile at plane F4 for the final design

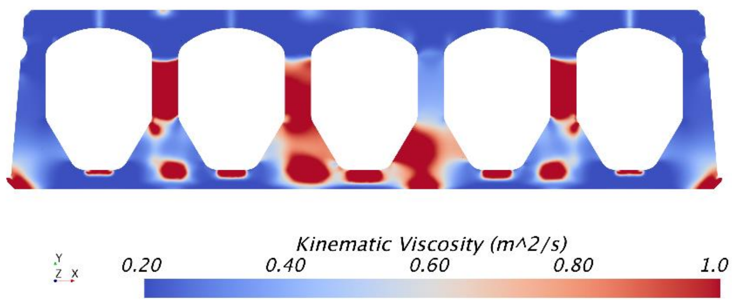

Figure C-28. Viscosity at plane F4 for the initial design

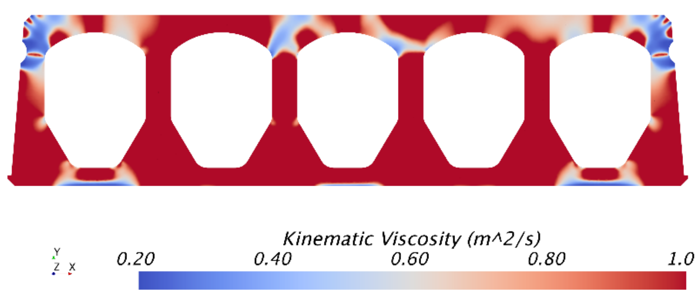

Figure C-29. Viscosity at plane F4 for the final design

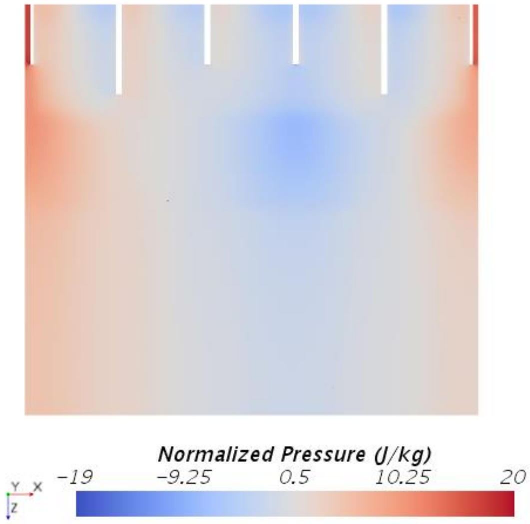

Figure C-30. Normalized pressure at plane T1 for the initial design

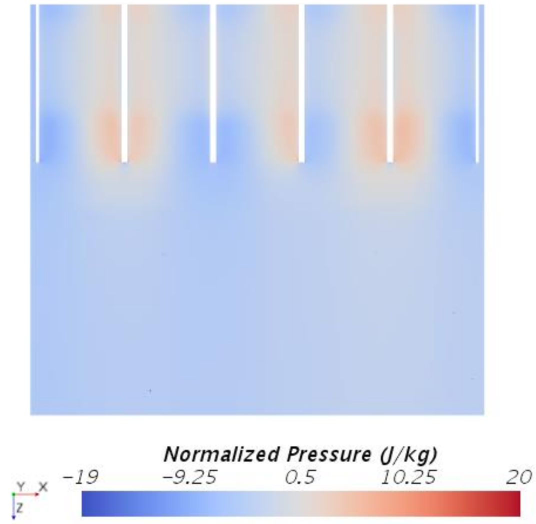

Figure C-32. Normalized pressure at plane T1 for the final design

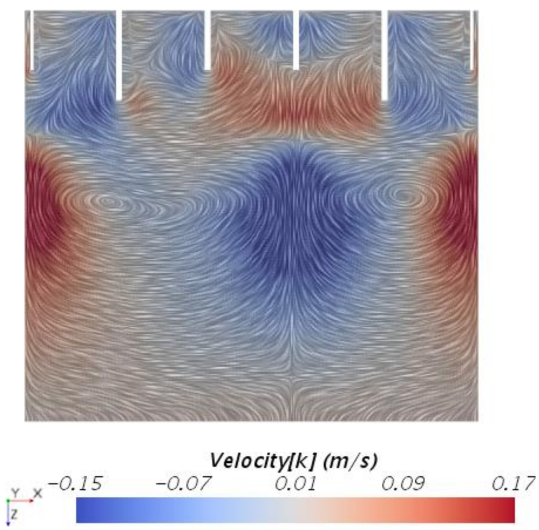

Figure C-31. Velocity profile at plane T1 for the initial design

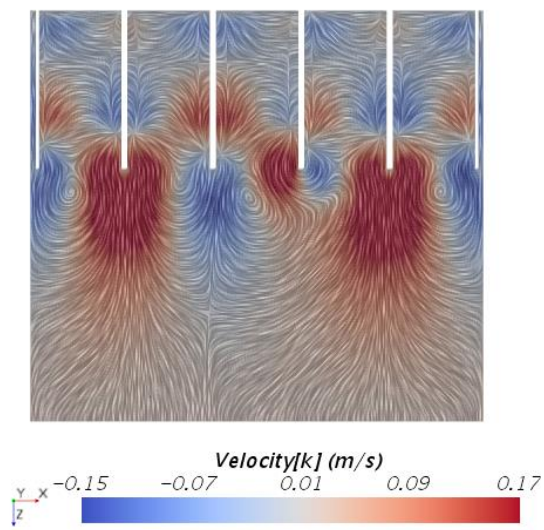

Figure C-33. Velocity profile at plane T1 for the final design

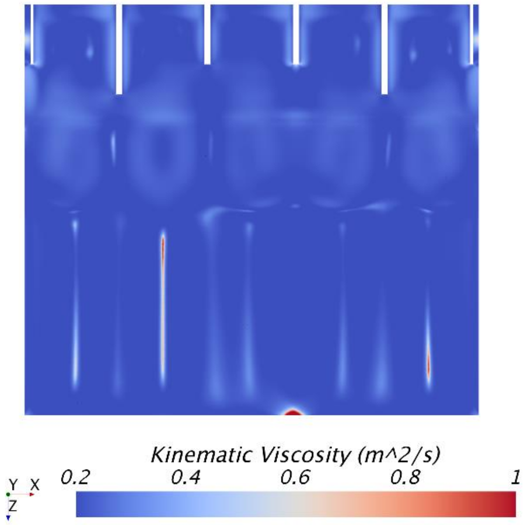

Figure C-34. Viscosity at plane T1 for the initial design

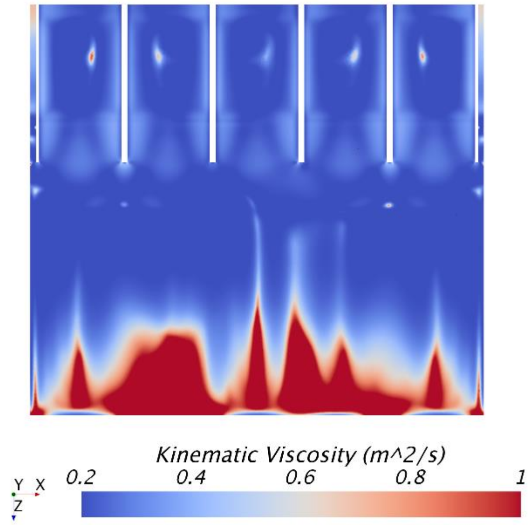

Figure C-36. Viscosity at plane T1 for the final design

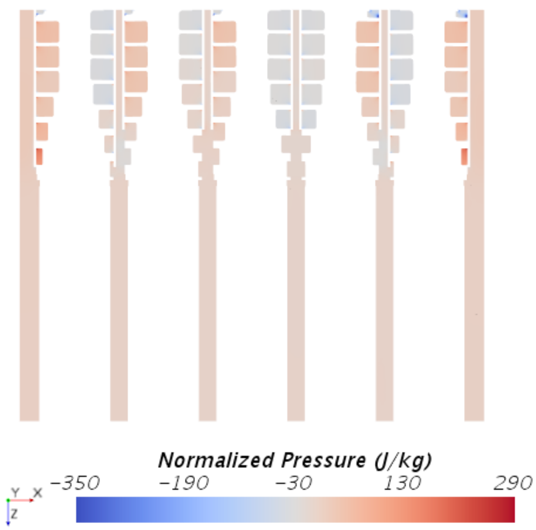

Figure C-35. Normalized pressure at plane T2 for the initial design

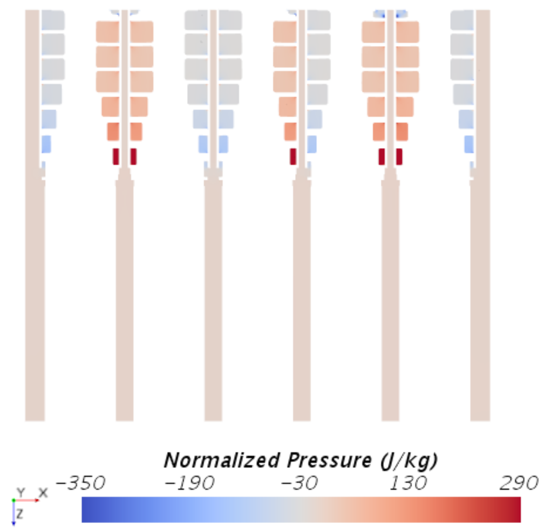

Figure C-37. Normalized pressure at plane T2 for the final design

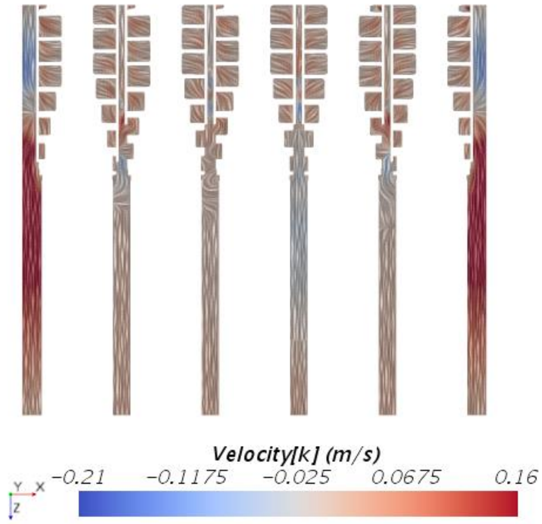

Figure C-38. Velocity profile at plane T2 for the initial design

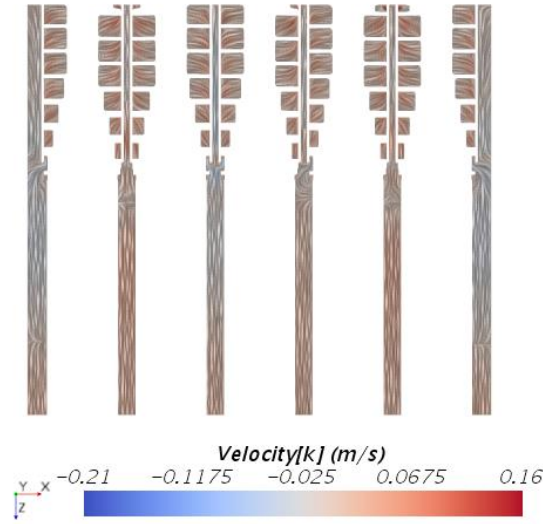

Figure C-40. Velocity profile at plane T2 for the final design

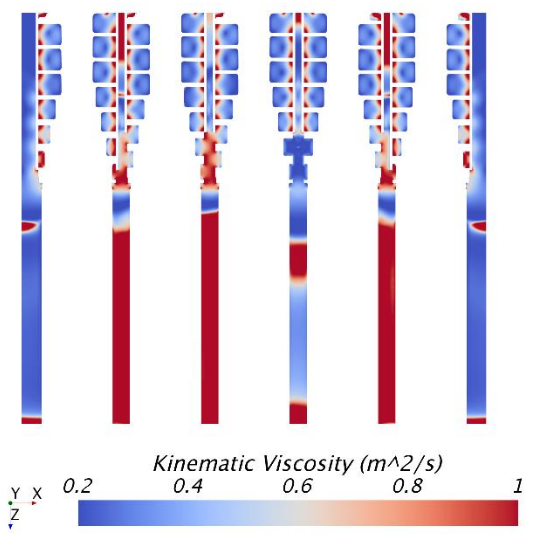

Figure C-39. Viscosity at plane T2 for the initial design

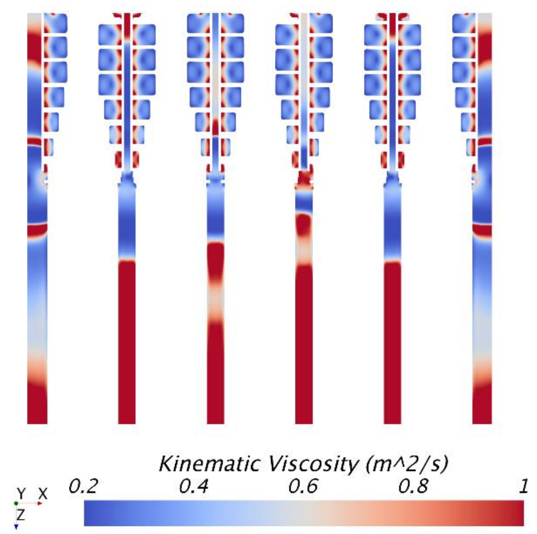

Figure C-41. Viscosity at plane T2 for the final design

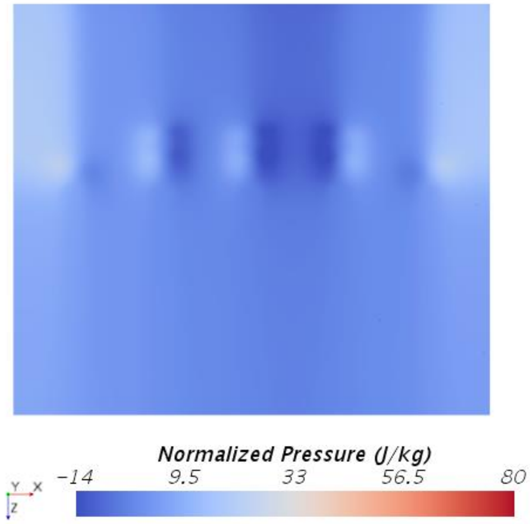

Figure C-42. Normalized pressure at plane T3 for the initial design

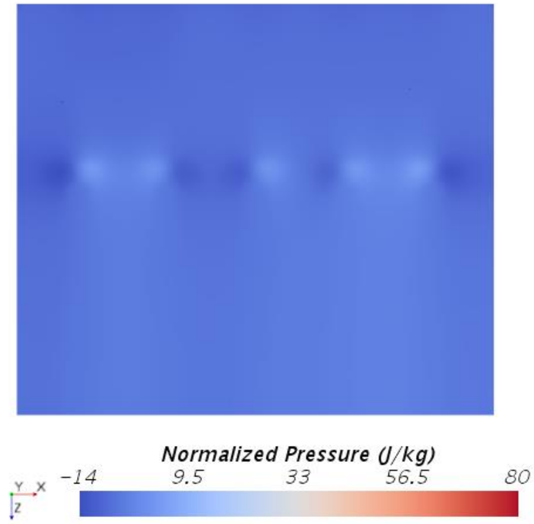

Figure C-44. Normalized pressure at plane T3 for the final design

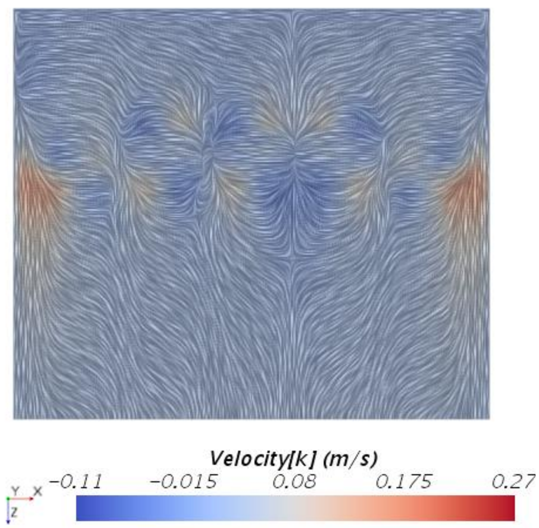

Figure C-43. Velocity profile at plane T3 for the initial design

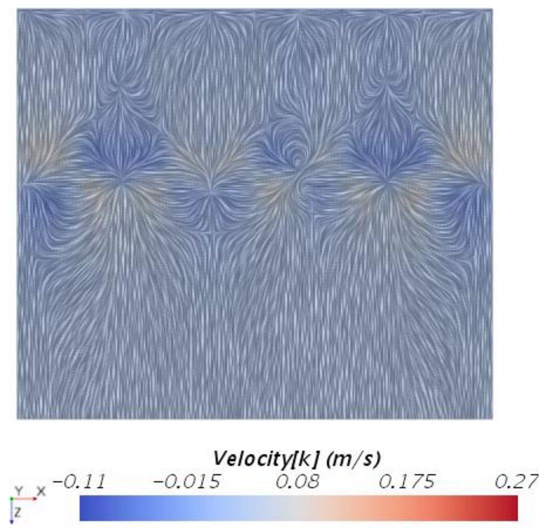

Figure C-45. Velocity profile at plane T3 for the final design

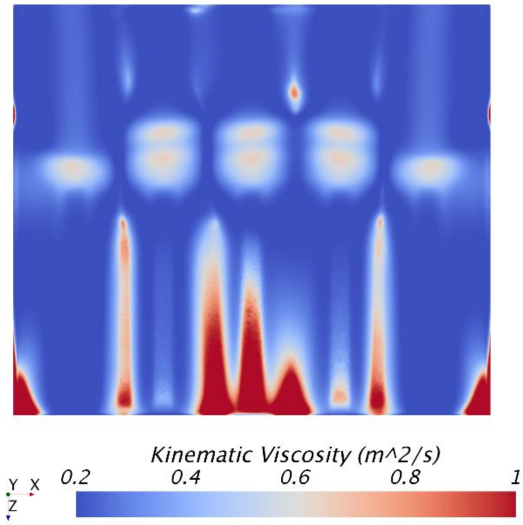

Figure C-46. Viscosity at plane T3 for the initial design

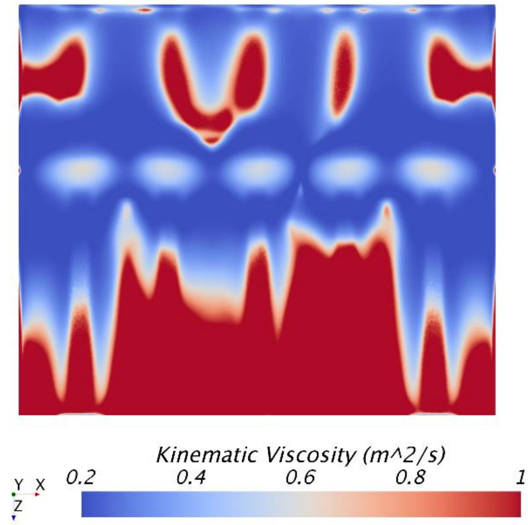

Figure C-48. Viscosity at plane T3 for the final design

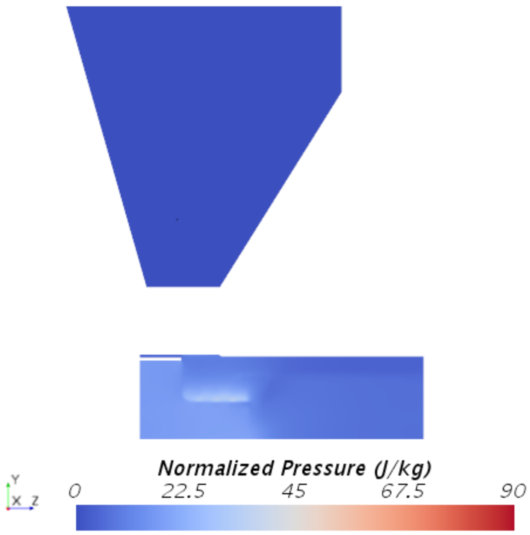

Figure C-47. Normalized pressure at plane S1 for the initial design

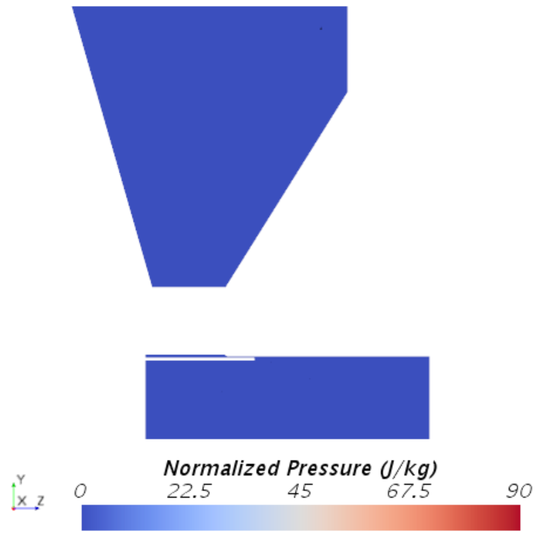

Figure C-49. Normalized pressure at plane S1 for the final design

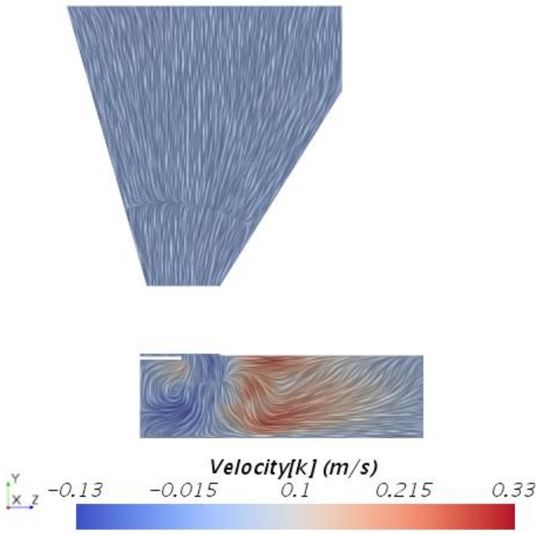

Figure C-50. Velocity profile at plane S1 for the initial design

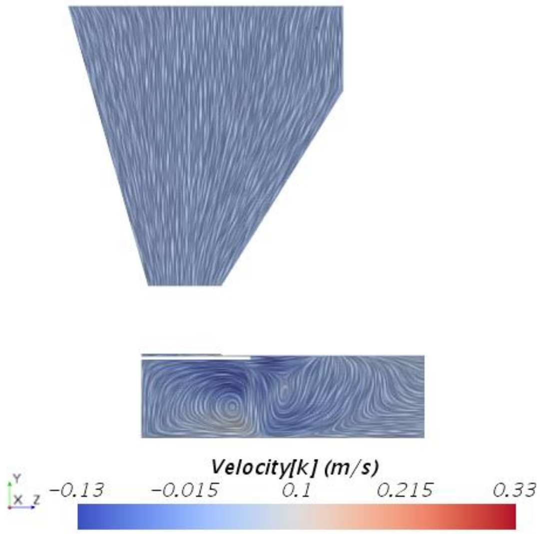

Figure C-52. Velocity profile at plane S1 for the final design

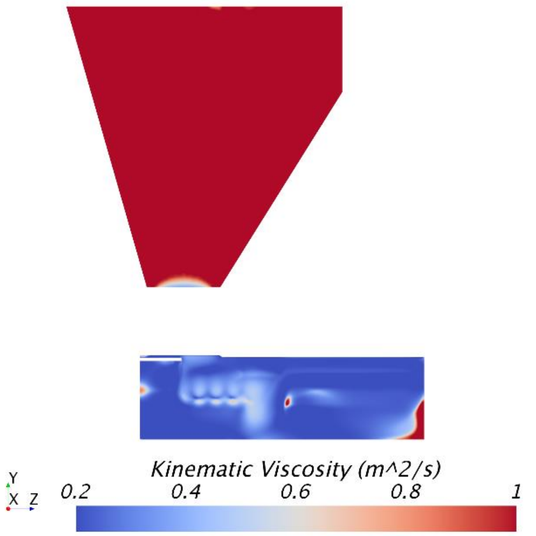

Figure C-51. Viscosity at plane S1 for the initial design

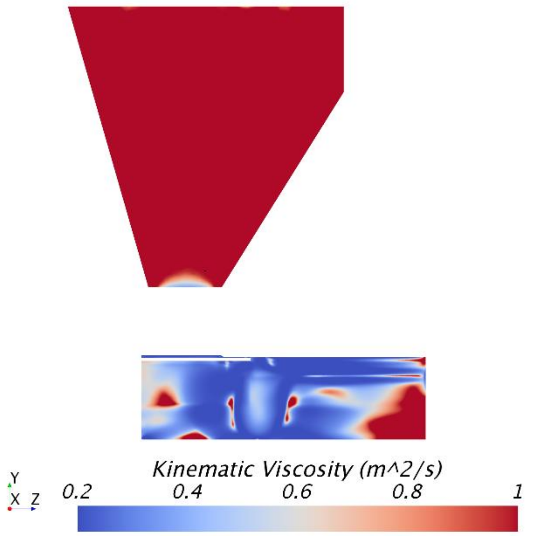

Figure C-53. Viscosity at plane S1 for the final design

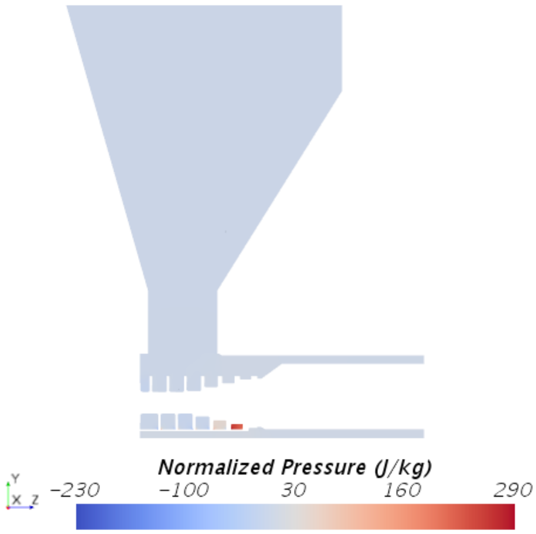

Figure C-54. Normalized pressure at plane S2 for the initial design

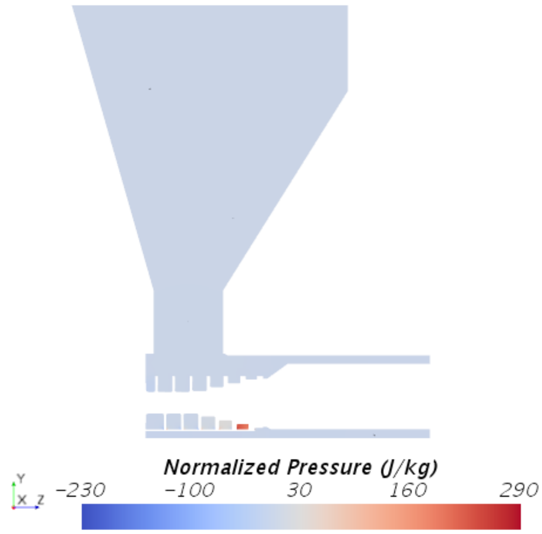

Figure C-56. Normalized pressure at plane S2 for the final design

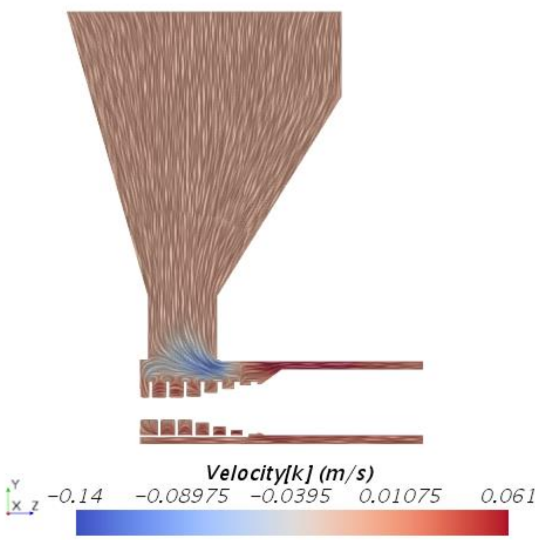

Figure C-55. Velocity profile at plane S2 for the initial design

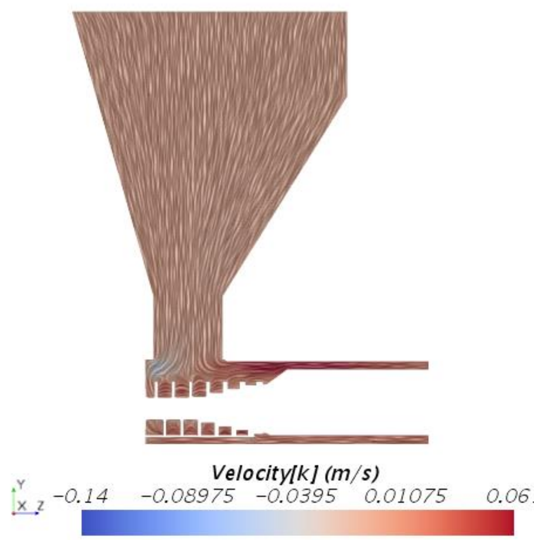

Figure C-57. Velocity profile at plane S2 for the final design

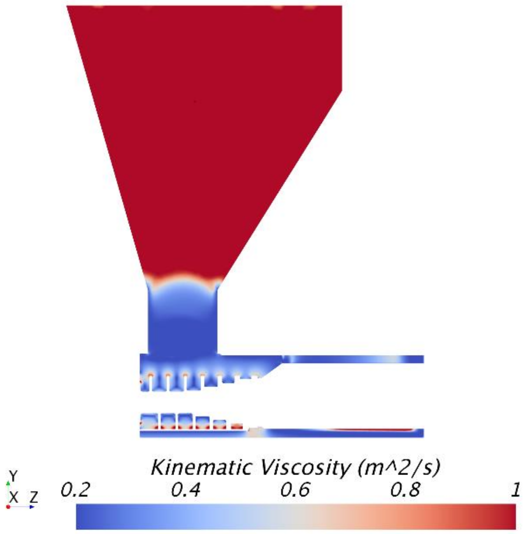

Figure C-58. Viscosity at plane S2 for the initial design

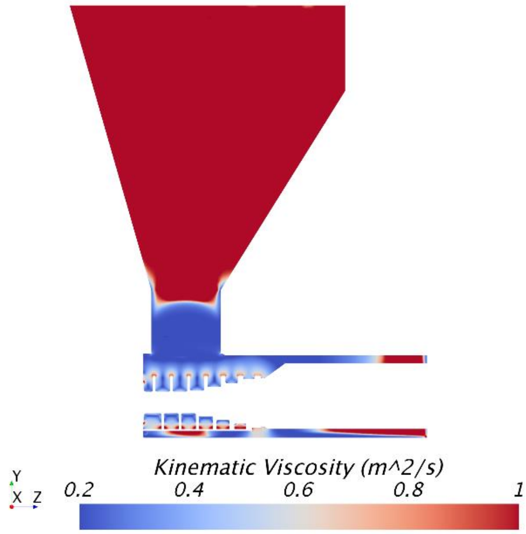

Figure C-60. Viscosity at plane S2 for the final design

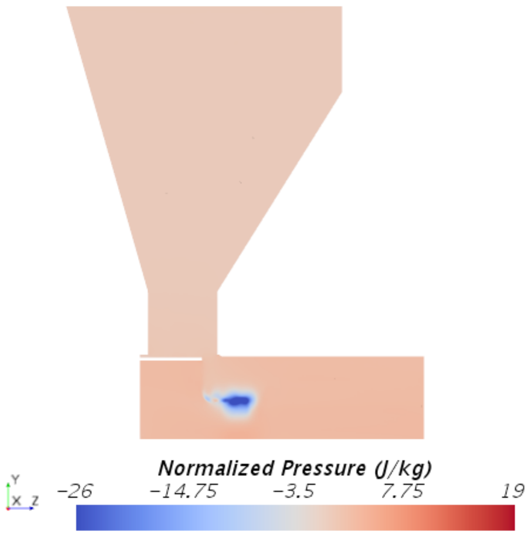

Figure C-59. Normalized pressure at plane S3 for the initial design

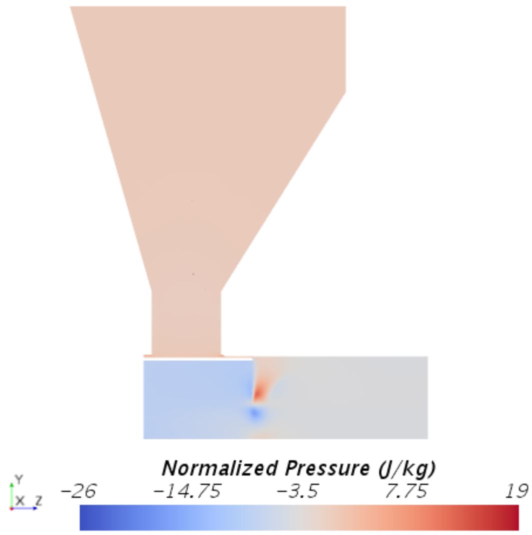

Figure C-61. Normalized pressure at plane S3 for the final design

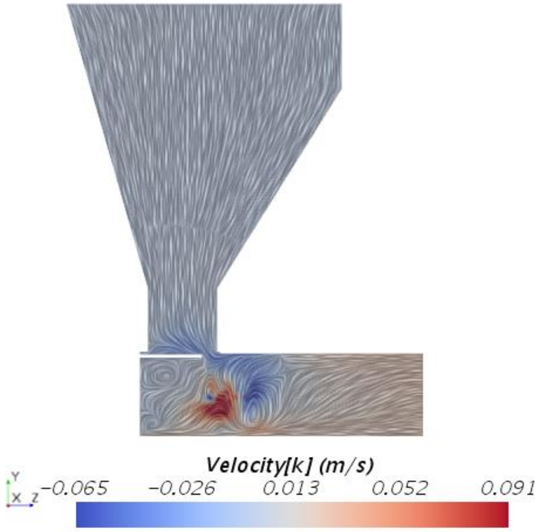

Figure C-62. Velocity profile at plane S3 for the initial design

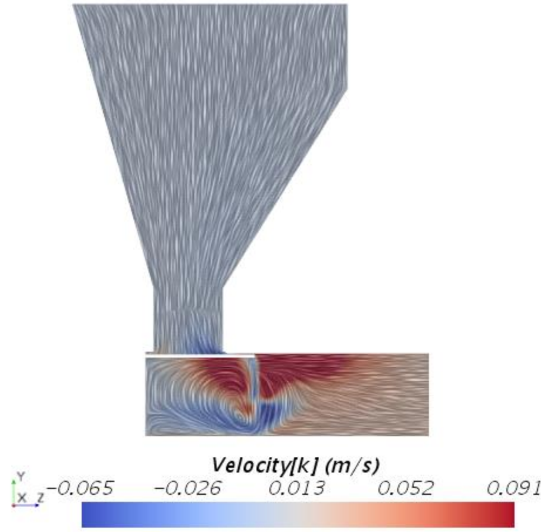

Figure C-64. Velocity profile at plane S3 for the final design

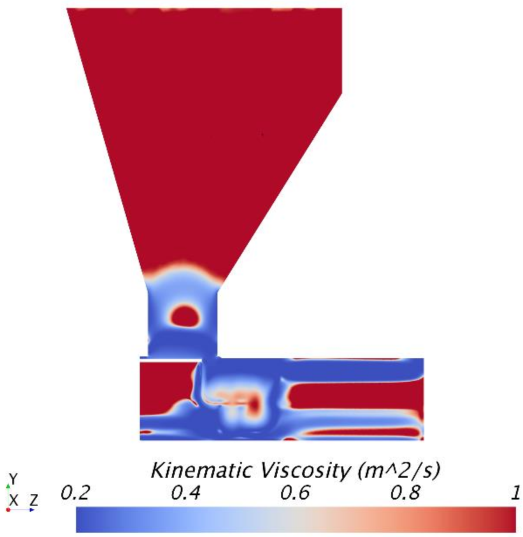

Figure C-63. Viscosity at plane S3 for the initial design

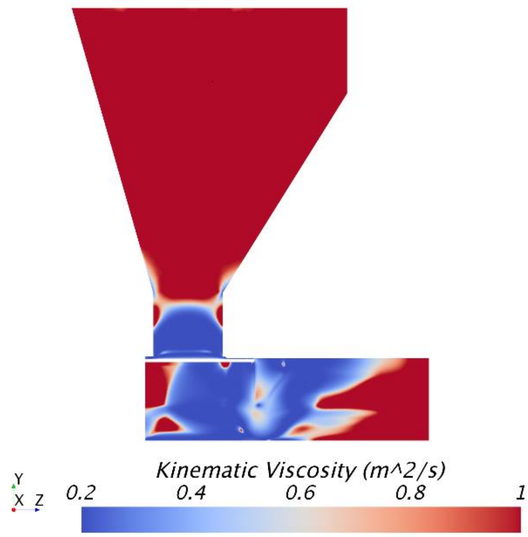

Figure C-65. Viscosity at plane S3 for the final design

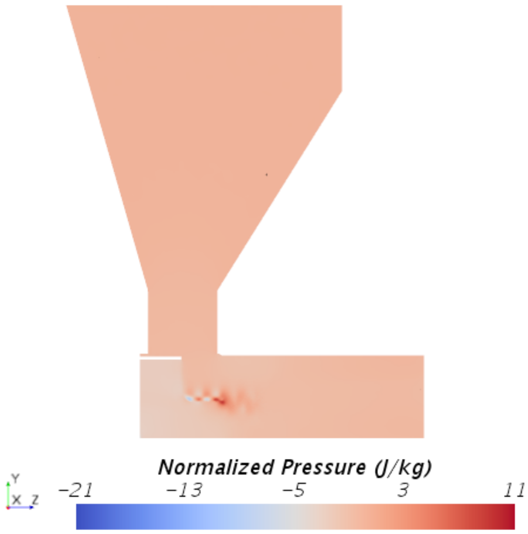

Figure C-66. Normalized pressure at plane S4 for the initial design

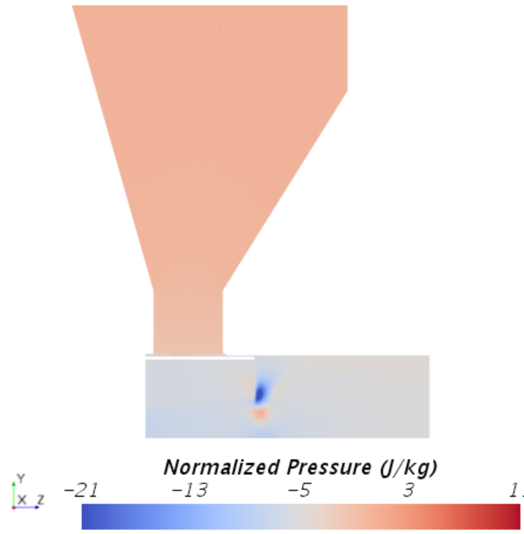

Figure C-68. Normalized pressure at plane S4 for the final design

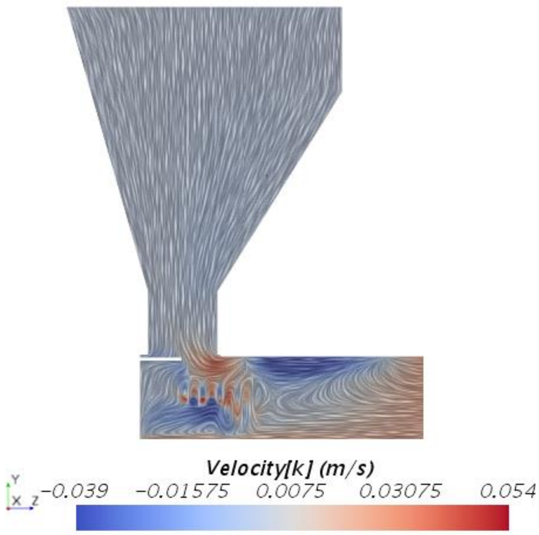

Figure C-67. Velocity profile at plane S4 for the initial design

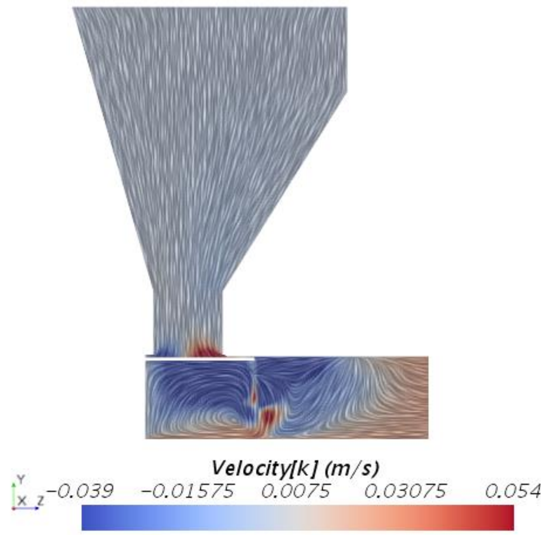

Figure C-69. Velocity profile at plane S4 for the final design

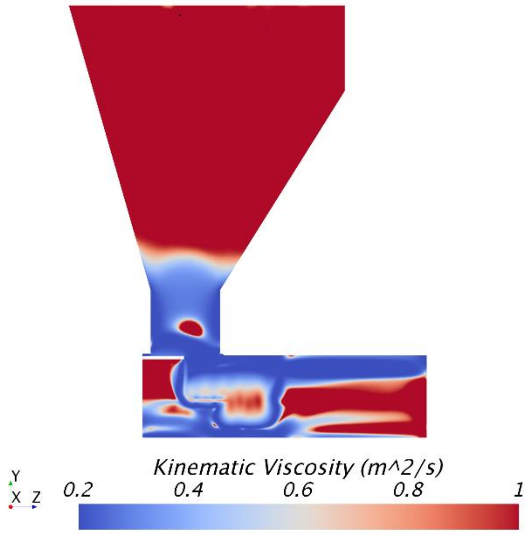

Figure C-70. Viscosity at plane S4 for the initial design

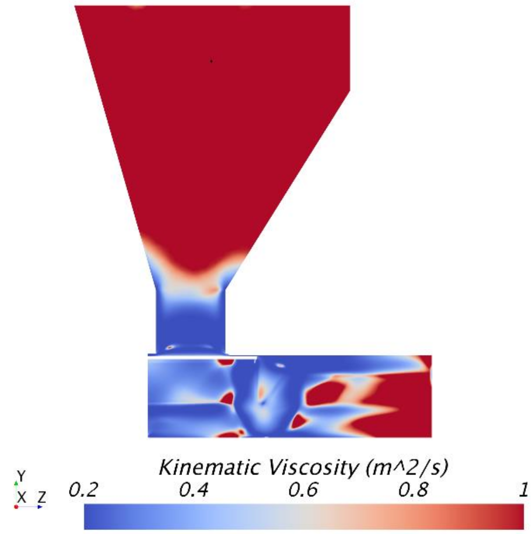

Figure C-72. Viscosity at plane S4 for the final design

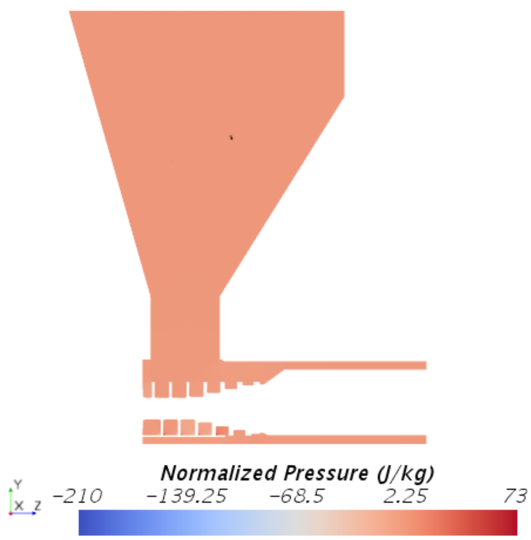

Figure C-71. Normalized pressure at plane S5 for the initial design

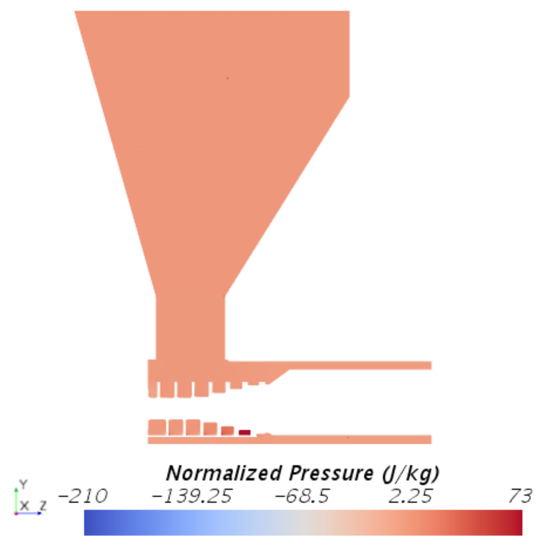

Figure C-73. Normalized pressure at plane S5 for the final design

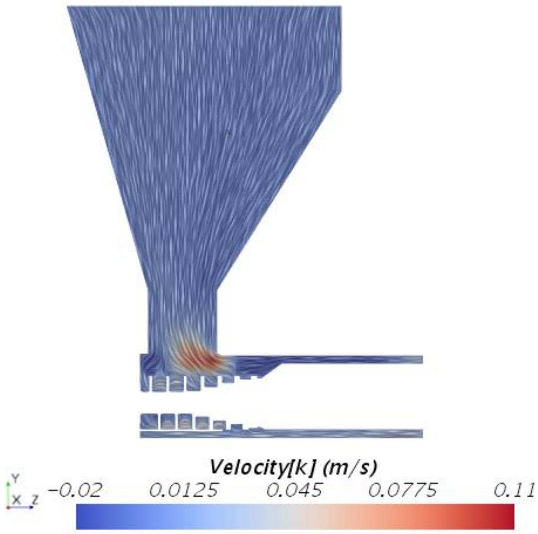

Figure C-74. Velocity profile at plane S5 for the initial design

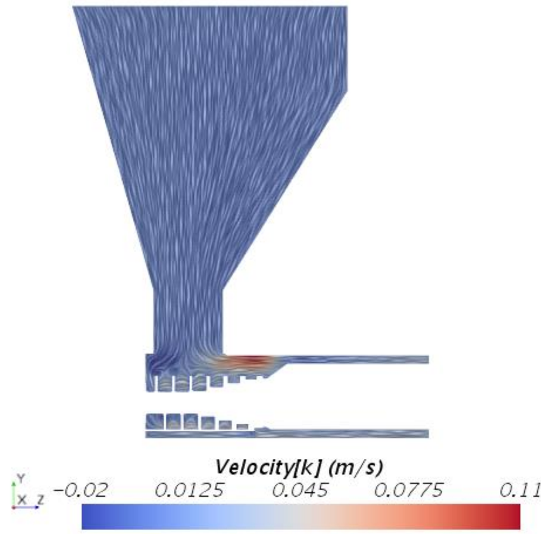

Figure C-76. Velocity profile at plane S5 for the final design

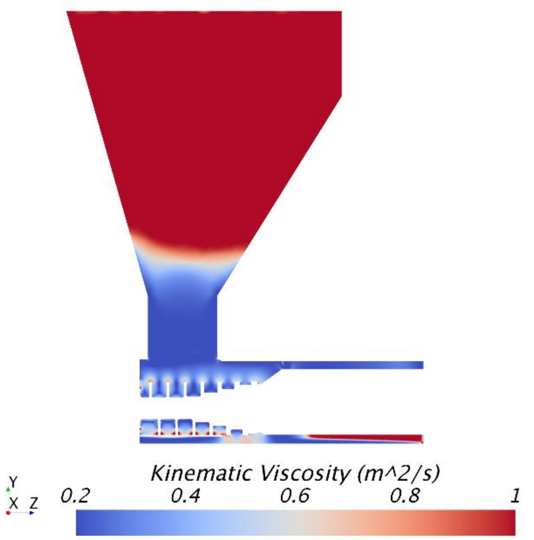

Figure C-75. Viscosity at plane S5 for the initial design

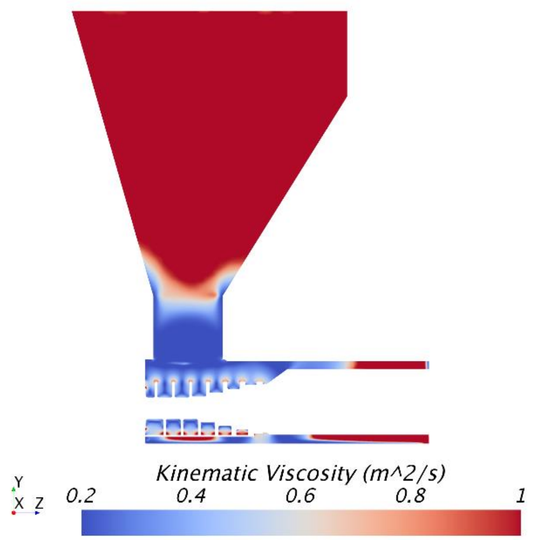

Figure C-77. Viscosity at plane S5 for the final design

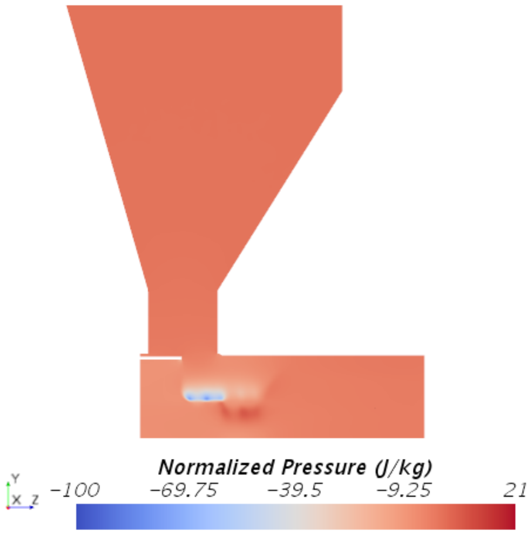

Figure C-78. Normalized pressure at plane S6 for the initial design

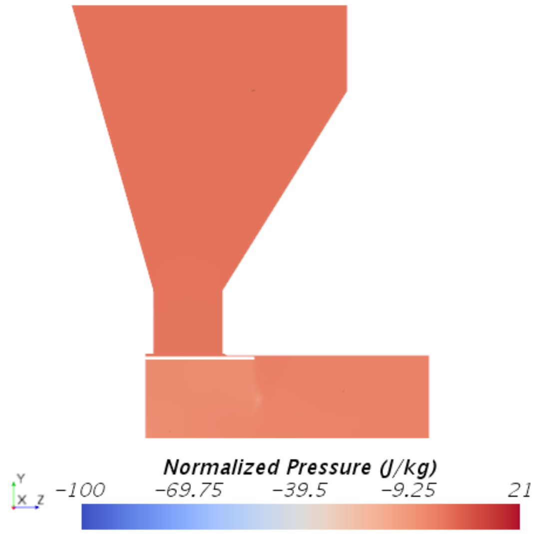

Figure C-80. Normalized pressure at plane S6 for the final design

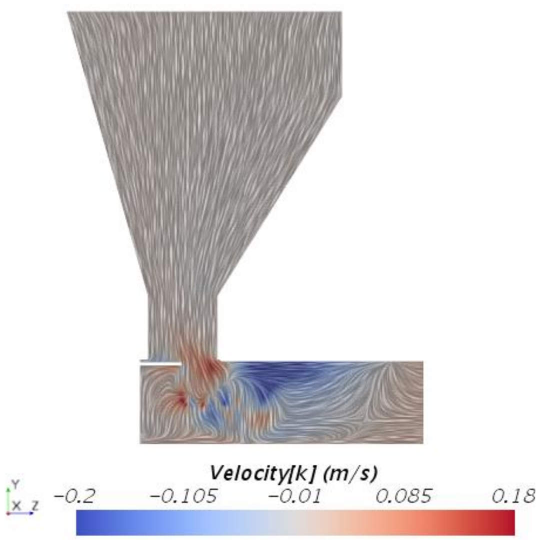

Figure C-79. Velocity profile at plane S6 for the initial design

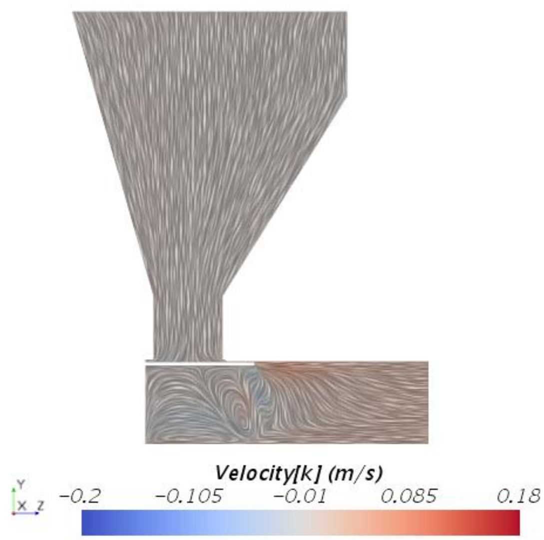

Figure C-81. Velocity profile at plane S6 for the final design

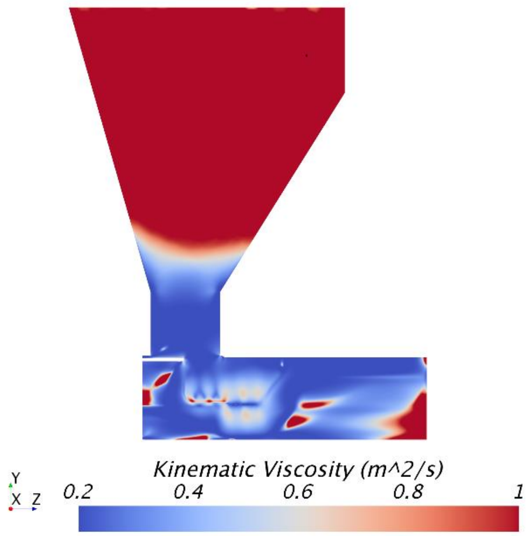

Figure C-82. Viscosity at plane S6 for the initial design

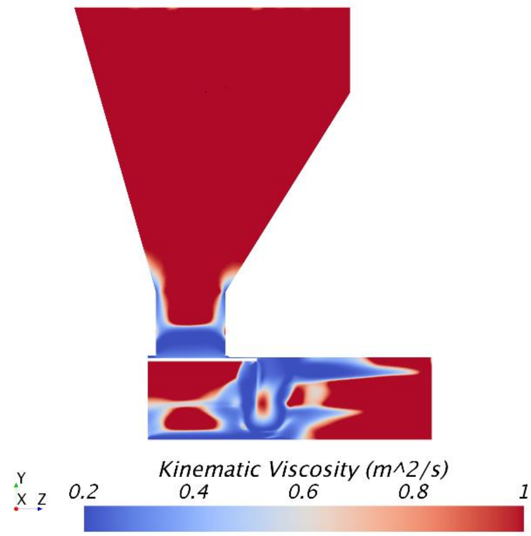

Figure C-84. Viscosity at plane S6 for the final design

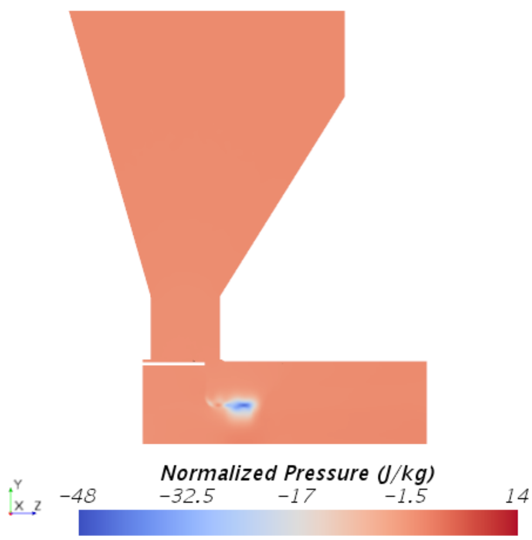

Figure C-83. Normalized pressure at plane S7 for the initial design

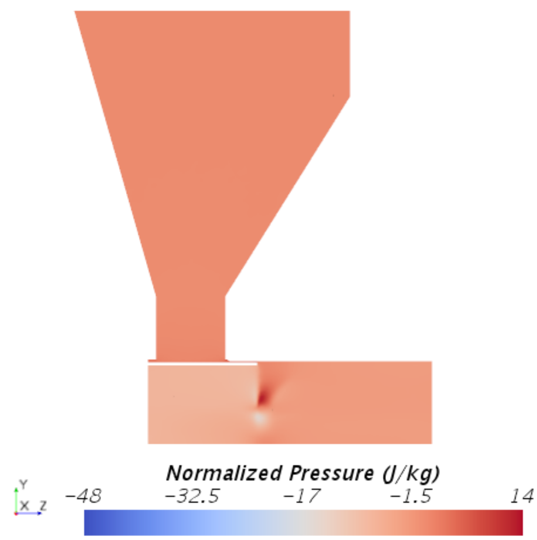

Figure C-85. Normalized pressure at plane S7 for the final design

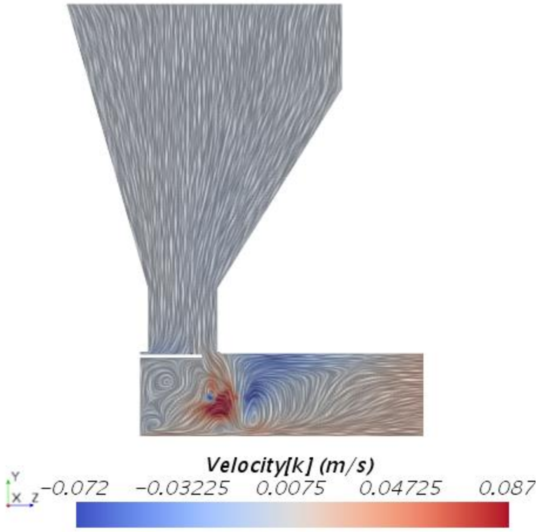

Figure C-86. Velocity profile at plane S7 for the initial design

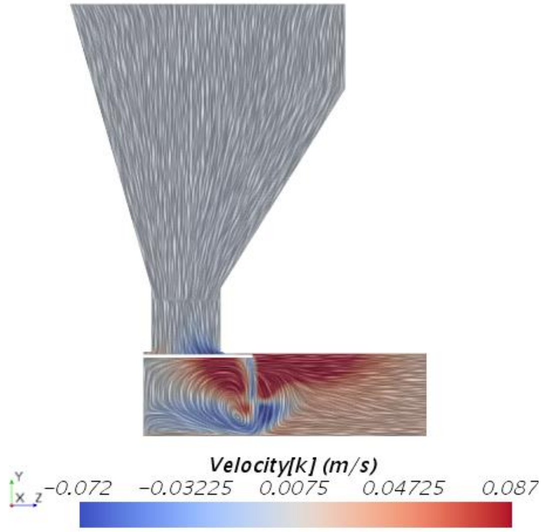

Figure C-88. Velocity profile at plane S7 for the final design

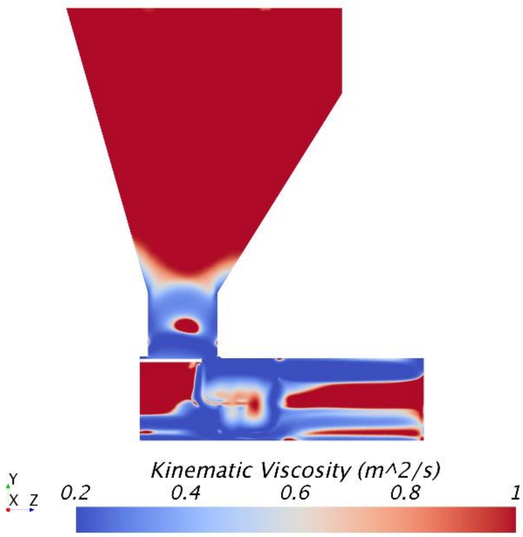

Figure C-87. Viscosity at plane S7 for the initial design

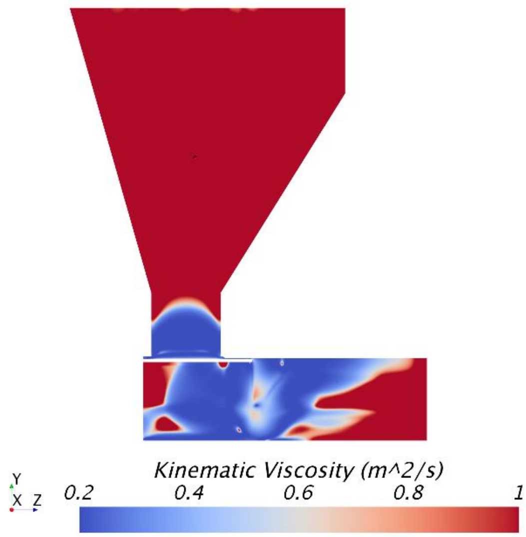

Figure C-89. Viscosity at plane S7 for the final design

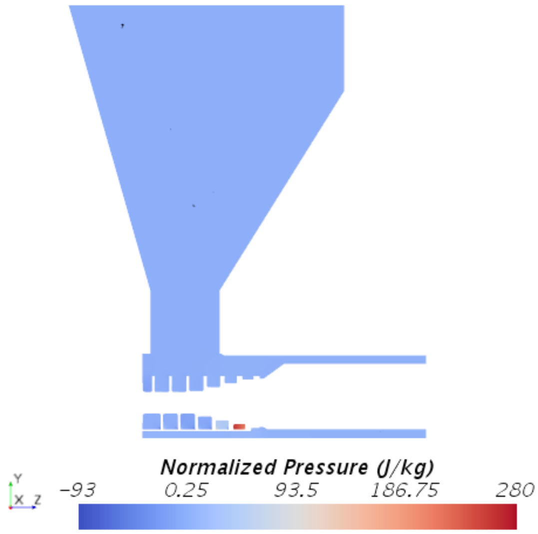

Figure C-90. Normalized pressure at plane S8 for the initial design

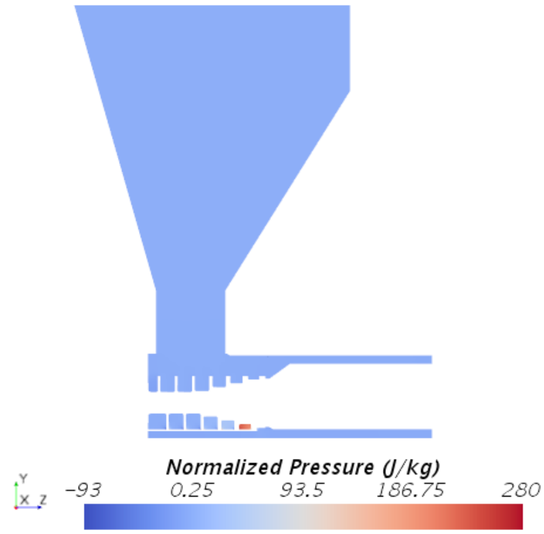

Figure C-92. Normalized pressure at plane S8 for the final design

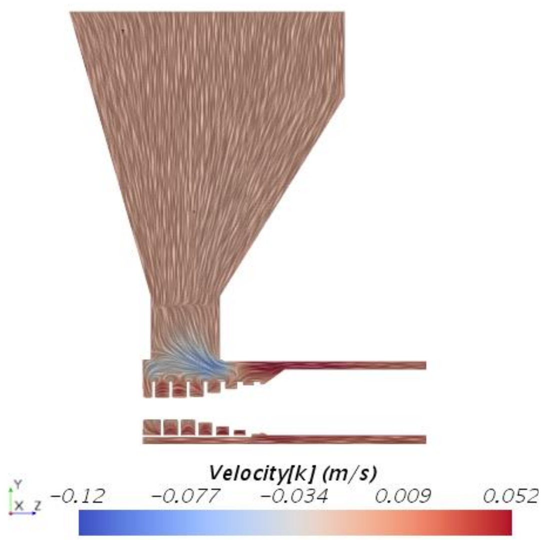

Figure C-91. Velocity profile at plane S8 for the initial design

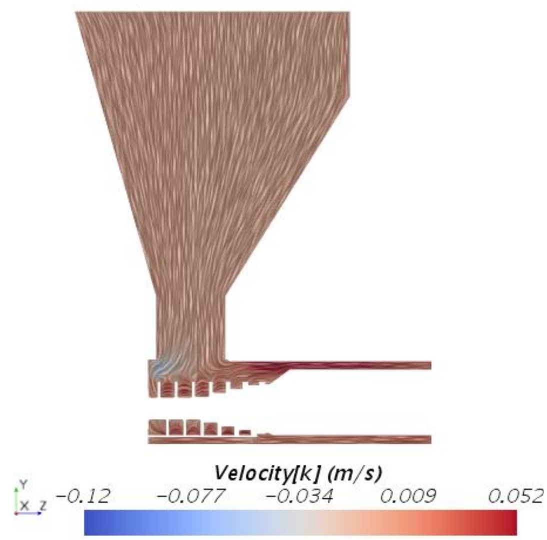

Figure C-93. Velocity profile at plane S8 for the final design

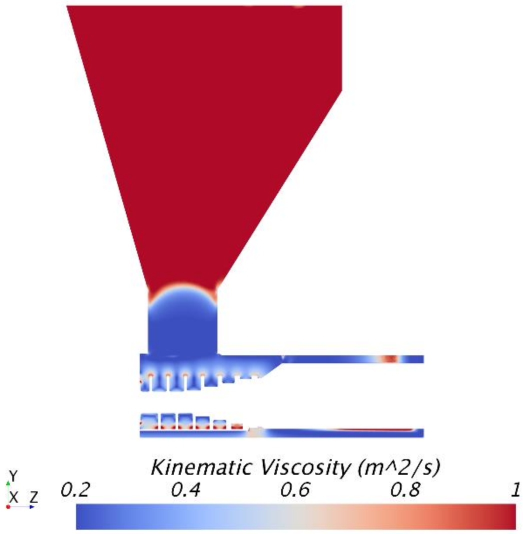

Figure C-94. Viscosity at plane S8 for the initial design

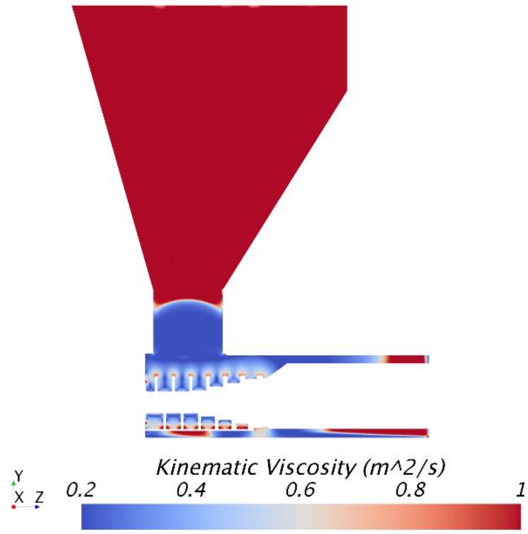

Figure C-96. Viscosity at plane S8 for the final design

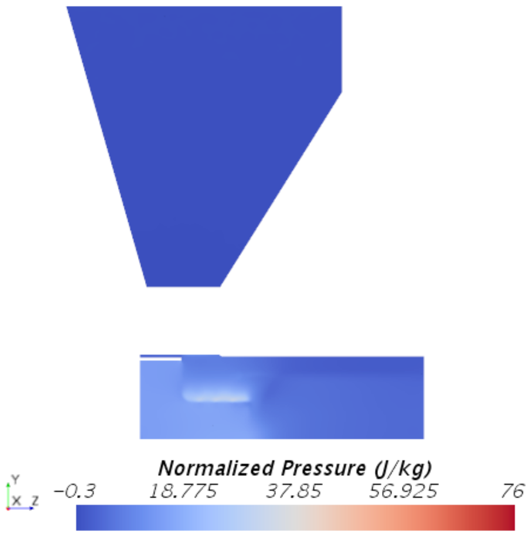

Figure C-95. Normalized pressure at plane S9 for the initial design

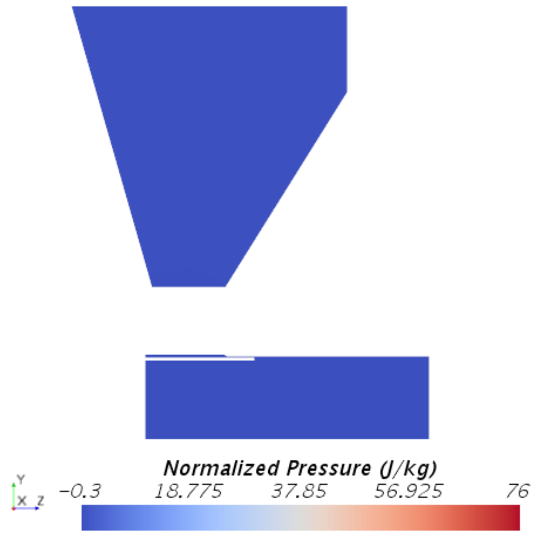

Figure C-97. Normalized pressure at plane S9 for the final design

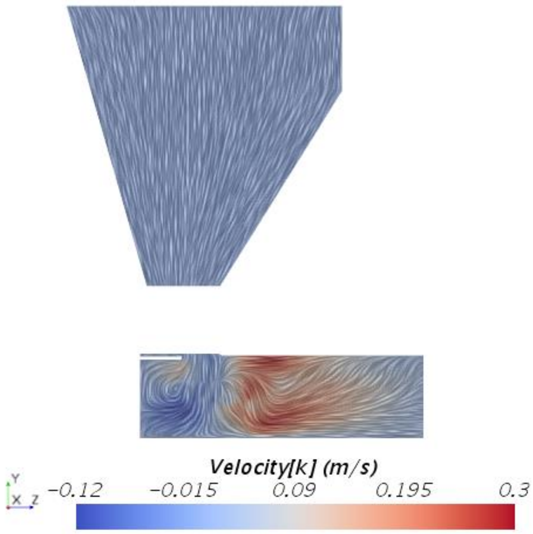

Figure C-98. Velocity profile at plane S9 for the initial design

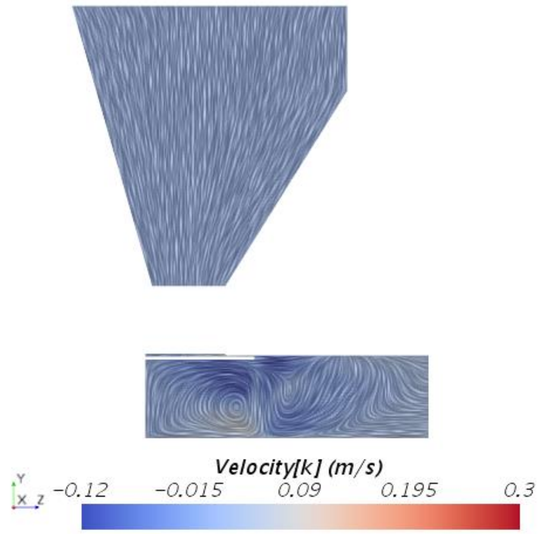

Figure C-100. Velocity profile at plane S9 for the final design

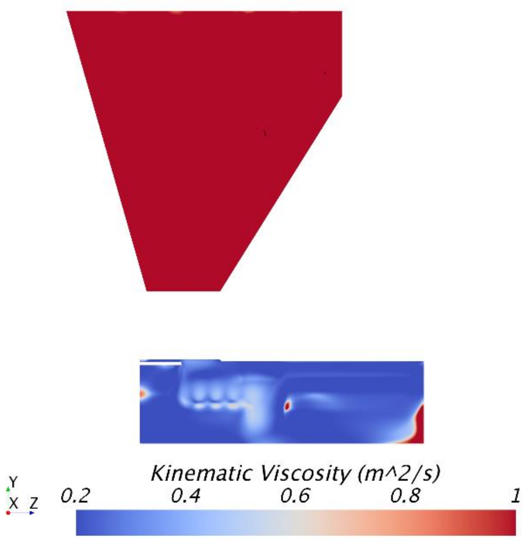

Figure C-99. Viscosity at plane S9 for the initial design

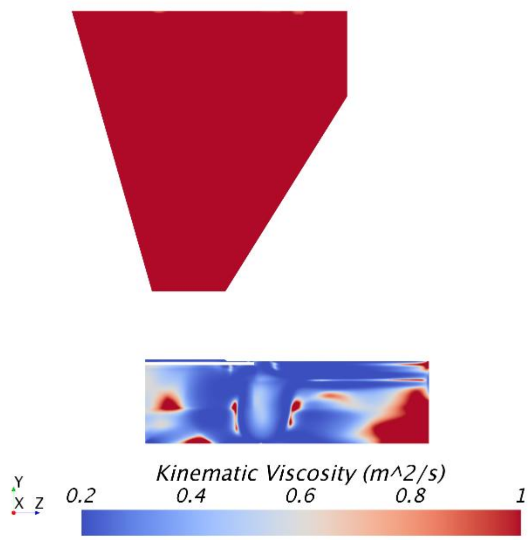

Figure C-101. Viscosity at plane S9 for the final design